The Pennsylvania State University

The Graduate School

Department of Mathematics

ON THE CONVERGENCE OF SOME LOW ORDER MIXED FINITE ELEMENTS FOR INCOMPRESSIBLE FLUIDS

A Thesis in

Mathematics

by

Jinshui Qin

Submitted in Partial Fulfillment
of the Requirements
for the Degree of

Doctor of Philosophy

April 1994

ABSTRACT

In this thesis, we study the approximation properties of three low order mixed finite elements which preserve the incompressibility condition for incompressible fluids. More precisely, we study the mixed finite elements $\mathcal{P}^n$–$\mathcal{P}^{n-1}$ for $n = 1, 2, 3$ for which the velocity space consists of continuous piecewise polynomials of degree at most n and the pressure space consists of discontinuous piecewise polynomials of degree at most $n-1$. In addition to its practical applications, the study of the elements sheds light upon questions in the approximation theory of divergence-free piecewise polynomials and continuously differentiable piecewise polynomials.

The performance of the $\mathcal{P}^n$–$\mathcal{P}^{n-1}$ elements depends on the mesh configuration and the analysis of their stability and convergence is far from complete. In this thesis, we extend the existing theory to many new analytical and computational results.

CONTENTS

LIST OF FIGURES

LIST OF TABLES

ACKNOWLEDGMENTS

I am extremely grateful to Professor Douglas N. Arnold for his encouragement, advice, and support during the years of my graduate study. I could not complete this work without his superb teaching and guidance for my study and research.

I wish to thank Professors Jesse Barlow, Diane Henderson, Simon Tavener, and Jinchao Xu who kindly agreed to serve on my thesis committee. Thanks also go to Professors Jerry Bona, William Pritchard, Ridgway Scott, and Jinchao Xu for their wonderful lectures on applied mathematics and numerical analysis.

I thank all my friends who have made my stay at Pennsylvania State University a very enjoyable and memorable one.

There are simply no words to express my gratitude to my parents and my brothers and sister, who supported me with all they had as farmers during the years of my education in China, to my parents-in-law, who take care of my family and my sons Dennis and Richard for all these years, and to my wife B. Lin, who has constantly supported and encouraged me since I met her 12 years ago.

Chapter 1

INTRODUCTION

1.1. Problem and Motivations

In this thesis, we mainly study the approximation properties of some low order mixed finite elements that preserve the incompressibility condition for incompressible fluids. Our principal equations in this work are the Stokes equations

$$\begin{aligned} -\Delta \boldsymbol{u} + \nabla p &= \boldsymbol{f} \quad \text{in } \Omega, \\ \operatorname{div} \boldsymbol{u} &= 0 \quad \text{in } \Omega, \end{aligned} \tag{1.1.1}$$

where $\boldsymbol{u} = (u_1, u_2)$ is the velocity of the fluid, p is its pressure, $\boldsymbol{f} = (f_1, f_2)$ is the external force, and Ω is a polygonal domain in $\mathbb{R}^2$. More precisely, the mixed finite elements $\mathcal{P}^n$–$\mathcal{P}^{n-1}$ for $n = 1, 2, 3$, i.e., the velocity space, consisting of continuous piecewise polynomials of degree n, and the pressure space consisting of discontinuous piecewise polynomials with degree $n-1$, are investigated in this work. It is known, by the work of Scott and Vogelius [21], that for $n \geq 4$ these elements are stable and have optimal rate of convergence for almost all of the regular mesh configurations. However, there are very few results, see Scott and Vogelius [22], that are valid for these three low order elements—mainly due to the uncertain stability of the elements on different mesh families. In this thesis, we present many new theoretical results and numerical experiments concerning these elements.

Let us first discuss our motivations in undertaking an in depth study of the $\mathcal{P}^n$–$\mathcal{P}^{n-1}$ elements. First of all, the $\mathcal{P}^n$–$\mathcal{P}^{n-1}$ elements are simple in structure and relatively easy to implement, and they often achieve good approximation in practical computations. For example, the $\mathcal{P}^2$–$\mathcal{P}^1$ element has been used in viscoplastic analysis, see Lee and Dawson [16] and Kitahama and Dawson [15]. Numerical experiments on $\mathcal{P}^2$–$\mathcal{P}^1$ element for the Stokes equations also show that this element does provide good approximation for the velocity and sometimes for the pressure as well. In the other words, this finite element method is able to provide numerical solutions with an optimal rate of convergence even though the method fails the stability test in general. This suggests that a gap sometimes exists between error estimates based on the classical stability theory and the true approximation properties of mixed finite element methods. Implementation of these elements are relatively simple in practical computations. Since the pressure space does not impose any interelement continuity, the finite element discretization of system (1.1.1) can be approximated by the penalty method, leading to a positive definite system for the velocity. Then the pressure can be recovered easily triangle by triangle.

Second, all the three elements preserve the incompressibility condition of the incompressible fluids. This is a direct consequence of the fact that the divergence of each velocity function in any of the three finite element spaces belongs to the corresponding pressure space. Almost all of the low order finite elements (see, e.g., Girault and Raviart [11], Brezzi and Fortin [7]) for the Stokes

equations do not have this property—this is because the usual way to achieve stability of a low order element is to relax the incompressibility condition, thereby sacrificing the incompressibility of the numerical solutions.

Third, the three elements provide examples in which the stability and convergence of finite element solutions depend heavily on the mesh configuration, a situation which has not been fully understood yet. As will be seen, they provide a remarkably rich set of behaviors depending on the boundary conditions and especially mesh geometries.

Finally, by analyzing the error estimates of the finite element solutions provided by these elements, we can understand the approximation properties of the space of all the divergence-free functions of the continuous piecewise linear, quadratic, or cubic polynomials. Via the introduction of a stream function, the best approximation to the velocity by $\mathcal{P}^n$–$\mathcal{P}^{n-1}$ element for $n = 1, 2, 3$ is intimately related to the best approximation of C^1 piecewise polynomials of $\mathcal{P}^{n+1}$ to a C^1 function.

1.2. Stability and Approximability of Mixed Finite Elements

To simplify the exposition we are assuming that the Stokes equations (1.1.1) is subject to either the homogeneous Dirichlet boundary conditions, $\boldsymbol{u} = 0$ on $\partial\Omega$, or to the traction boundary conditions $\partial\boldsymbol{u}/\partial\boldsymbol{n} - p\boldsymbol{n} = \boldsymbol{g}$ on $\partial\Omega$, where $\boldsymbol{n}$ is the outward normal unit to $\partial\Omega$.

For the Dirichlet condition, the weak formulation of (1.1.1) seeks $(\boldsymbol{u}, p)$ in $\boldsymbol{V} \times P := \mathring{\boldsymbol{H}}^1(\Omega) \times L^2(\Omega)$ such that

$$\begin{aligned} \int_\Omega \nabla\boldsymbol{u} : \nabla\boldsymbol{v} - \int_\Omega p \operatorname{div}\boldsymbol{v} &= \int_\Omega \boldsymbol{f}\cdot\boldsymbol{v}, \quad \forall \boldsymbol{v} \in \boldsymbol{V}, \\ \int_\Omega q \operatorname{div}\boldsymbol{u} &= 0, \quad \forall q \in P. \end{aligned} \tag{1.2.1}$$

Note that the velocity $\boldsymbol{u}$ is uniquely determined but the pressure p is only determined up to an additive constant—if $(\boldsymbol{u}, p)$ solves (1.1.1) then $(\boldsymbol{u}, p + c)$ also solves (1.1.1) for any constant c. To obtain a unique pressure, we impose the side condition

$$\int_\Omega p = 0.$$

For the traction boundary condition, the weak formulation of (1.1.1) is given by following with the space $\boldsymbol{V} \times P$ is taken to be $\boldsymbol{H}^1(\Omega) \times L^2(\Omega)$:

$$\begin{aligned} \int_\Omega \nabla\boldsymbol{u} : \nabla\boldsymbol{v} - \int_\Omega p \operatorname{div}\boldsymbol{v} &= \int_\Omega \boldsymbol{f}\cdot\boldsymbol{v} + \int_{\partial\Omega} \boldsymbol{g}\cdot\boldsymbol{v}, \quad \forall \boldsymbol{v} \in \boldsymbol{V}, \\ \int_\Omega q \operatorname{div}\boldsymbol{u} &= 0, \quad \forall q \in P. \end{aligned}$$

The pressure p is unique under the traction boundary condition but the velocity $\boldsymbol{u}$ is determined only up to an additive constant vector.

In the following, we always refer to the Stokes equations with the Dirichlet boundary condition unless stated otherwise. Parallel discussions can be carried out quite similarly for the traction boundary condition.

On the finite element level, we consider solving a discrete analogue of the system (1.2.1) in a finite element space $\boldsymbol{V}_h \times P_h$ contained in $\boldsymbol{V} \times P$:

$$\begin{aligned} \int_\Omega \nabla\boldsymbol{u}_h : \nabla\boldsymbol{v} - \int_\Omega p_h \operatorname{div}\boldsymbol{v} &= \int_\Omega \boldsymbol{f}\cdot\boldsymbol{v}, \quad \forall \boldsymbol{v} \in \boldsymbol{V}_h, \\ \int_\Omega q \operatorname{div}\boldsymbol{u}_h &= 0, \quad \forall q \in P_h. \end{aligned} \tag{1.2.2}$$

Here the parameter h usually refers to the meshsize. The velocity $\boldsymbol{u}_h$ is still unique, but the pressure p_h may be determined up to addition of any function in the kernel

$$N_h = \{p \in P_h \mid \int_\Omega p \operatorname{div} \boldsymbol{v} = 0, \quad \forall \boldsymbol{v} \in \boldsymbol{V}_h\},$$

of the discrete gradient operator. The nonconstant pressure modes in N_h are called spurious pressure modes. In order for (1.2.2) to be a reasonable discretization, the spaces $\boldsymbol{V}_h$ and P_h will have to be appropriately chosen; not just any combination will work. Loosely speaking, we want to choose $\boldsymbol{V}_h$ and P_h so that the resulting method is both stable and accurate in some sense. These demands tend to be in conflict and one has to find a reasonable compromise. Many low order finite elments for (1.2.2) are known to be both stable and accurate, however almost none of them can provide a divergence-free numerical solution $\boldsymbol{u}_h$.

The stability properties of the finite element method based on $\boldsymbol{V}_h \times P_h$ is determined by the inf–sup condition (or Brezzi's condition, or LBB condition), see Brezzi [6]: that the inf–sup constant

$$\gamma_h := \inf_{0 \neq p \in \hat{P}_h} \sup_{0 \neq \boldsymbol{v} \in \boldsymbol{V}_h} \frac{\int_\Omega p \operatorname{div} \boldsymbol{v}}{\|\boldsymbol{v}\|_{1,\Omega} \|p\|_{0,\Omega}} > 0.$$

(The circumflex in $\hat{P}_h$ indicates the subspace of P_h consisting of functions with a mean value of zero for Dirichlet problems; P_h is used instead of $\hat{P}_h$ for traction problems.) If the finite element space $\boldsymbol{V}_h \times P_h$ satisfies the inf–sup condition and some other assumptions, we then have the following classical error estimates:

$$\|\boldsymbol{u} - \boldsymbol{u}_h\|_{1,\Omega} \leq \frac{C}{\gamma_h} \inf_{\boldsymbol{v} \in \boldsymbol{V}_h} \|\boldsymbol{u} - \boldsymbol{v}\|_{1,\Omega} + C \inf_{q \in P_h} \|p - q\|_{0,\Omega}, \tag{1.2.3}$$

$$\|p - p_h\|_{0,\Omega} \leq \frac{C}{\gamma_h^2} \inf_{\boldsymbol{v} \in \boldsymbol{V}_h} \|\boldsymbol{u} - \boldsymbol{v}\|_{1,\Omega} + \frac{C}{\gamma_h} \inf_{q \in P_h} \|p - q\|_{0,\Omega}, \tag{1.2.4}$$

where C is a generic constant which may vary in different locations, but it is independent of h. See Brezzi [6], Brezzi and Fortin [7], and Girault and Raviart [11].

A finite element method is called stable if there exists $\gamma > 0$ independent of h such that $\gamma_h \geq \gamma$ holds for any mesh of Ω and for any meshsize $h > 0$. Similarly, a finite element is said to be stable for a mesh family if γ_h can be bounded below by a positive number for any mesh of the mesh family. For a stable finite element method, the combination of (1.2.3) and (1.2.4) gives an estimate of the finite element solution $(\boldsymbol{u}_h, p_h)$ as

$$\|\boldsymbol{u} - \boldsymbol{u}_h\|_{1,\Omega} + \|p - p_h\|_{0,\Omega} \leq \frac{C}{\gamma^2} \inf_{\boldsymbol{v} \in \boldsymbol{V}_h} \|\boldsymbol{u} - \boldsymbol{v}\|_{1,\Omega} + \frac{C}{\gamma} \inf_{q \in P_h} \|p - q\|_{0,\Omega}. \tag{1.2.5}$$

Therefore, for a stable finite element method, the good convergence of the finite element solution is guaranteed as long as the finite element space $\boldsymbol{V}_h \times P_h$ has good approximation properties. It is easy to achieve the stability by simply taking $\boldsymbol{V}_h$ large enough; the real challenge is to achieve a good balance between $\boldsymbol{V}_h$ and P_h. Since the estimate of the finite element solution is tied together with the approximation properties of both the velocity and pressure spaces, shown by (1.2.5), a large $\boldsymbol{V}_h$ will not improve the error estimate in any way.

The three finite elements considered, i.e., $\mathcal{P}^n$–$\mathcal{P}^{n-1}$ for $n = 1, 2, 3$, have divergence-free velocity solutions and well matched velocity and pressure spaces in the sense of approximation abilities of the two spaces. However the stability of these elements does not hold for general mesh families. As we shall see the inf–sup constant γ_h is zero for some meshes, while for certain mesh

families γ_h will be shown to tend to zero with h, and while for other mesh families γ_h will be shown to be positive and bounded above zero uniformly.

When $\gamma_h = 0$, the pressure space P_h contains spurious pressure modes. A natural idea is to define the reduced pressure space M_h as the L^2-orthogonal complement of N_h in P_h, so there are no spurious pressure modes in M_h. The reduced inf–sup constant is defined by

$$\bar{\gamma}_h := \inf_{0 \neq p \in M_h} \sup_{0 \neq \boldsymbol{v} \in \boldsymbol{V}_h} \frac{\int_\Omega p \operatorname{div} \boldsymbol{v}}{\|\boldsymbol{v}\|_{1,\Omega} \|p\|_{0,\Omega}},$$

and is always positive. Consequently, the pair $(\bar{\boldsymbol{u}}_h, \bar{p}_h) \in \boldsymbol{V}_h \times M_h$ which solves (1.2.2) with P_h replaced by M_h is uniquely determined. With a simple calculation one can show that $\bar{\boldsymbol{u}}_h$ equals $\boldsymbol{u}_h$ and $\bar{p}_h$ is the orthogonal part of p_h to N_h. A finite element is said to be reduced-stable if there is $\bar{\gamma} > 0$ such that $\bar{\gamma}_h \geq \bar{\gamma}$ uniformly for all the regular meshes of Ω. It is obvious that stability implies reduced stability. Applying the classical error estimate theory to $\boldsymbol{V}_h \times M_h$, we shall see that the approximation of $\boldsymbol{u}_h$ to $\boldsymbol{u}$ and $\bar{p}_h$ to p depends on $\bar{\gamma}_h$ and the approximation properties of $\boldsymbol{V}_h$ and M_h.

The three elements we consider are stable on some mesh families. Therefore, the classical theory can be applied. But stability fails on many mesh families for these elements. To determine the reduced stability and the approximation properties of M_h is valuable but difficult. The structures of the reduced pressure space M_h and N_h are far from being understood for general mesh families. If the elements are reduced-stable on some mesh families, we are able to conclude that

$$\|\boldsymbol{u} - \boldsymbol{u}_h\|_{1,\Omega} \leq \frac{C}{\bar{\gamma}} \inf_{\boldsymbol{v} \in \boldsymbol{V}_h} \|\boldsymbol{u} - \boldsymbol{v}\|_{1,\Omega},$$

which implies that $\boldsymbol{u}_h$ is the best approximation of $\boldsymbol{u}$ in the velocity space $\boldsymbol{V}_h$. However the estimate for $p - \bar{p}_h$ is determined by the approximation property of the reduced pressure space M_h. As shown in late chapters M_h does have nice approximation ability on many mesh families, namely, the pressure $\bar{p}_h$ is a good approximation for p for a lot of cases. The computation for $(\boldsymbol{u}_h, \bar{p}_h)$ is usually not practical because M_h does not usually admit a local basis, but fortunately we can solve $(\boldsymbol{u}_h, p_h)$ in $\boldsymbol{V}_h \times P_h$ instead of $(\boldsymbol{u}_h, \bar{p}_h)$ in $\boldsymbol{V}_h \times M_h$ as long as there is an inexpensive post-processing procedure (or filtering) to compute $\bar{p}_h$ from p_h. If even reduced stability fails, we will see that velocity (also pressure) may or may not converge optimally.

1.3. The Organization of This Thesis

In this work, we study the three finite elements theoretically, and also investigate the numerical performance of the $\mathcal{P}^2$–$\mathcal{P}^1$ element. Each of the three elements has its own character, but they share many common properties. We shall recall some basic knowledge of Stokes equations and present the major tools used in our analysis in the next two chapters, then treat each of the elements afterward. The organization of this thesis and the content of each chapter are as following.

In Chapter 2 we recall some theoretical results on the Stokes equations which shall be used frequently in this thesis. Most of these can be found in Brezzi and Fortin [7] and Girault and Raviart [11]. More specifically, the theorems on the uniqueness, existence, and error estimates of finite element solutions of Stokes equations shall be introduced in this chapter.

Chapter 3 concerns macroelement techniques for verifying the inf–sup condition. The main idea of such techniques (see, e.g., Boland and Nicolaides [2], [3], Stenberg [24], [25], and Brezzi and Fortin [7, § VI.5.3]) is to reduce the stability analysis of a finite element discretization to the analysis

of the stability on macroelements composed of only a few triangles, combined with some minimal global information. Our approach is based on several types of macroelement techniques.

Chapter 4 contains some theoretical results on the $\mathcal{P}^2$–$\mathcal{P}^1$ finite element. The approximation order for this finite element space is 2; that is, the error in the best approximation of $(\boldsymbol{u}, p)$ in $\mathring{\boldsymbol{H}}^1(\Omega) \times L^2(\Omega)$ by functions in $\boldsymbol{V}_h \times P_h$ tends to zero like $O(h^2)$. However, the convergence and stability properties of the $\mathcal{P}^2$–$\mathcal{P}^1$ finite element method depend essentially on the mesh family used.

Based on the analysis of the Fraeijs de Veubeke–Sander element by Ciavaldini and Nedelec [10], Mercier [17] observed that for a triangulation composed of convex quadrilaterals each of which is partitioned into four triangles by its two diagonals, $\boldsymbol{u}_h$ converges to $\boldsymbol{u}$ with optimal order h^2 in H^1. We shall strengthen this result by showing that for such meshes the pair $\boldsymbol{V}_h \times M_h$ is actually stable, and that the subspace M_h gives the same order of approximation as P_h does. The recovery of $\bar{p}_h$ from p_h is quite simple in this case.

A negative result can be deduced from the work of de Boor and Höllig [5]; see also de Boor and Devore [4]. They considered the triangulation of the unit square obtained by subdividing it into equal subsquares and then bisecting each of these by its positively sloped diagonal. They showed that for this mesh family the space of C^1 piecewise cubic polynomials has approximation properties that are one order suboptimal, which is equivalent to suboptimal approximation of $\boldsymbol{u}$ by $\boldsymbol{u}_h$. (The norms considered by de Boor and Höllig are not exactly those pertinent to this discussion. However their argument can be adapted. Cf., Babuška and Suri [1].) It is known that the dimension of N_h is 6 for this diagonal mesh. We explicitly determine a basis for N_h.

For a triangulation of the unit square, which is a mixture of diagonal and crisscross subdivisions, i.e. a partition into equal small squares with each of the squares divided either by its positively sloped diagonal or by both its diagonals, what is the approximation property and reduced stability of the $\mathcal{P}^2$–$\mathcal{P}^1$ element? We know that the element has optimal approximation for both velocity and pressure if the mesh is formed only by crisscross subdivisions; but on the other extreme, the element has only suboptimal approximation for the velocity if the mesh is diagonal. Our main result is that the element is both reduced-stable and optimal after the removal of local spurious pressure modes associated with the singular vertices, as long as the proportion of crisscross subdivisions is not vanishingly small in any part of the domain.

We also show that for some mesh families the $\mathcal{P}^2$–$\mathcal{P}^1$ finite element method is stable, and consequently the velocity and the pressure converge with optimal order.

Chapter 5 continues the investigation of the $\mathcal{P}^2$–$\mathcal{P}^1$ element, mostly based on numerical experiments. In particular we show extensive numerical computations of the inf–sup and reduced inf–sup constants, as well as numerical computations of the finite element solutions. Some of these results serve to verify the theoretical considerations of the previous chapter, but for some cases the finite element solution is more accurate then we are able to explain theoretically.

In Chapter 6 we consider the $\mathcal{P}^3$–$\mathcal{P}^2$ element. Generally, $\mathcal{P}^3$–$\mathcal{P}^2$ element performs better than the $\mathcal{P}^2$–$\mathcal{P}^1$ element, and the results of Chapter 4 carry over to this element. Using ideas similar to those of the proofs in Chapter 4, we show that the $\mathcal{P}^3$–$\mathcal{P}^2$ element is reduced-stable on the irregular crisscross family and as well on the mixed family of crisscross and diagonal subdivisions. The $\mathcal{P}^3$–$\mathcal{P}^2$ element is stable on many mesh configurations, for example on barycentric trisected triangulations.

Chapter 7 is devoted to the $\mathcal{P}^1$–$\mathcal{P}^0$ element. This element is probably the simplest finite element that preserves the incompressibility of fluids. However, this element is not reduced-stable for almost any mesh since the system is over constrained. The best mesh we known of is the crisscross mesh. Even on this mesh $\boldsymbol{V}_h \times M_h$ is unstable and $ch \le \bar{\gamma}_h \le Ch$ with c and C two positive constants independent of h. However, with further analysis, we can show that, on the crisscross mesh, this simplest element provides optimal approximations for the velocity $\boldsymbol{u}$ and the pressure p. We also prove some similar results for a general mesh family of a polygonal domain.

An interesting relation between the stabilities of the quadrilateral element $\mathcal{Q}^1$–$\mathcal{P}^0$ and the $\mathcal{P}^1$–$\mathcal{P}^0$ is also established in this chapter. Because of the relation, if the element $\mathcal{Q}^1$–$\mathcal{P}^0$ is stable on a family of partitions $\mathcal{Q}_h$ for a polygonal domain, then the $\mathcal{P}^1$–$\mathcal{P}^0$ element is reduced-stable on a corresponding mesh family. More precisely, the reduced inf–sup constant is bounded below by a fixed positive number on the triangulations $\mathcal{T}_h$ resulting from dividing each quadrilateral in $\mathcal{Q}_h$ by its two diagonals. Moreover the numerical solution for velocity converges with the optimal rate and the pressure can be recovered by a simple postprocess. We have obtained some theoretical results on the $\mathcal{Q}^1$–$\mathcal{P}^0$ element. Since this element does not preserve the incompressibility condition, we will not discuss these results in this thesis.

Chapter 2

STOKES EQUATIONS AND THEIR FINITE ELEMENT APPROXIMATIONS

In this chapter, we briefly introduce some fundamental concepts and theorems underlying the Stokes equations and their mixed finite element discretization. In Section 1 we discuss the Stokes equations and their weak formulation. In Section 2 we present some abstract approximation results for the mixed formulation of the equations. In Section 3 we recall some basic approximation properties of finite element spaces of piecewise polynomials; these properties will often be used in our analysis. Finally, in Section 4 we give a short introduction to the three finite elements considered in this thesis. All results stated in this chapter are for the Stokes equations with Dirichlet boundary conditions, however they are also valid for the same problem with traction boundary conditions.

2.1. The Stokes Equations and Their Weak Formulation

Consider the Stokes equations

$$\begin{aligned} -\Delta \boldsymbol{u} + \nabla p &= \boldsymbol{f} \quad \text{in } \Omega, \\ \operatorname{div} \boldsymbol{u} &= 0 \quad \text{in } \Omega, \end{aligned} \tag{2.1.1}$$

with either the Dirichlet or traction boundary conditions. Here Ω is a bounded polygonal domain in $\mathbb{R}^2$. The velocity and the pressure of the fluid governed by the equations are denoted by $\boldsymbol{u}$ and p respectively.

As our model problem we consider (2.1.1) with Dirichlet boundary condition. The weak formulation of this problem is

$$\begin{aligned} a(\boldsymbol{u},\boldsymbol{v}) - b(\boldsymbol{v},p) &= (\boldsymbol{f},\boldsymbol{v}), \quad \forall \boldsymbol{v} \in \boldsymbol{V}, \\ b(\boldsymbol{u},q) &= 0, \quad \forall q \in P. \end{aligned} \tag{2.1.2}$$

This is obtained by multiplying the equations of (2.1.1) by $\boldsymbol{v} \in \boldsymbol{V}$ and $q \in P$, integrating them over Ω, and using the Green's formula. Here

$$\begin{aligned} \boldsymbol{V} \times P &:= \mathring{\boldsymbol{H}}^1(\Omega) \times L^2(\Omega), \\ a(\boldsymbol{u},\boldsymbol{v}) &:= \int_\Omega \nabla \boldsymbol{u} : \nabla \boldsymbol{v}, \qquad \text{for any } \ \boldsymbol{u},\boldsymbol{v} \in \boldsymbol{V}, \\ b(\boldsymbol{u},q) &:= \int_\Omega q \operatorname{div} \boldsymbol{u}, \qquad \text{for any } \ \boldsymbol{u} \in \boldsymbol{V}, q \in P, \text{ and} \\ (\boldsymbol{f},\boldsymbol{v}) &:= \int_\Omega \boldsymbol{f} \cdot \boldsymbol{u}, \qquad \text{for any } \ \boldsymbol{f},\boldsymbol{v} \in \boldsymbol{V}. \end{aligned}$$

The formulation (2.1.2) is usually called the mixed formulation of (2.1.1). It is known that finding a solution $(\boldsymbol{u},p) \in \boldsymbol{V} \times P$ of (2.1.1) is equivalent to finding a solution $(\boldsymbol{u},p) \in \boldsymbol{V} \times P$ of (2.1.2).

Obviously, the velocity $\boldsymbol{u} \in \boldsymbol{V}$ is unique and the pressure p is determined only up to an additive constant.

Let

$$N := \{q \in P \mid b(\boldsymbol{v}, q) = 0, \quad \forall \boldsymbol{v} \in \boldsymbol{V}\}$$

denote the kernel of the gradient operator. Let $\boldsymbol{Z}$ denote the space of all divergence-free functions in $\boldsymbol{V}$. Since the divergence of each function in $\boldsymbol{V}$ belongs to P, the space $\boldsymbol{Z}$ can be defined by

$$\boldsymbol{Z} = \{\boldsymbol{v} \in \boldsymbol{V} \mid b(\boldsymbol{v}, q) = 0, \quad \forall q \in P\}.$$

If we choose velocity functions in (2.1.2) from the space $\boldsymbol{Z}$, then the second equation of (2.1.2) is automatically satisfied. Consequently, the solution $\boldsymbol{u}$ of (2.1.2) satisfies

$$a(\boldsymbol{u}, \boldsymbol{v}) = (\boldsymbol{f}, \boldsymbol{v}), \quad \forall \boldsymbol{v} \in \boldsymbol{Z}. \tag{2.1.3}$$

The formulation (2.1.3) is a simpler formulation of the model problem than (2.1.2) in that it results in a much smaller positive definite system. However, finding a discretization of $\boldsymbol{Z}$ is quite hard in practical computations.

2.2. Abstract Approximation Results

We devote this section to the study of solutions of (2.1.2) from a finite dimensional space $\boldsymbol{V}_h \times P_h$. We shall first introduce the main theorem on the approximability of the solutions, then discuss two parallel techniques of checking the inf–sup condition. The results stated in this section can be found in Brezzi and Fortin [7, §II] and Girault and Raviart [11, §II.1.1-3].

Let h denote a discretization parameter (usually the mesh size) tending to zero. For each h let $\boldsymbol{V}_h \subset \boldsymbol{V}$ and $P_h \subset P$ be two finite dimensional spaces. $\boldsymbol{V}_h$ is called the velocity space and P_h the pressure space. The discretization of (2.1.2) based on $\boldsymbol{V}_h \times P_h$ is

$$\begin{aligned} a(\boldsymbol{u}_h, \boldsymbol{v}) - b(\boldsymbol{v}, p_h) &= (\boldsymbol{f}, \boldsymbol{v}), \quad \forall \boldsymbol{v} \in \boldsymbol{V}_h, \\ b(\boldsymbol{u}_h, q) &= 0, \quad \forall q \in P_h. \end{aligned} \tag{2.2.1}$$

The velocity $\boldsymbol{u}_h$ is uniquely determined since $a(\cdot, \cdot)$ corresponds to an elliptic operator, but p_h is not. The algebraic system that results from (2.2.1) is symmetric and indefinite.

As on the continuous level in the previous section, we define a finite dimensional space $\boldsymbol{Z}_h$ corresponding to $\boldsymbol{Z}$ by

$$\boldsymbol{Z}_h = \{\boldsymbol{v} \in \boldsymbol{V}_h \mid b(\boldsymbol{v}, q) = 0, \quad \forall q \in P_h\}.$$

Clearly, $\boldsymbol{Z}_h$ may not be contained in $\boldsymbol{Z}$, i.e., $\boldsymbol{u}_h$ may not satisfy the incompressibility condition. However, solving for $\boldsymbol{u}_h$ from (2.2.1) is equivalent to solving for $\boldsymbol{u}_h \in \boldsymbol{Z}_h$ from

$$a(\boldsymbol{u}_h, \boldsymbol{v}) = (\boldsymbol{f}, \boldsymbol{v}), \quad \forall \boldsymbol{v} \in \boldsymbol{Z}_h. \tag{2.2.2}$$

The uniqueness, existence, and error estimates for the solution of (2.2.1) are established in the following theorem.

Theorem 2.2.1. *Assume that the following conditions hold:*

(1) *There exists a constant $\alpha > 0$ such that*

$$a(\boldsymbol{v}, \boldsymbol{v}) \geq \alpha \|\boldsymbol{v}\|_{1,\Omega}, \forall \boldsymbol{v} \in \boldsymbol{Z}_h; \tag{2.2.3}$$

(2) *there exists a constant $\gamma_h > 0$ such that*

$$\inf_{0 \neq p \in P_h} \sup_{0 \neq \boldsymbol{v} \in \boldsymbol{V}_h} \frac{b(\boldsymbol{v}, q)}{\|\boldsymbol{v}\|_{1,\Omega} \|p\|_{0,\Omega}} = \gamma_h. \tag{2.2.4}$$

Then (2.2.1) *has a unique solution* $(\boldsymbol{u}_h, p_h) \in \boldsymbol{V}_h \times P_h$ *such that*

$$\|\boldsymbol{u}-\boldsymbol{u}_h\|_{1,\Omega} \le \left(1+\frac{\|a\|}{\alpha}\right) \inf_{\boldsymbol{z}\in\boldsymbol{Z}_h} \|\boldsymbol{u}-\boldsymbol{z}\|_{1,\Omega} + \frac{\|b\|}{\alpha} \inf_{q\in P_h} \|p-q\|_{0,\Omega}, \tag{2.2.5}$$

$$\|\boldsymbol{u}-\boldsymbol{u}_h\|_{1,\Omega} \le \left(1+\frac{\|a\|}{\alpha}\right)\left(1+\frac{\|b\|}{\gamma_h}\right) \inf_{\boldsymbol{v}\in\boldsymbol{V}_h} \|\boldsymbol{u}-\boldsymbol{v}\|_{1,\Omega} + \frac{\|b\|}{\alpha} \inf_{q\in P_h} \|p-q\|_{0,\Omega}, \ \textit{and} \tag{2.2.6}$$

$$\|p-p_h\|_{0,\Omega} \le \frac{\|a\|}{\gamma_h}\|\boldsymbol{u}-\boldsymbol{u}_h\|_{1,\Omega} + \left(1+\frac{\|b\|}{\gamma_h}\right) \inf_{q\in P_h} \|p-q\|_{0,\Omega}. \tag{2.2.7}$$

Proof. Because of the condition (2.2.3) and the formulation (2.2.2), there exists a unique $\boldsymbol{u}_h$ which satisfies (2.2.1). The pressure p_h of (2.2.1) must be also unique since if $\tilde{p}_h \in P_h$ $(p_h \neq \tilde{p}_h)$ is another solution for the pressure, then we have

$$b(\boldsymbol{v}, p_h - \tilde{p}_h) = 0, \quad \forall \boldsymbol{v} \in \boldsymbol{V}_h,$$

which obviously violates the condition (2.2.4).

Let $\boldsymbol{z}$ be an arbitrary vector of $\boldsymbol{Z}_h$, then $\boldsymbol{v} = \boldsymbol{u}_h - \boldsymbol{z}$ belongs to $\boldsymbol{Z}_h \subset \boldsymbol{V}_h$ and

$$a(\boldsymbol{v}, \boldsymbol{v}) = (\boldsymbol{f}, \boldsymbol{v}) - a(\boldsymbol{z}, \boldsymbol{v}). \tag{2.2.8}$$

Since $\boldsymbol{v} \in \boldsymbol{V}_h$, from (2.1.2) we have

$$a(\boldsymbol{u}, \boldsymbol{v}) - b(\boldsymbol{v}, p) = (\boldsymbol{f}, \boldsymbol{v}). \tag{2.2.9}$$

Combining (2.2.8) and (2.2.9) we get

$$\begin{aligned} a(\boldsymbol{v}, \boldsymbol{v}) &= a(\boldsymbol{u}-\boldsymbol{z}, \boldsymbol{v}) - b(\boldsymbol{v}, p) \\ &= a(\boldsymbol{u}-\boldsymbol{z}, \boldsymbol{v}) - b(\boldsymbol{v}, p-q). \end{aligned}$$

The $\boldsymbol{Z}_h$-ellipticity of the operator a and the continuity of the operators a and b yield

$$\|\boldsymbol{v}\|_{1,\Omega} \le \frac{\|a\|}{\alpha}\|\boldsymbol{u}-\boldsymbol{z}\|_{1,\Omega} + \frac{\|b\|}{\alpha}\|p-q\|_{0,\Omega}.$$

Therefore we have

$$\|\boldsymbol{u}-\boldsymbol{u}_h\|_{1,\Omega} \le \left(1+\frac{\|a\|}{\alpha}\right)\|\boldsymbol{u}-\boldsymbol{z}\|_{1,\Omega} + \frac{\|b\|}{\alpha}\|p-q\|_{0,\Omega}$$

for any $\boldsymbol{z} \in \boldsymbol{Z}_h$ and $q \in P_h$. This proves (2.2.5).

In order to derive the estimate (2.2.6), we need only prove that

$$\inf_{\boldsymbol{z}\in\boldsymbol{Z}_h} \|\boldsymbol{u}-\boldsymbol{z}\|_{1,\Omega} \le \left(1+\frac{\|b\|}{\gamma_h}\right) \inf_{\boldsymbol{v}\in\boldsymbol{V}_h} \|\boldsymbol{u}-\boldsymbol{v}\|_{1,\Omega}. \tag{2.2.10}$$

Let $\boldsymbol{v}$ be an arbitrary vector in $\boldsymbol{V}_h$. By condition (2.2.4), there exists a unique $\boldsymbol{w}$ in the $\boldsymbol{H}^1$ complement of $\boldsymbol{Z}_h$ (a subspace of $\boldsymbol{V}_h$) such that

$$b(\boldsymbol{w}, q) = b(\boldsymbol{u}-\boldsymbol{v}, q), \quad \forall q \in P_h,$$

and

$$\|\boldsymbol{w}\|_{1,\Omega} \le \frac{1}{\gamma_h} \sup_{q\in P_h} \frac{b(\boldsymbol{u}-\boldsymbol{v},q)}{\|q\|_{0,\Omega}} \le \frac{1}{\gamma_h}\|b\|\|\boldsymbol{u}-\boldsymbol{v}\|_{1,\Omega}.$$

If we set $\boldsymbol{z} = \boldsymbol{w} + \boldsymbol{v}$, we have

$$b(\boldsymbol{z},q) = b(\boldsymbol{u}-\boldsymbol{v},q) + b(\boldsymbol{v},q) = 0, \quad \forall q \in P_h.$$

This shows that $\boldsymbol{z}$ is in $\boldsymbol{Z}_h$. Furthermore,

$$\begin{aligned}\|\boldsymbol{u}-\boldsymbol{z}\|_{1,\Omega} &\le \|\boldsymbol{u}-\boldsymbol{v}\|_{1,\Omega} + \|\boldsymbol{w}\|_{1,\Omega} \\ &\le \left(1+\frac{\|b\|}{\gamma_h}\right)\|\boldsymbol{u}-\boldsymbol{v}\|_{1,\Omega}.\end{aligned}$$

Since $\boldsymbol{v}$ is arbitrary, the above estimates prove (2.2.10).

It remains to estimate $\|p-p_h\|_{0,\Omega}$. From (2.1.2) and (2.2.1) we are able to derive

$$b(\boldsymbol{v},p_h-q) = a(\boldsymbol{u}-\boldsymbol{u}_h,\boldsymbol{v}) + b(\boldsymbol{v},p-q), \quad \forall \boldsymbol{v}\in \boldsymbol{V}_h, \quad \forall q \in P_h.$$

Therefore the condition (2.2.4) ensures

$$\begin{aligned}\|p_h-q\|_{0,\Omega} &\le \frac{1}{\gamma_h}\sup_{\boldsymbol{v}\in\boldsymbol{V}_h}\frac{1}{\|\boldsymbol{v}\|_{1,\Omega}}\{a(\boldsymbol{u}-\boldsymbol{u}_h,\boldsymbol{v}) + b(\boldsymbol{v},p-q)\} \\ &\le \frac{1}{\gamma_h}\{\|a\|\|\boldsymbol{u}-\boldsymbol{u}_h\|_{1,\Omega} + \|b\|\|p-q\|_{0,\Omega}\}.\end{aligned}$$

Hence

$$\|p-p_h\|_{0,\Omega} \le \frac{\|a\|}{\gamma_h}\|\boldsymbol{u}-\boldsymbol{u}_h\|_{1,\Omega} + \left(1+\frac{\|b\|}{\gamma_h}\right)\inf_{q\in P_h}\|p-q\|_{0,\Omega}. \quad \square$$

Remark 2.2.1. *Under the assumption* (2.2.3)*, we have*

$$\|\boldsymbol{u}-\boldsymbol{u}_h\|_{1,\Omega} \le \left(1+\frac{\|a\|}{\alpha}\right)\inf_{\boldsymbol{z}\in\boldsymbol{Z}_h}\|\boldsymbol{u}-\boldsymbol{z}\|_{1,\Omega}. \tag{2.2.11}$$

Moreover, under the assumptions (2.2.3) *and* (2.2.4)*, if $\boldsymbol{Z}_h$ is contained in $\boldsymbol{Z}$, then we have following estimate:*

$$\|\boldsymbol{u}-\boldsymbol{u}_h\|_{1,\Omega} \le \left(1+\frac{\|a\|}{\alpha}\right)\left(1+\frac{\|b\|}{\gamma_h}\right)\inf_{\boldsymbol{v}\in\boldsymbol{V}_h}\|\boldsymbol{u}-\boldsymbol{v}\|_{1,\Omega}. \tag{2.2.12}$$

The condition (2.2.4) in the above theorem, called the Brezzi's condition (or LBB condition, or inf–sup condition), plays a crucial role in the uniqueness and error estimate for the solution $(\boldsymbol{u}_h,p_h)$. From the estimates (2.2.6) and (2.2.7), we can see that the estimate for $\|p-p_h\|_{0,\Omega}$ depends on $1/\gamma_h^2$, but the one for $\|\boldsymbol{u}-\boldsymbol{u}_h\|_{1,\Omega}$ only depends on $1/\gamma_h$ (γ_h is called the inf–sup constant). Therefore, the inf–sup constant affects the error estimate for the pressure much more than it does for the velocity if γ_h is small. The inf–sup condition is a measure of the compatibility between the velocity space $\boldsymbol{V}_h$ and the pressure space P_h. If P_h is too large, $\gamma_h = 0$, and if P_h is too small the rates of convergence for both velocity and pressure fall. The finite dimensional spaces $\boldsymbol{V}_h$ and P_h have to be carefully chosen such that γ_h does not tend to zero when h goes to zero, or at least not too quickly. Checking whether the inf–sup condition holds is a primary step in analyzing the approximation properties of a finite element.

The following theorem due to Fortin offers a criterion for checking the inf–sup condition.

Theorem 2.2.2. *The inf–sup condition holds for $\boldsymbol{V}_h \times P_h$ if and only if there exists a linear operator $\Pi_h : \boldsymbol{V} \to \boldsymbol{V}_h$ satisfying*

$$b(\boldsymbol{v} - \Pi_h \boldsymbol{v}, q) = 0, \quad \forall q \in P_h, \quad \forall \boldsymbol{v} \in \boldsymbol{V}, \tag{2.2.13}$$

and

$$\|\Pi_h \boldsymbol{v}\|_{1,\Omega} \leq C \|\boldsymbol{v}\|_{1,\Omega}, \quad \forall \boldsymbol{v} \in \boldsymbol{V}, \tag{2.2.14}$$

with a constant $C > 0$.

Proof. Suppose such an operator Π_h exists. From (2.2.13) we conclude

$$\sup_{\boldsymbol{v} \in \boldsymbol{V}_h} \frac{b(\boldsymbol{v}, q)}{\|\boldsymbol{v}\|_{1,\Omega}} \geq \sup_{\boldsymbol{v} \in \boldsymbol{V}} \frac{b(\Pi_h \boldsymbol{v}, q)}{\|\Pi_h \boldsymbol{v}\|_{1,\Omega}} = \sup_{\boldsymbol{v} \in \boldsymbol{V}} \frac{b(\boldsymbol{v}, q)}{\|\Pi_h \boldsymbol{v}\|_{1,\Omega}},$$

for all $q \in P_h$. Since the inf–sup condition holds on the continuous level, (2.2.14) implies

$$\sup_{\boldsymbol{v} \in \boldsymbol{V}} \frac{b(\boldsymbol{v}, q)}{\|\Pi_h \boldsymbol{v}\|_{1,\Omega}} \geq C \sup_{\boldsymbol{v} \in \boldsymbol{V}} \frac{b(\boldsymbol{v}, q)}{\|\boldsymbol{v}\|_{1,\Omega}} \geq C \|q\|_{0,\Omega}.$$

Therefore (2.2.4) follows with $\gamma_h \geq C$.

Conversely, suppose (2.2.4) holds with a constant $\gamma_h > 0$. For each $\boldsymbol{v} \in \boldsymbol{V}$ there exists a unique vector $\Pi_h \boldsymbol{v} \in \boldsymbol{Z}_h^{\perp}$ such that

$$b(\Pi_h \boldsymbol{v}, q) = b(\boldsymbol{v}, q), \quad \forall q \in P_h,$$

and

$$\|\Pi_h \boldsymbol{v}\|_{1,\Omega} \leq \frac{1}{\gamma_h} \sup_{q \in P_h} \frac{b(\boldsymbol{v}, q)}{\|q\|_{0,\Omega}} \leq \frac{1}{\gamma_h} \|b\| \|\boldsymbol{v}\|_{1,\Omega}.$$

Clearly, Π_h is a linear operator and satisfies (2.2.14). □

Another useful way to state the inf–sup condition (2.2.4) is given in the following theorem.

Theorem 2.2.3. *The inf–sup condition* (2.2.4) *is equivalent to the condition: for each $q \in P_h$ there exists a $\boldsymbol{v} \in \boldsymbol{V}_h$ such that*

$$b(\boldsymbol{v}, q) = \|q\|_{0,\Omega}^2, \tag{2.2.15}$$

$$\|\boldsymbol{v}\|_{1,\Omega} \leq \frac{1}{\gamma_h} \|q\|_{0,\Omega}. \tag{2.2.16}$$

Proof. If the inf–sup condition (2.2.4) holds, then for any $q \in P_h$ there exists a $\bar{\boldsymbol{v}} \in \boldsymbol{V}_h$ such that

$$\frac{b(\bar{\boldsymbol{v}}, q)}{\|\bar{\boldsymbol{v}}\|_{1,\Omega}} \geq \gamma_h \|q\|_{0,\Omega}.$$

Let $\boldsymbol{v}$ be a multiple of $\bar{\boldsymbol{v}}$ such that

$$b(\boldsymbol{v}, q) = \|q\|_{0,\Omega}^2.$$

Then

$$\|\boldsymbol{v}\|_{1,\Omega} \leq \frac{1}{\gamma_h} \frac{b(\boldsymbol{v}, q)}{\|q\|_{0,\Omega}} \leq \frac{1}{\gamma_h} \|q\|_{0,\Omega}.$$

The proof for the other direction is trivial. □

This result is also valid on the continuous level.

The above two theorems are useful in checking the inf–sup condition for mixed finite element discretizations. The former is popularly used in stability analysis of finite element methods, while the latter is frequently employed in developing macroelement techniques.

2.3. Approximation Properties of Piecewise Polynomials

If we know the approximation properties of the finite dimensional spaces $\boldsymbol{V}_h$ and P_h, the right hand sides of the estimates (2.2.5)—(2.2.7) can be simplified. In this section, we present some approximation results for finite element spaces of piecewise polynomials.

Let Ω be a polygonal domain and $\mathcal{T}_h$ be a triangulation of Ω such that $\Omega = \bigcup_{\tau\in\mathcal{T}_h} \tau$. For any triangle $\tau \in \mathcal{T}_h$, we define

$$h_\tau = \text{the diameter of } \tau \text{ (the longest side of } \tau),$$
$$\rho_\tau = \text{the diameter of the circle inscribed in } \tau,$$

and set $h = \max_{\tau\in\mathcal{T}_h} h_\tau$. A family of triangulations of Ω is said to be quasi-uniform if there is a positive number β independent of h such that the quasi-uniformality constant

$$\beta_h := \frac{h}{\min_{\tau\in\mathcal{T}_h} h_\tau} \le \beta, \tag{2.3.1}$$

for every triangulation $\mathcal{T}_h$ in the family. A family of triangulations is said to be regular if there is a positive number θ independent of h such that

$$\frac{\rho_\tau}{h_\tau} \ge \theta, \tag{2.3.2}$$

for every triangle $\tau \in \mathcal{T}_h$ and for every triangulation $\mathcal{T}_h$ in the family (The condition (2.3.2) is also called the shape constraint). Roughly speaking, this condition means that no angle of any triangle in $\mathcal{T}_h$ is too small or too big.

On a triangulation $\mathcal{T}_h$ of Ω, we define finite element spaces

$$M_m^l(\mathcal{T}_h) = \{f \in C^m(\Omega) \mid f|_\tau \text{ is a polynomial with degree} \le l \ , \forall \tau \in \mathcal{T}_h\},$$
$$\mathring{M}_m^l(\mathcal{T}_h) = \{f \in M_m^l(\mathcal{T}_h) \mid f|_{\partial\Omega} = 0\},$$

where $l \ge 0$ and $m \ge 0$ are integers. $M_{-1}^l(\mathcal{T}_h)$ denotes the space of all discontinuous piecewise polynomials with degree $\le l$.

The following results can be found in Ciarlet [9, §3] and Johnson [12, §4].

Theorem 2.3.1. *Assume that the triangulation $\mathcal{T}_h$ is regular. If function $u \in H^{l+1}(\Omega)$, then*

$$\inf_{v\in M_0^l(\mathcal{T}_h)} \|u - v\|_{r,\Omega} \le Ch^{l+1-r}\|u\|_{l+1,\Omega},$$
$$\inf_{v\in M_{-1}^l(\mathcal{T}_h)} \|u - v\|_{0,\Omega} \le Ch^{l+1}\|u\|_{l+1,\Omega},$$

where r is 0 or 1 and l is a nonnegative integer. Similarly, if $u \in \mathring{H}^{l+1}(\Omega)$, we have

$$\inf_{v\in \mathring{M}_0^l(\mathcal{T}_h)} \|u - v\|_{r,\Omega} \le Ch^{l+1-r}\|u\|_{l+1,\Omega},$$

for $r = 0$ or 1. Here C is a generic constant which depends only on θ, the degree l, and the domain Ω.

For the elements considered in this thesis, the best error estimate, also called the optimal estimate, of $\|\boldsymbol{u} - \boldsymbol{u}_h\|_{1,\Omega} + \|p - p_h\|_{0,\Omega}$ is $O(h^n)$ for $\mathcal{P}^n$–$\mathcal{P}^{n-1}$, $n = 1, 2, 3$.

For convenience, we denote $M_m^l(\mathcal{T}_h) \times M_m^l(\mathcal{T}_h)$ by $\boldsymbol{M}_m^l(\mathcal{T}_h)$ in this thesis. Most of the time we use M_m^l to denote $M_m^l(\mathcal{T}_h)$.

2.4. $\mathcal{P}^n$–$\mathcal{P}^{n-1}$ Elements for Stokes Equations

In this section, we will define the elements $\mathcal{P}^n$–$\mathcal{P}^{n-1}$ for $n = 1, 2, 3$, and discuss their stability or reduced stability. The stability and performance of these elements depend on the mesh configurations in most of the cases.

The mixed finite elements $\mathcal{P}^n$–$\mathcal{P}^{n-1}$ are defined as

$$\boldsymbol{V}_h = \mathring{\boldsymbol{M}}_0^n \text{ (or } \boldsymbol{M}_0^n) \quad \text{and} \quad P_h = M_{-1}^{n-1},$$

for $n = 1, 2, 3$. For $\mathcal{P}^n$–$\mathcal{P}^{n-1}$ elements the degrees of freedom in each triangle are distributed as shown in Figure 2.1. For example, any velocity function for the $\mathcal{P}^2$–$\mathcal{P}^1$ element is a continuous piecewise quadratic polynomial which is determined on each triangle by its values at the three vertices and the three middle points of the edges of the triangle; any pressure function for the $\mathcal{P}^2$–$\mathcal{P}^1$ element is a discontinuous piecewise linear polynomial which is determined on each triangle by its values at three interior points of the triangle.

Analogous to the continuous level, we define

$$\begin{aligned}
\hat{P}_h &= \{q \in P_h \mid \int_\Omega q = 0\}, \\
N_h &= \{q \in P_h \mid b(\boldsymbol{v}, q) = 0, \quad \forall \boldsymbol{v} \in \boldsymbol{V}_h\}, \\
\boldsymbol{Z}_h &= \{\boldsymbol{v} \in \boldsymbol{V} \mid b(\boldsymbol{v}, q) = 0, \quad \forall q \in P_h\}, \\
M_h &= \text{ the } L^2 \text{ orthogonal complement of } N_h \text{ in } P_h.
\end{aligned} \tag{2.4.1}$$

Here M_h is called the reduced pressure space of P_h.

Due to the finite element discretization, N_h may contain some nonconstant functions. For many meshes this happens for the three finite elements defined above and it causes a lot of trouble in the analysis.

Since the divergence of any function in $\boldsymbol{V}_h$ is in P_h, $\boldsymbol{Z}_h$ is a subspace of $\boldsymbol{Z}$ for these elements. Namely, all these three elements preserve the incompressibility condition of incompressible flows.

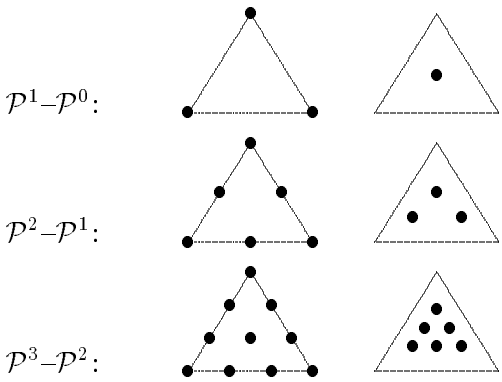

Figure 2.1. $\mathcal{P}^n$–$\mathcal{P}^{n-1}$ **elements.**

In order to study $\boldsymbol{V}_h \times \hat{P}_h$ and $\boldsymbol{V}_h \times M_h$, we consider inf–sup constant γ_h and define the reduced inf–sup constant

$$\bar{\gamma}_h = \inf_{0 \neq p \in M_h} \sup_{0 \neq \boldsymbol{v} \in \boldsymbol{V}_h} \frac{b(\boldsymbol{v}, q)}{\|\boldsymbol{v}\|_{1,\Omega} \|p\|_{0,\Omega}}.$$

It is clear that $\bar{\gamma}_h$ is always positive, $\gamma_h = \bar{\gamma}_h$ if and only if $N_h = N$, and $\gamma_h = 0$ if and only if N_h contains some nonconstant functions.

A finite element method is said to be stable (resp. reduced-stable) on a mesh family of Ω if there is a fixed positive lower bound for all the inf–sup constants γ_h (resp. $\bar{\gamma}_h$).

The solution $(\boldsymbol{u}_h, p_h) \in \boldsymbol{V}_h \times P_h$ of

$$\begin{aligned} a(\boldsymbol{u}_h, \boldsymbol{v}) - b(\boldsymbol{v}, p_h) &= (\boldsymbol{f}, \boldsymbol{v}), \quad \forall \boldsymbol{v} \in \boldsymbol{V}_h, \\ b(\boldsymbol{u}_h, q) &= 0, \quad \forall q \in P_h, \end{aligned} \tag{2.4.2}$$

and the solution $(\bar{\boldsymbol{u}}_h, \bar{p}_h) \in \boldsymbol{V}_h \times M_h$ of

$$\begin{aligned} a(\bar{\boldsymbol{u}}_h, \boldsymbol{v}) - b(\boldsymbol{v}, \bar{p}_h) &= (\boldsymbol{f}, \boldsymbol{v}), \quad \forall \boldsymbol{v} \in \boldsymbol{V}_h, \\ b(\bar{\boldsymbol{u}}_h, q) &= 0, \quad \forall q \in M_h, \end{aligned} \tag{2.4.3}$$

satisfy the relations

$$\boldsymbol{u}_h = \bar{\boldsymbol{u}}_h \quad \text{and} \quad p_h / N_h = \bar{p}_h.$$

Here p_h is determined only up to addition of a constant of N_h and p_h/N_h denotes the uniquely determined part of p_h in $N_h^{\perp}$. The convergence of $(\boldsymbol{u}_h, p_h)$ could be analyzed by studying the reduced stability and the approximation properties of the space $\boldsymbol{V}_h \times M_h$ if $\gamma_h = 0$. However, the analysis is usually difficult because of two reasons: first, to check the reduced stability is not easy and second, the approximation properties of M_h are not always known and may be different from those of P_h.

Chapter 3

TECHNIQUES FOR CHECKING THE INF–SUP CONDITION

A major part in analyzing any mixed finite element method for the Stokes equations is to check the stability of the element. In this thesis the main technique used to check the stability of the three finite elements is the use of macroelements to localize the stability condition. Namely, the stability is tested by checking local stabilities and a relatively simple global stability. Many variations of the macroelement technique have been introduced; see for example, Boland and Nicolaides [2] and [3], Stenberg [24] and [25], and Brezzi and Fortin [7, §VI.5.3]. In this chapter, we present some different versions and some lemmas to justify them. First we shall state two results about the macroelement technique, one for the case of macroelement partitions, and the other one for the coverings by overlapping macroelements. Secondly we shall introduce a criterion for checking the inf–sup condition by testing subspaces of the velocity and pressure spaces. Finally we provide some technical lemmas for checking the local inf–sup condition.

In this chapter, we consider a finite element space $\boldsymbol{V}_h \times P_h$ for $h > 0$ with $\boldsymbol{V}_h \subset \mathring{\boldsymbol{H}}^1(\Omega)$ (the velocity space) and $P_h \subset L^2(\Omega)$ (the pressure space) over a triangulation $\mathcal{T}_h$ of a polygonal domain Ω. All the related definitions, like N_h, M_h, $\boldsymbol{Z}_h$, etc., are defined as in Section 2.4.

3.1. Some Concepts about Macroelements

Given a triangulation $\mathcal{T}_h$ of a polygonal domain Ω, a macroelement with respect to $\mathcal{T}_h$ is a polygonal region U formed by some triangles in $\mathcal{T}_h$. The triangles of $\mathcal{T}_h$, which are contained in U form a triangulation of U, denoted by $\mathcal{T}_h^U$. A macroelement covering is a covering of Ω by macroelements. Such a covering is called a macroelement partition if the intersection of a pair of distinct, nondisjoint macroelements is either a single vertex of the triangulation $\mathcal{T}_h$ or a connected set consisting of some edges of the triangulation. Usually we denote a macroelement partition or covering by $\mathcal{U}_h$.

For a macroelement U we define localizations to U of the finite element spaces $\boldsymbol{V}_h$, P_h, N_h, and M_h (see (2.4.1)) as follows:

$$
\begin{aligned}
\boldsymbol{V}_h^U &= \left\{ \boldsymbol{v} \in \boldsymbol{V}_h \;\middle|\; \operatorname{spt} \boldsymbol{v} \subset U \right\}, \\
P_h^U &= \left\{ \chi^U p \;\middle|\; p \in P_h \right\}, \\
N_h^U &= \left\{ p \in P_h^U \;\middle|\; b(\boldsymbol{v}, p) = 0 \quad \forall \boldsymbol{v} \in \boldsymbol{V}_h^U \right\}, \\
M_h^U &= \text{ the } L^2\text{-orthogonal complement of } N_h^U \text{ in } P_h^U.
\end{aligned}
$$

Here χ^U denotes the characteristic function of U and $\operatorname{spt} \boldsymbol{v}$ is the support of $\boldsymbol{v}$.

Given a macroelement covering $\mathcal{U}_h$ of Ω, for any $e \in \mathcal{E}_h$, the set of edges of triangles in $\mathcal{T}_h$, we define L_e to be the number of macroelements in $\mathcal{U}_h$ that contain e in their interior. The covering

is said to possess the overlap property if $L_e \geq 1$ for all edges e of $\mathring{\mathcal{E}}_h$, which is the set of all the interior edges in $\mathcal{T}_h$. The quantity $\max_e L_e$ is called the covering constant of $\mathcal{U}_h$.

3.2. Macroelement Partition Theorem

This section deals with the macroelement partition theorem. The macroelement partition theorem is based on local stabilities over macroelements and the stability of a special element over the $\mathcal{T}_h$. It is a useful tool to check the inf–sup condition of a mixed finite element.

Theorem 3.2.1 (Macroelement partition theorem). *Let $\mathcal{U}_h$ be a macroelement partition of Ω with respect to some triangulation $\mathcal{T}_h$. Let $\boldsymbol{V}_h \times P_h$ be a finite element defined on $\mathcal{T}_h$. We define*

$$\bar{\gamma}_h^U = \inf_{0 \neq p \in M_h^U} \sup_{0 \neq \boldsymbol{v} \in \boldsymbol{V}_h^U} \frac{b(\boldsymbol{v}, p)}{\|\boldsymbol{v}\|_{1,\Omega} \|p\|_{0,\Omega}}, \tag{3.2.1}$$

for each $U \in \mathcal{U}_h$, and

$$\beta_h = \inf_{0 \neq p \in Q_h} \sup_{0 \neq v \in \boldsymbol{V}_h} \frac{b(\boldsymbol{v}, p)}{\|\boldsymbol{v}\|_{1,\Omega} \|p\|_{0,\Omega}}.$$

Here

$$Q_h := \{ q \in \sum_{U \in \mathcal{U}_h} N_h^U \mid \int_\Omega qr = 0 \quad \forall r \in N_h \}. \tag{3.2.2}$$

If $\beta_h > 0$, then the reduced inf–sup constant $\bar{\gamma}_h$ is strictly positive. Moreover, if α is a positive lower bound for β_h and $\bar{\gamma}_h^U$ for all U, then $\bar{\gamma}_h$ can be bounded below by a positive constant depending only on α.

Proof. Assume α is a positive lower bound for all γ_h^U and β_h. Since $\chi^U P_h = N_h^U + M_h^U$, for any $q \in M_h$ and $U \in \mathcal{U}_h$ we have

$$\chi^U q = q_1^U + q_2^U,$$

for some q_1^U contained in N_h^U and q_2^U contained M_h^U. Since q_2^U is orthogonal to N_h^U and $\chi^U N_h$ is contained in N_h^U, we have $q_2^U \perp N_h$.

Putting

$$q_i := \sum_{U \in \mathcal{U}_h} q_i^U \quad \text{for } i = 1, 2,$$

we have a decomposition for q: $q = q_1 + q_2$. Here $\int_\Omega q_2 r = 0$ for all $r \in N_h$. Therefore, $\int_\Omega q_1 r = \int_\Omega (q - q_2) r = 0$ for all $r \in N_h$, so $q_1 \in Q_h$. Moreover, the following hold:

$$\begin{aligned}
\int_\Omega q_1 q_2 &= 0, \\
\|q\|_{0,\Omega}^2 &= \|q_1\|_{0,\Omega}^2 + \|q_2\|_{0,\Omega}^2, \\
\|q_1\|_{0,\Omega}^2 &= \sum_{U \in \mathcal{U}_h} \|q_1^U\|_{0,U}^2, \\
\|q_2\|_{0,\Omega}^2 &= \sum_{U \in \mathcal{U}_h} \|q_2^U\|_{0,U}^2.
\end{aligned}$$

By Theorem 2.2.3, there exists a function $\boldsymbol{v}_1 \in \boldsymbol{V}_h$ such that

$$b(\boldsymbol{v}_1, q_1) = \|q_1\|_{0,\Omega}^2, \quad \text{and} \quad \|\boldsymbol{v}_1\|_{1,\Omega} \leq \frac{1}{\beta_h} \|q_1\|_{0,\Omega}.$$

Similarly, for each U there is a function $\boldsymbol{v}^U \in \boldsymbol{V}_h^U$ such that

$$b(\boldsymbol{v}^U, q_2^U) = \|q_2^U\|_{0,U}^2, \quad \text{and} \quad \|\boldsymbol{v}^U\|_{1,\Omega} \le \frac{1}{\alpha}\|q_2^U\|_{0,U}.$$

Setting

$$\boldsymbol{v}_2 = \sum_{U \in \mathcal{U}_h} \boldsymbol{v}^U,$$

we have

$$b(\boldsymbol{v}_2, q_2) = \|q_2\|_{0,\Omega}^2, \quad \text{and} \quad \|\boldsymbol{v}_2\|_{1,\Omega} \le \frac{1}{\alpha}\|q_2\|_{0,\Omega}.$$

Put $\boldsymbol{v} = \lambda \boldsymbol{v}_1 + \boldsymbol{v}_2$, where $\lambda > 0$. We get

$$\begin{aligned}
b(\boldsymbol{v}, q) &= b(\lambda \boldsymbol{v}_1 + \boldsymbol{v}_2, q_1 + q_2) \\
&= \lambda b(\boldsymbol{v}_1, q_1) + b(\boldsymbol{v}_2, q_2) + \lambda b(\boldsymbol{v}_1, q_2) \\
&= \lambda \|q_1\|_{0,\Omega}^2 + \|q_2\|_{0,\Omega}^2 + \lambda b(\boldsymbol{v}_1, q_2) \\
&\ge \lambda \|q_1\|_{0,\Omega}^2 + \|q_2\|_{0,\Omega}^2 - \frac{\sqrt{2}\lambda}{\beta_h}\|q_1\|_{0,\Omega}\|q_2\|_{0,\Omega} \\
&\ge \lambda \|q_1\|_{0,\Omega}^2 + \|q_2\|_{0,\Omega}^2 - \frac{\sqrt{2}\lambda}{\beta_h}(\epsilon\|q_1\|_{0,\Omega}^2 + \frac{1}{4\epsilon}\|q_2\|_{0,\Omega}^2) \\
&\ge \lambda(1 - \frac{\sqrt{2}\epsilon}{\beta_h})\|q_1\|_{0,\Omega}^2 + (1 - \frac{\sqrt{2}\lambda}{4\epsilon\beta_h})\|q_2\|_{0,\Omega}^2,
\end{aligned}$$

for any $\epsilon > 0$ and $\lambda > 0$. The special choice $\epsilon = \beta_h/(2\sqrt{2})$ and $\lambda = \beta_h^2/2$ gives

$$b(\boldsymbol{v}, q) \ge \frac{\beta_h^2}{4}\|q_1\|_{0,\Omega}^2 + \frac{1}{2}\|q_2\|_{0,\Omega}^2 \ge \min(\frac{\beta_h^2}{4}, \frac{1}{2})\|q\|_{0,\Omega}^2. \tag{3.2.3}$$

On the other hand,

$$\begin{aligned}
\|\boldsymbol{v}\|_{1,\Omega} \le& \lambda\|\boldsymbol{v}_1\|_{1,\Omega} + \|\boldsymbol{v}_2\|_{1,\Omega} \\
=& \frac{\beta_h^2}{2}\|\boldsymbol{v}_1\|_{1,\Omega} + \|\boldsymbol{v}_2\|_{1,\Omega} \\
\le& \frac{\beta_h}{2}\|q_1\|_{0,\Omega} + \frac{1}{\alpha}\|q_2\|_{0,\Omega} \\
\le& \max(\frac{\beta_h}{2}, \frac{1}{\alpha})(\|q_1\|_{0,\Omega} + \|q_2\|_{0,\Omega}) \\
\le& \sqrt{2}\max(\frac{\beta_h}{2}, \frac{1}{\alpha})\|q\|_{0,\Omega}.
\end{aligned} \tag{3.2.4}$$

Now, (3.2.3) and (3.2.4) combine to give

$$\sup_{0 \ne \boldsymbol{v} \in \boldsymbol{V}_h} \frac{b(\boldsymbol{v}, p)}{\|\boldsymbol{v}\|_{1,\Omega}\|p\|_{0,\Omega}} \ge C, \forall p \in M_h,$$

where C is dependent on α and β_h. $\square$

Remark 3.4.1. *If $\chi^U P_h \subset P_h$ for all $U \in \mathcal{U}_h$, then* (3.2.2) *in the above theorem is equivalent to*

$$Q_h := M_h \bigcap \sum_{U \in \mathcal{U}_h} N_h^U. \tag{3.2.5}$$

This can be seen from the above proof. Since q_2^U is orthogonal to N_h^U and $\chi^U N_h$ is contained in N_h^U, q_2^U is orthogonal to $\chi^U N_h$. That is, $q_2^U \in \chi^U P_h \subset P_h$ is orthogonal to N_h. therefore, we have $q_2^U \in M_h$. In particular, q_2 is in M_h and then, $q_1 = q - q_2$ is in $M_h \cap \Sigma_{U \in \mathcal{U}_h} N_h^U$. Since all the $\mathcal{P}^n$–$\mathcal{P}^{n-1}$ elements have discontinous pressure space, we use (3.2.5) *instead of* (3.2.2) *sometimes in this thesis.*

There are two major concerns regarding the application of this theorem. The first is whether there exists a common positive lower bound for all γ_h^U, and the second is how to handle the stability of the composite element $\boldsymbol{V}_h \times Q_h$. The first question can be answered easily if we only consider special meshes (for example if all the macroelements in $\mathcal{U}_h$ are congruent). However, the second question may not be simple if $\dim N_h^U > 1$. All these issues will be addressed in later sections.

3.3. Macroelement Covering Theorem

In order to present the result on overlapping macroelement coverings we need to assume an approximation property of the velocity space $\boldsymbol{V}_h$: For each $\boldsymbol{w} \in \mathring{\boldsymbol{H}}^1(\Omega)$ there exists a function $\boldsymbol{w}_h \in \boldsymbol{V}_h$ such that

$$\sum_{\tau \in \mathcal{T}_h} h_\tau^{-2} \|\boldsymbol{w} - \boldsymbol{w}_h\|_{0,\tau}^2 + \sum_{e \in \mathcal{E}_h} h_e^{-1} \|\boldsymbol{w} - \boldsymbol{w}_h\|_{0,e}^2 + \|\boldsymbol{w}_h\|_{1,\Omega}^2 \le C \|\boldsymbol{w}\|_{1,\Omega}^2, \tag{3.3.1}$$

where h_τ is the diameter of τ, h_e is the length of e, and C is a positive number independent of h. This holds, for example as long as $\mathring{\boldsymbol{M}}_0^1 \subset \boldsymbol{V}_h$ (Scott and Zhang [23]).

The covering theorem is more flexible than the partition theorem in terms of the choice of macroelements, and therefore more arbitrary triangulations can be treated by using this theorem.

Theorem 3.3.1 (Macroelement covering theorem). *Let $\mathcal{U}_h$ be a macroelement covering of a quasi-uniform and regular triangulation $\mathcal{T}_h$ satisfying the overlap property. For each $U \in \mathcal{U}_h$ define $\bar{\gamma}_h^U$ by* (3.2.1). *Assume that $\boldsymbol{V}_h$ satisfies* (3.3.1) *and*

$$\chi^U p \in M_h^U + \mathbb{R}\chi^U, \quad \forall p \in M_h. \tag{3.3.2}$$

Then the reduced inf–sup constant $\bar{\gamma}_h$ is strictly positive. Moreover, if α is a positive lower bound for the $\bar{\gamma}_h^U$, then $\bar{\gamma}_h$ can be bounded below by a positive constant depending only on α and the covering constant for $\mathcal{U}_h$.

Proof. By (3.3.2), any $p \in M_h$ can be decomposed as

$$\chi^U p = p_1^U + p_2^U,$$

on each $U \in \mathcal{U}_h$ $p_1^U \in \mathbb{R}\chi^U$, $p_2^U \in M_h^U$.

On any macroelement U we define a seminorm over P_h^U by

$$|p|_U^2 := \sum_{\tau \in \mathcal{T}_h^U} h_\tau^2 \|\nabla p\|_{0,\tau}^2 + \sum_{e \in \mathring{\mathcal{E}}_h^U} h_e \int_e |[p]_e|^2 ds,$$

for each $p \in P_h^U$. Globally we define

$$\|p\|_{h,\Omega}^2 := \sum_{\tau \in \mathcal{T}_h} h_\tau^2 \|\nabla p\|_{0,\tau}^2 + \sum_{e \in \mathring{\mathcal{E}}_h} h_e \int_e |[p]_e|^2 ds.$$

Here $\mathring{\mathcal{E}}_h^U$ is the set of interior edges in $\mathcal{T}_h^U$ and $[p]_e$ is the jump of p across the edge e. By using the inverse inequality, it is easy to show that

$$\|p\|_{0,U}^2 \geq C|p|_U^2,$$

with constant C independent of h. Therefore the local inf–sup constant on each macroelement is also bounded below by a multiple of α in terms of the seminorm. This implies that for each p_2^U there exists a function $\boldsymbol{v}^U \in \boldsymbol{V}_h^U$ such that

$$b(\boldsymbol{v}^U, p_2^U) \geq |p_2^U|_U^2 \text{ and } \|\boldsymbol{v}^U\|_{1,U} \leq \frac{C}{\alpha}|p_2^U|_U.$$

Namely

$$b(\boldsymbol{v}^U, p) \geq |p|_U^2 \text{ and } \|\boldsymbol{v}^U\|_{1,U} \leq \frac{C}{\alpha}|p|_U.$$

By setting $\boldsymbol{v} = \Sigma_{U \in \mathcal{U}_h} \boldsymbol{v}^U$, we have

$$b(\boldsymbol{v}, p) = \sum_{U \in \mathcal{U}_h} b(\boldsymbol{v}^U, p) \geq \sum_{U \in \mathcal{U}_h} |p|_U^2 \geq C_1 \|p\|_{h,\Omega}^2, \tag{3.3.3}$$

with C_1 depending on the covering constant and α. Moreover

$$\|\boldsymbol{v}\|_{1,\Omega} \leq \sum_{U \in \mathcal{U}_h} \|\boldsymbol{v}^U\|_{1,U} \leq \frac{C}{\alpha} \sum_{U \in \mathcal{U}_h} |p|_U \leq C_2 \|p\|_{h,\Omega}, \tag{3.3.4}$$

where C_2 depends only on α and the covering constant. Inequalities (3.3.3) and (3.3.4) together imply

$$\sup_{0 \neq \boldsymbol{v} \in \boldsymbol{V}_h} \frac{b(\boldsymbol{v}, p)}{\|\boldsymbol{v}\|_{1,\Omega}} \geq C_3 \|p\|_{h,\Omega} = \|p\|_{0,\Omega} \big(C_3 \frac{\|p\|_{h,\Omega}}{\|p\|_{0,\Omega}} \big),$$

where C_3 depends only on the covering constant and α.

Since $p \in M_h \subset \hat{L}^2(\Omega)$, there is a function $\boldsymbol{w} \in \mathring{\boldsymbol{H}}^1(\Omega)$ such that

$$b(\boldsymbol{w}, p) \geq C_4 \|p\|_{0,\Omega}^2 \text{ and } \|\boldsymbol{w}\|_{1,\Omega} \leq \|p\|_{0,\Omega}.$$

By the second assumption, for the function $\boldsymbol{w}$ there is a $\boldsymbol{w}_h \in \boldsymbol{V}_h$ such that the condition (3.3.1) holds. Therefore, we have

$$\begin{aligned}
b(\boldsymbol{w}_h, p) &= b(\boldsymbol{w}_h - \boldsymbol{w}, p) + b(\boldsymbol{w}, p) \\
&\geq b(\boldsymbol{w}_h - \boldsymbol{w}, p) + C_4 \|p\|_{0,\Omega}^2 \\
&\geq \sum_{\tau \in \mathcal{T}_h} \int_\tau (\boldsymbol{w}_h - \boldsymbol{w}) \cdot \nabla p + \sum_{e \in \mathring{\mathcal{E}}_h} \int_e (\boldsymbol{w}_h - \boldsymbol{w}) \cdot \boldsymbol{n} [p]_e) ds + C_4 \|p\|_{0,\Omega}^2 \\
&\geq -\big(\sum_{\tau \in \mathcal{T}_h} h_\tau^{-2} \|\boldsymbol{w}_h - \boldsymbol{w}\|_{0,\tau}^2 + \sum_{e \in \mathring{\mathcal{E}}_h} h_e^{-1} \|\boldsymbol{w}_h - \boldsymbol{w}\|_{0,e}^2 \big)^{1/2} \|p\|_{h,\Omega} + C_4 \|p\|_{0,\Omega}^2 \\
&\geq -C_5 \|\boldsymbol{w}\|_{1,\Omega} \|p\|_{h,\Omega} + C_4 \|p\|_{0,\Omega}^2 \\
&\geq \|p\|_{0,\Omega}^2 \big(C_4 - C_5 \frac{\|p\|_{h,\Omega}}{\|p\|_{0,\Omega}} \big).
\end{aligned}$$

Considering the following inequality

$$\|\boldsymbol{w}_h\|_{1,\Omega} \leq C_6\|p\|_{0,\Omega},$$

we then have

$$\frac{b(\boldsymbol{w}_h,p)}{\|\boldsymbol{w}_h\|_{1,\Omega}} \geq \|p\|_{0,\Omega}(C_7 - C_8\frac{\|p\|_{h,\Omega}}{\|p\|_{0,\Omega}}). \tag{3.3.5}$$

Combining (3.3.4) and (3.3.5), we have

$$\begin{aligned}\sup_{0\neq\boldsymbol{v}\in\boldsymbol{V}_h}\frac{b(\boldsymbol{v},p)}{\|\boldsymbol{v}\|_{1,\Omega}} &\geq \min_t[\max(C_7 - C_8t, C_3t)]\|p\|_{0,\Omega}\\ &= \frac{C_3C_7}{C_3+C_8}\|p\|_{0,\Omega}.\end{aligned}$$

Taking $\gamma = C_3C_7/(C_3+C_8)$, $\bar{\gamma}_h \geq \gamma$. Obviously, γ is only dependent on α and the covering constant. □

Allowing overlapping in $\mathcal{U}_h$ makes the analysis easier in applications. However, (3.3.2) is a strict condition, and many meshes fail to fulfill it.

3.4. Subspace Theorem

We present a more abstract theorem for checking the inf–sup condition in this section. The main idea of the theorem is to find two subspaces in each of the velocity and pressure spaces, and to check whether the four subspaces satisfy some conditions.

Let $\boldsymbol{V}_h \subset \boldsymbol{H}^1$ be the velocity space and $P_h \subset L^2$ the pressure space.

Theorem 3.4.1 (Subspace theorem). *Let $\boldsymbol{V}_1$ and $\boldsymbol{V}_2$ be two subspaces of $\boldsymbol{V}_h$ and P_1 and P_2 be two subspaces of P_h. Let the following four conditions hold:*

(1)
$$P_h = P_1 + P_2,$$

(2) *there exists $\alpha_1 > 0$ such that*

$$\sup_{\boldsymbol{v}_1\in\boldsymbol{V}_1}\frac{b(\boldsymbol{v}_1,q_1)}{\|\boldsymbol{v}_1\|_{1,\Omega}} \geq \alpha_1\|q_1\|_{0,\Omega}, \forall q_1 \in P_1, \tag{3.4.1}$$

(3) *there exists $\alpha_2 > 0$ such that*

$$\sup_{\boldsymbol{v}_2\in\boldsymbol{V}_2}\frac{b(\boldsymbol{v}_2,q_2)}{\|\boldsymbol{v}_2\|_{1,\Omega}} \geq \alpha_2\|q_2\|_{0,\Omega}, \forall q_2 \in P_2, \tag{3.4.2}$$

(4) *there exist $\beta_1, \beta_2 \geq 0$ such that*

$$\begin{aligned}|b(\boldsymbol{v}_1,q_2)| &\leq \beta_1\|\boldsymbol{v}_1\|_{1,\Omega}\|q_2\|_{0,\Omega}, \forall \boldsymbol{v}_1 \in \boldsymbol{V}_1 \text{ and } \forall q_2 \in P_2,\\ |b(\boldsymbol{v}_2,q_1)| &\leq \beta_2\|\boldsymbol{v}_2\|_{1,\Omega}\|q_1\|_{0,\Omega}, \forall \boldsymbol{v}_2 \in \boldsymbol{V}_2 \text{ and } \forall q_1 \in P_1,\end{aligned}$$

with

$$\beta_1\beta_2 < \alpha_1\alpha_2.$$

Then $\boldsymbol{V}_h \times P_h$ satisfies the inf–sup condition with the inf–sup constant depending only on $\alpha_1, \alpha_2, \beta_1$, and β_2.

Proof. The idea is to construct a $\boldsymbol{v} \in \boldsymbol{V}_h$ for each $q \in P_h$ such that

$$\frac{b(\boldsymbol{v}, q)}{\|\boldsymbol{v}\|_{1,\Omega}} \geq C\|q\|_{0,\Omega}, \tag{3.4.3}$$

where C is a positive constant.

For each $q \in P_h$, there exist $q_1 \in P_1$ and $q_2 \in P_2$ such that

$$q = q_1 + q_2. \tag{3.4.4}$$

By Theorem 2.2.3, the condition (3.4.1) is equivalent to

$$\begin{aligned} &\text{for any } q_1 \in P_1, \text{ there is } \boldsymbol{v}_1 \in \boldsymbol{V}_1 \text{ such that} \\ &b(\boldsymbol{v}_1, q_1) = \|q_1\|_{0,\Omega}^2 \quad \text{and} \quad \|\boldsymbol{v}_1\|_{1,\Omega} \leq \frac{1}{\alpha_1}\|q_1\|_{0,\Omega}. \end{aligned} \tag{3.4.5}$$

Similarly, the condition (3.4.2) implies that for each $q_2 \in P_2$ there exists a $\boldsymbol{v}_2 \in \boldsymbol{V}_2$ such that

$$b(\boldsymbol{v}_2, q_2) = \|q_2\|_{0,\Omega}^2 \quad \text{and} \quad \|\boldsymbol{v}_2\|_{1,\Omega} \leq \frac{1}{\alpha_2}\|q_2\|_{0,\Omega}. \tag{3.4.6}$$

For the q in (3.4.4), we are going to construct a $\boldsymbol{v}$ such that (3.4.3) holds. There are two cases, $\beta_1 + \beta_2 = 0$ ($\beta_1 = \beta_2 = 0$) and $\beta_1 + \beta_2 \neq 0$.

Case 1. $\beta_1 = \beta_2 = 0$

Let $\boldsymbol{v}_1$ and $\boldsymbol{v}_2$ be the functions corresponding to q_1 and q_2 in (3.4.4) such that the condition (3.4.5) and (3.4.6) hold. Setting

$$\boldsymbol{v} := \boldsymbol{v}_1 + \boldsymbol{v}_2,$$

we have

$$\begin{aligned} b(\boldsymbol{v}, q) &= b(\boldsymbol{v}_1 + \boldsymbol{v}_2, q_1 + q_2) \\ &= b(\boldsymbol{v}_1, q_1) + b(\boldsymbol{v}_2, q_2) \\ &= \|q_1\|_{0,\Omega}^2 + \|q_2\|_{0,\Omega}^2. \end{aligned}$$

Since

$$\begin{aligned} \|\boldsymbol{v}\|_{1,\Omega} &= \|\boldsymbol{v}_1 + \boldsymbol{v}_2\|_{1,\Omega} \\ &\leq \|\boldsymbol{v}_1\|_{1,\Omega} + \|\boldsymbol{v}_2\|_{1,\Omega} \\ &\leq \frac{1}{\alpha_1}\|q_1\|_{0,\Omega} + \frac{1}{\alpha_2}\|q_2\|_{0,\Omega} \\ &\leq \max(\frac{1}{\alpha_1}, \frac{1}{\alpha_2})(\|q_1\|_{0,\Omega} + \|q_2\|_{0,\Omega}), \end{aligned}$$

we get

$$\begin{aligned} \frac{b(\boldsymbol{v}, q)}{\|\boldsymbol{v}\|_{1,\Omega}} &\geq \frac{\|q_1\|_{0,\Omega}^2 + \|q_2\|_{0,\Omega}^2}{\max(\frac{1}{\alpha_1}, \frac{1}{\alpha_2})(\|q_1\|_{0,\Omega} + \|q_2\|_{0,\Omega})} \\ &\geq \frac{1}{2\max(\frac{1}{\alpha_1}, \frac{1}{\alpha_2})}(\|q_1\|_{0,\Omega} + \|q_2\|_{0,\Omega}) \\ &\geq \frac{1}{2\max(\frac{1}{\alpha_1}, \frac{1}{\alpha_2})}\|q\|_{0,\Omega}. \end{aligned}$$

Case 2. $\beta_1 + \beta_2 \neq 0$
Without loss of generality, we assume $\beta_2 \neq 0$. Setting

$$\boldsymbol{v} := \boldsymbol{v}_1 + \sigma \boldsymbol{v}_2,$$

where σ is a scalar, we immediately have

$$\begin{aligned} b(\boldsymbol{v}, q) &= b(\boldsymbol{v}_1 + \sigma \boldsymbol{v}_2, q_1 + q_2) \\ &= b(\boldsymbol{v}_1, q_1) + \sigma b(\boldsymbol{v}_2, q_2) + b(\boldsymbol{v}_1, q_2) + \sigma b(\boldsymbol{v}_2, q_1) \\ &= \|q_1\|_{0,\Omega}^2 + \sigma \|q_2\|_{0,\Omega}^2 + b(\boldsymbol{v}_1, q_2) + \sigma b(\boldsymbol{v}_2, q_1). \end{aligned}$$

Since

$$\begin{aligned} |b(\boldsymbol{v}_1, q_2) + \sigma b(\boldsymbol{v}_2, q_1)| \leq & \beta_1 \|\boldsymbol{v}_1\|_{1,\Omega} \|q_2\|_{0,\Omega} + \sigma \beta_2 \|\boldsymbol{v}_2\|_{1,\Omega} \|q_1\|_{0,\Omega} \\ \leq & (\frac{\beta_1}{\alpha_1} + \frac{\sigma \beta_2}{\alpha_2}) \|q_1\|_{0,\Omega} \|q_2\|_{0,\Omega} \\ \leq & (\frac{\beta_1}{\alpha_1} + \frac{\sigma \beta_2}{\alpha_2})(\epsilon \|q_1\|_{0,\Omega}^2 + \frac{1}{4\epsilon} \|q_2\|_{0,\Omega}^2) \\ \leq & \epsilon(\lambda_1 + \sigma \lambda_2) \|q_1\|_{0,\Omega}^2 + \frac{1}{4\epsilon}(\lambda_1 + \sigma \lambda_2) \|q_2\|_{0,\Omega}^2, \end{aligned}$$

where $\lambda_1 := \beta_1/\alpha_1$ and $\lambda_2 := \beta_2/\alpha_2$, we have

$$b(\boldsymbol{v}, q) \geq [1 - \epsilon(\lambda_1 + \sigma \lambda_2)] \|q_1\|_{0,\Omega}^2 + [\sigma - \frac{1}{4\epsilon}(\lambda_1 + \sigma \lambda_2)] \|q_2\|_{0,\Omega}^2.$$

We hope to choose $\sigma > 0$ and $\epsilon > 0$ such that

$$1 - \epsilon(\lambda_1 + \sigma \lambda_2) > 0 \quad \text{and} \quad \sigma - \frac{1}{4\epsilon}(\lambda_1 + \sigma \lambda_2) > 0.$$

Namely, to choose $\sigma > 0$ and $\epsilon > 0$ such that

$$\epsilon < \frac{1}{\lambda_1 + \sigma \lambda_2} \quad \text{and} \quad 4\sigma\epsilon > \lambda_1 + \sigma \lambda_2.$$

Therefore σ must satisfy

$$\frac{4\sigma}{\lambda_1 + \sigma \lambda_2} > \lambda_1 + \sigma \lambda_2.$$

Simplifying the above inequality, we get

$$\lambda_2^2 \sigma^2 + (2\lambda_1 \lambda_2 - 4)\sigma + \lambda_1^2 < 0. \tag{3.4.7}$$

The inequality (3.4.7) implies

$$\lambda_2^2 t^2 + (2\lambda_1 \lambda_2 - 4)t + \lambda_1^2 = 0,$$

has two different real roots. This is equivalent to the fact that λ_1 and λ_2 satisfy the inequality

$$(2\lambda_1 \lambda_2 - 4)^2 - 4\lambda_1^2 \lambda_2^2 > 0,$$

or

$$\lambda_1 \lambda_2 < 1.$$

Namely, α_1, α_2, β_1, and β_2 satisfy the relation

$$\beta_1\beta_2 < \alpha_1\alpha_2.$$

Picking σ as

$$\sigma = \frac{2 - \lambda_1\lambda_2 + 2\sqrt{1-\lambda_1\lambda_2}}{\lambda_2^2},$$

and selecting ϵ such that

$$\frac{\lambda_1 + \sigma\lambda_2}{4\sigma} < \epsilon < \frac{1}{\lambda_1 + \sigma\lambda_2},$$

we have

$$b(\boldsymbol{v}, q) \geq \min(C_1, C_2)(\|q_1\|_{0,\Omega}^2 + \|q_2\|_{0,\Omega}^2).$$

Here $C_1 = 1 - \epsilon(\lambda_1 + \sigma\lambda_2)$ and $C_2 = \sigma - 4\epsilon(\lambda_1 + \sigma\lambda_2)/(4\epsilon)$. On the other hand, we have

$$\begin{aligned}
\|\boldsymbol{v}\|_{1,\Omega} &= \|\boldsymbol{v}_1 + \sigma\boldsymbol{v}_2\|_{1,\Omega} \\
&\leq \|\boldsymbol{v}_1\|_{1,\Omega} + \sigma\|\boldsymbol{v}_2\|_{1,\Omega} \\
&\leq \frac{1}{\alpha_1}\|q_1\|_{0,\Omega} + \frac{\sigma}{\alpha_2}\|q_2\|_{0,\Omega} \\
&\leq \max(\frac{1}{\alpha_1}, \frac{\sigma}{\alpha_2})(\|q_1\|_{0,\Omega} + \|q_2\|_{0,\Omega}).
\end{aligned}$$

Finally,

$$\begin{aligned}
\frac{b(\boldsymbol{v}, q)}{\|\boldsymbol{v}\|_{1,\Omega}} &\geq \frac{\min(C_1, C_2)}{2\max(\frac{1}{\alpha_1}, \frac{\sigma}{\alpha_2})}(\|q_1\|_{0,\Omega} + \|q_2\|_{0,\Omega}) \\
&\geq \frac{\min(C_1, C_2)}{2\max(\frac{1}{\alpha_1}, \frac{\sigma}{\alpha_2})}\|q\|_{0,\Omega}. \quad \square
\end{aligned}$$

As an application, we use this subspace theorem to prove the macroelement partition theorem. Define

$$\begin{aligned}
\boldsymbol{V}_1 &:= \boldsymbol{V}_h, & P_1 &:= Q_h, \\
\boldsymbol{V}_2 &:= \sum_{U\in\mathcal{U}_h} \boldsymbol{V}_h^U, & P_2 &:= \sum_{U\in\mathcal{U}_h} M_h^U.
\end{aligned}$$

For this choice of spaces we will show that the four assumptions of the subspace theorem are satisfied under the assumptions of the macroelement partion theorem. Then the inf–sup constant is bounded below by a positive number with independent of h. Therefore the macroelement partition theorem holds. By the assumptions in the partition theorem, conditions (1) and (2) hold. Since $b(\boldsymbol{v}, p) = 0$ holds for any $\boldsymbol{v} \in \boldsymbol{V}_2$ and any $p \in P_1$, $\beta_2 = 0$. Consequently, condition (4) holds. It only remains to verify condition (3). According to the definition of P_2, any $p \in P_2$ can be written as

$$p = \sum_{U\in\mathcal{U}_h} p^U,$$

with some $p^U \in M_h^U$. For each p^U there is a $\boldsymbol{v}^U \in \boldsymbol{V}_h^U$ such that

$$b(\boldsymbol{v}^U, q^U) = \|q^U\|_{0,\Omega}^2 \quad \text{and} \quad \|\boldsymbol{v}^U\|_{1,\Omega} \leq \frac{1}{\alpha}\|q^U\|_{0,\Omega}.$$

Taking $\boldsymbol{v} = \Sigma_{U \in \mathcal{U}_h} \boldsymbol{v}^U$, we have

$$b(\boldsymbol{v}, p) = \sum_{U \in \mathcal{U}_h} b(\boldsymbol{v}^U, p^U) = \sum_{U \in \mathcal{U}_h} \|p^U\|_{0,\Omega}^2 = \|p\|_{0,\Omega}^2,$$

and

$$\|\boldsymbol{v}\|_{1,\Omega}^2 = \sum_{U \in \mathcal{U}_h} \|\boldsymbol{v}^U\|_{1,\Omega}^2 \leq \frac{1}{\alpha^2} \sum_{U \in \mathcal{U}_h} \|p^U\|_{0,\Omega}^2 = \frac{1}{\alpha^2} \|p\|_{0,\Omega}^2.$$

Therefore condition (3) holds. This proves the macroelement partition theorem.

Another application of the subspace theorem is to prove that results on stability or reduced stability of a finite element method for the Stokes equations with Dirichlet boundary conditions are also valid for the equations traction boundary conditions. To simplify the exposition, we only consider $\mathcal{P}^n$–$\mathcal{P}^{n-1}$ elements in the following discussion (similar arguments work for other elements). In order to distinguish the finite element spaces for problems with different boundary conditions, we use $\boldsymbol{V}_h$, P_h, N_h, and M_h to denote the spaces in problems with the Dirichlet condition and use $\boldsymbol{V}_h^N$, P_h^N (which actually equals P_h), N_h^N, and M_h^N to denote the corresponding spaces for traction boundary condition problems.

Theorem 3.4.2. *If a finite element $\boldsymbol{V}_h \times P_h$ is stable, so is $\boldsymbol{V}_h^N \times P_h^N$.*

Proof. Since $\boldsymbol{V}_h \times P_h$ is stable, N_h only contains constants. Define

$$\begin{aligned} \boldsymbol{V}_1 &:= \boldsymbol{V}_h, \quad & P_1 &:= M_h, \\ \boldsymbol{V}_2 &:= \boldsymbol{V}_h^N, \quad & P_2 &:= \mathbb{R}. \end{aligned}$$

Obviously, conditions (1) and (2) of the subspace theorem hold.

For any constant $c \in P_2$ (without loss of generality we assume $c > 0$), we have

$$\frac{b(\boldsymbol{u}, c)}{\|\boldsymbol{u}\|_{1,\Omega} \|c\|_{0,\Omega}} \geq \gamma(\Omega) > 0,$$

where $\boldsymbol{u} = (x, 0)$. Therefore, $\boldsymbol{V}_2 \times P_2$ is stable i.e. the third condition holds.

Since $b(\boldsymbol{v}, q) = 0$ holds for any $\boldsymbol{v} \in \boldsymbol{V}_1$ and $q \in P_2$, the condition (4) of the subspace theorem holds.

Hence, the proof. □

Theorem 3.4.3. *If $\boldsymbol{V}_h \times P_h$ is reduced-stable and* $\dim N_h = \dim N_h^N + 1$, *then $\boldsymbol{V}_h^N \times P_h^N$ is stable.*

Proof. Since $\boldsymbol{V}_h \times P_h$ is reduced-stable and more importantly since $\dim N_h = \dim N_h^N + 1$, $N_h^N + \mathbb{R} = N_h$ and $M_h^N = M_h + \mathbb{R}$. Define

$$\begin{aligned} \boldsymbol{V}_1 &:= \boldsymbol{V}_h, \quad & P_1 &:= M_h, \\ \boldsymbol{V}_2 &:= \boldsymbol{V}_h^N, \quad & P_2 &:= \mathbb{R}. \end{aligned}$$

The theorem results from applying similar arguments as in the proof of Theorem 3.4.2 to the above four spaces. □

3.5. Support Lemmas

In order to apply the macroelement partition or covering theorem to a finite element method on some mesh families, we have to check if there is a common positive lower bound for every local inf–sup constant. In this section, we present some technical lemmas designed for checking the local inf–sup condition on various macroelements.

3.5.1. Equivalence Classes of Macroelements

We shall introduce the concepts of macroelement equivalence classes and equivalence classes under certain sets in this subsection. All these concepts are important in the analysis of the three finite elements.

Let $\mathcal{T}_{h_1}$ and $\mathcal{T}_{h_2}$ be two triangulations of Ω. Let $\mathcal{U}_{h_i}$ denote a set of macroelements for $\mathcal{T}_{h_i}$, for $i = 1, 2$.

A pair of macroelement U in $\mathcal{U}_{h_1}$ and O in $\mathcal{U}_{h_2}$ are called equivalent if the number of triangles in the two macroelements are equal, if $\mathcal{T}_{h_1}^U$ consists of triangles $\tau_1, \tau_2, \ldots, \tau_k$, and if $\mathcal{T}_{h_2}^O$ consists of triangles $\omega_1, \omega_2, \ldots, \omega_k$ so that there is a 1–1 continuous map H of U onto O which maps τ_i to ω_i, such that H is linear on each triangle τ_i. We call such a mapping H a topological mapping.

Let G denote a set of topological mappings that map a macroelement U to some other macroelements O. The macroelement equivalence class of U under the set G is defined as

$$E(U, G) := \{H(U) \mid H \in G\}.$$

Any two macroelements $U, O \in E(U, G)$ are called G–equivalent and denoted by

$$U \overset{G}{\sim} O.$$

3.5.2. The Equivalence Class under Invertible Linear Mappings

In this subsection, we investigate several equivalence classes of macroelements that correspond to some subsets of the set of all invertible linear mappings.

We consider an affine linear map from the coordinate system (x, y) to (ξ, ζ) given by

$$\begin{pmatrix} \xi(x,y) \\ \zeta(x,y) \end{pmatrix} = \begin{pmatrix} d_{11} & d_{12} \\ d_{21} & d_{22} \end{pmatrix} \begin{pmatrix} x \\ y \end{pmatrix} + \begin{pmatrix} d_1 \\ d_2 \end{pmatrix}.$$

A macroelement U is transformed to $\hat{U}$ under this map. Here the matrix of the mapping, denoted by D, is an invertible matrix with constant coefficients, and d_1, and d_2 are two constants. We let $\boldsymbol{V}_h^U$ and $\boldsymbol{V}_h^{\hat{U}}$ denote the velocity spaces and P_h^U and $P_h^{\hat{U}}$ denote the pressure spaces for the two macroelements.

Define

$$\hat{\boldsymbol{v}}(\xi, \zeta) := \boldsymbol{v}(x(\xi, \zeta), y(\xi, \zeta)), \forall \boldsymbol{v} \in \boldsymbol{V}_h^U,$$
$$\hat{q}(\xi, \zeta) := q(x(\xi, \zeta), y(\xi, \zeta)), \forall q \in P_h^U.$$

We assume that

$$\begin{aligned} \boldsymbol{V}_h^{\hat{U}} &= \{\hat{\boldsymbol{v}}(\xi,\zeta) \mid \boldsymbol{v} \in \boldsymbol{V}_h^U\}, \\ P_h^{\hat{U}} &= \{\hat{q}(\xi,\zeta) \mid q \in P_h^U\}. \end{aligned} \tag{3.5.1}$$

We also assume

$$\boldsymbol{V}_h^U = \{A\boldsymbol{v} \mid \boldsymbol{v} \in \boldsymbol{V}_h^U\} \quad \text{and} \quad \boldsymbol{V}_h^{\hat{U}} = \{A\boldsymbol{v} \mid \boldsymbol{v} \in \boldsymbol{V}_h^{\hat{U}}\}, \tag{3.5.2}$$

for any 2×2 nonsingular matrix A with constant coefficients. This assumption is valid for most of the mixed finite elements used for the Stokes equations, which reflects the symmetric structure of the two components of the velocity function $\boldsymbol{v}$.

Our first goal is to analyze the relation between the reduced inf–sup constants over the two macroelements U and $\hat{U}$. For this, we need to compute the inf–sup constant explicitly.

It is easy to verify that

$$\nabla \boldsymbol{v} = (\nabla \hat{\boldsymbol{v}})D,$$

and

$$\int_U q \operatorname{div} \boldsymbol{v} = \int_{\hat{U}} \hat{q} \operatorname{div}(D\hat{\boldsymbol{v}}) J_{D^{-1}} = J_{D^{-1}} \int_{\hat{U}} \hat{q} \operatorname{div}(D\hat{\boldsymbol{v}}) \tag{3.5.3}$$

where $J_{D^{-1}}$ stands for the absolute value of the determinant of D^{-1}.

Similar computations show that

$$\|q\|_{0,U}^2 = J_{D^{-1}} \|\hat{q}\|_{0,\hat{U}}^2, \tag{3.5.4}$$

and

$$\begin{aligned} |\boldsymbol{v}|_{1,U}^2 &= \int_U \nabla \boldsymbol{v} : \nabla \boldsymbol{v} = \int_{\hat{U}} (\nabla \hat{\boldsymbol{v}})D : (\nabla \hat{\boldsymbol{v}})D J_{D^{-1}} \\ &= J_{D^{-1}} \|(\nabla \hat{\boldsymbol{v}})D\|_F^2. \end{aligned}$$

Here $\|D\|_F$ denotes the Frobenius norm of the matrix D.

Since $\nabla D\hat{\boldsymbol{v}} = D\nabla \hat{\boldsymbol{v}}$, we have

$$\nabla \hat{\boldsymbol{v}} = D^{-1} \nabla D\hat{\boldsymbol{v}}.$$

Hence,

$$|\boldsymbol{v}|_{1,U}^2 = J_{D^{-1}} \int_{\hat{U}} \|D^{-1}(\nabla D\hat{\boldsymbol{v}})D\|_F^2. \tag{3.5.5}$$

Combining (3.5.3), (3.5.4), and (3.5.5), we get

$$\frac{\int_U q \operatorname{div} \boldsymbol{v}}{|\boldsymbol{v}|_{1,U} \|q\|_{0,U}} = \frac{\int_U q \operatorname{div} \boldsymbol{v}}{\left(\int_U \|\nabla \boldsymbol{v}\|_F^2\right)^{1/2} \|q\|_{0,U}} = \frac{\int_{\hat{U}} \hat{q} \operatorname{div}(D\hat{\boldsymbol{v}})}{\left(\int_{\hat{U}} \|D^{-1}(\nabla D\hat{\boldsymbol{v}})D\|_F^2\right)^{1/2} \|\hat{q}\|_{0,\hat{U}}}. \tag{3.5.6}$$

Since

$$\|D^{-1}(\nabla D\hat{\boldsymbol{v}})D\|_F \le \kappa_F(D) \|\nabla D\hat{\boldsymbol{v}}\|_F,$$

where $\kappa_F(D) = \|D^{-1}\|_F \|D\|_F$ is the condition number of the matrix D with respect to the Frobenius norm, we have

$$\frac{\int_U q \operatorname{div} \boldsymbol{v}}{\left(\int_U \|\nabla \boldsymbol{v}\|_F^2\right)^{1/2} \|q\|_{0,U}} \ge \frac{1}{\kappa_F(D)} \frac{\int_{\hat{U}} \hat{q} \operatorname{div}(D\hat{\boldsymbol{v}})}{\left(\int_{\hat{U}} \|\nabla D\hat{\boldsymbol{v}}\|_F^2\right)^{1/2} \|\hat{q}\|_{0,\hat{U}}}. \tag{3.5.7}$$

Now we are in the position to state some lemmas based on (3.5.6).

Lemma 3.5.1. *Let F be the set of all invertible linear mappings. For any $\hat{U}$ in $E(U,F)$, we have, under assumptions* (3.5.2) *and* (3.5.1),

$$\begin{aligned}\dim \boldsymbol{V}_h^U &= \dim \boldsymbol{V}_h^{\hat{U}},\\ \dim P_h^U &= \dim P_h^{\hat{U}},\\ \dim N_h^U &= \dim N_h^{\hat{U}}, \text{ and}\\ \dim M_h^U &= \dim M_h^{\hat{U}}.\end{aligned}$$

Proof. By assumption (3.5.1) and the equalities (3.5.3) and (3.5.6), we can clearly see that the lemma holds. □

Lemma 3.5.2. *Let $F_1 \subset F$ denote the set of all linear mappings with orthonormal matrices. For any $\hat{U} \in E(U,F_1)$,*

$$\bar{\gamma}_h^U = \bar{\gamma}_h^{\hat{U}}$$

holds under assumptions (3.5.2) *and* (3.5.1).

Proof. Since we have $\|D^{-1}(\nabla D\hat{\boldsymbol{v}})D\|_F = \|\nabla D\hat{\boldsymbol{v}}\|_F$, the equality (3.5.6) becomes

$$\frac{\int_U q \operatorname{div} \boldsymbol{v}}{\left(\int_U \|\nabla \boldsymbol{v}\|_F^2\right)^{1/2}\|q\|_{0,U}} = \frac{\int_{\hat{U}} \hat{q} \operatorname{div}(D\hat{\boldsymbol{v}})}{\left(\int_{\hat{U}} \|\nabla D\hat{\boldsymbol{v}}\|_F^2\right)^{1/2}\|\hat{q}\|_{0,\hat{U}}}.$$

The lemma then follows by (3.5.2). □

Lemma 3.5.3. *Let $F_2 \subset F$ be the set generated by all translations, dilations, reflections, and rotations. Then for any $\hat{U} \in E(U,F_2)$, we have*

$$\bar{\gamma}_h^U = \bar{\gamma}_h^{\hat{U}}$$

under the assumptions (3.5.2) *and* (3.5.1).

Proof. Since reflections and rotations correspond to orthonormal matrices, the previous lemma proves the result in these cases.

For dilations, the corresponding matrices are multiples of the identity matrix. We can then conclude that the reduced inf–sup constant does not change (equality (3.5.6)).

Since any translation corresponds to the identity matrix, the lemma holds trivially. □

The previous two lemmas are mainly for some special subsets. The question is whether we can conclude anything about the reduced inf–sup constant of the macroelements in $E(U,F)$. The answer is yes. However, since some triangles of $\mathcal{T}_h^{\hat{U}}$ for $\hat{U} \in E(U,F)$ could be degenerate, we need to add more restrictions to $E(U,F)$ in our discussion. Only a part of $E(U,F)$ is allowed to appear in triangulations $\mathcal{T}_h$, where h can be any small positive number.

Let $E_\theta(U,F)$ denote the subset of all the macroelements in $E(U,F)$ such that each of them satisfies the regularity assumption (2.3.2). That is, there is a positive number θ such that for any triangle τ in any macroelement of $E_\theta(U,F)$

$$\frac{\rho_\tau}{h_\tau} \geq \theta,$$

where ρ_τ is the diameter of the inscribed circle in τ and h_τ is the longest edge of τ.

Lemma 3.5.4. *Under assumptions* (3.5.2) *and* (3.5.1), *there exists* $\alpha_U > 0$ *with*

$$\bar{\gamma}^{\hat{U}} \geq \alpha_U, \quad \forall \hat{U} \in E_\theta(U, F).$$

Proof. Let $u_1, \ldots, u_k$ denote the vertices of U and $\hat{u}_1, \ldots, \hat{u}_k$ be the vertices of any $\hat{U}$ in $E_\theta(U, F)$. Here $\hat{u}_i$ corresponds u_i for $i = 1, \ldots, k$, under some mapping in F.

Since translations or dilations leave the reduced inf–sup constant unchanged, we assume $\hat{u}_1 = (0, 0)$ and $\max_{\tau \in \hat{U}}\{h_\tau\} = 1$ for any $\hat{U}$ in $E_\theta(U, F)$. Define

$$W := \{(\hat{u}_1, \ldots, \hat{u}_k) \mid \hat{U} \in E_\theta(U, F)\},$$

which is a set in $\mathbb{R}^{2k}$.

We first show that W is a closed set in $\mathbb{R}^{2k}$. Suppose there is a sequence of macroelements $\hat{U}^{(1)}, \hat{U}^{(2)}, \hat{U}^{(3)}, \ldots$ that converges to $\hat{U}$. That is, the vertices $\hat{u}_1^{(n)}, \ldots, \hat{u}_k^{(n)}$ of $U^{(n)}$ converge to the vertices $\hat{u}_1, \ldots, \hat{u}_k$ of $\hat{U}$ respectively as n goes to infinity. Since any triangle $\hat{\tau}^{(n)}$ in $\hat{U}^{(n)}$ satisfies

$$\frac{\rho_{\hat{\tau}^{(n)}}}{h_{\hat{\tau}^{(n)}}} \geq \theta,$$

we have

$$\frac{\rho_{\hat{\tau}}}{h_{\hat{\tau}}} \geq \theta,$$

for the corresponding triangle $\hat{\tau}$ in $\hat{U}$. Therefore the triangles in $\hat{U}$ satisfy (2.3.2).

It is quite straightforward to see that there is a continuous, 1–1, and onto mapping H of U to $\hat{U}$ such that H is linear on each triangle. Let H_n denote the linear mapping that maps U to $U^{(n)}$. Our goal is to prove that H is a linear mapping over the whole of U. If that is the case, W is closed.

Let D_n denote the matrix associated with H_n and D_τ denote the matrix associated with $H|_\tau$ for each τ in $\mathcal{T}_h^U$. For any triangle τ in $\mathcal{T}_h^U$, we assume that τ has vertices u_1, u_2, and u_3. We know that

$$H_n|_\tau(u_i) \to H|_\tau(u_i) \text{ as } n \to \infty,$$

for $i = 1, 2, 3$. This implies

$$\begin{aligned} D_n(u_2 - u_1) &\to D_\tau(u_2 - u_1), \text{ and} \\ D_n(u_3 - u_1) &\to D_\tau(u_3 - u_1), \end{aligned}$$

as $n \to \infty$. Since $u_2 - u_1$ and $u_3 - u_1$ are linearly independent vectors,

$$D_n \to D_\tau \text{ as } n \to \infty.$$

Consequently, we have

$$D_{\tau_i} = D_{\tau_j}, \forall \tau_i, \tau_j \in \mathcal{T}_h^U.$$

Similarly, we can show that the constant vector associated with $H|_\tau$ is also same for all τ in $\mathcal{T}_h^U$. Hence, we have proved that H is a nonsingular linear mapping.

Since

$$\bar{\gamma}_h^{\hat{U}}(\hat{u}_1, \ldots, \hat{u}_k) = \sqrt{\lambda_{\dim N_h^{\hat{U}}+1}\left(M_{\hat{U}}^{-1/2} B_{\hat{U}} A_{\hat{U}}^{-1} B_{\hat{U}}^t M_{\hat{U}}^{-1/2}\right)},$$

(please see the relevant sections of Chapter 5) and the entries of matrices $M_{\hat{U}}$, $A_{\hat{U}}$, and $B_{\hat{U}}$ depend continuously on vertices $\hat{u}_1, \ldots, \hat{u}_k$, $\bar{\gamma}^{\hat{U}}$ must continuously depend on the vertices in $\hat{U}$. Since W is a bounded closed domain, there is α_U such that

$$\bar{\gamma}^{\hat{U}} \geq \alpha_U, \forall \hat{U} \in E_\theta(U, F). \quad \square$$

3.5.3. Stability of Finite Elements on Macroelement Partitions

When applying the macroelement partition theorem, we have to estimate the stability of $\boldsymbol{V}_h \times (M_h \cap \Sigma_{U \in \mathcal{U}_h} N_h^U)$. In this section, we state some basic results that can be used to analyze this stability.

Let $\mathcal{U}_h$ be a macroelement partition of a triangulation $\mathcal{T}_h$ of Ω. Let $\boldsymbol{V}_h$ be the velocity space with $\mathring{\boldsymbol{M}}_0^k \subset \boldsymbol{V}_h$ and let $P_h := M_{-1}^l$ be the pressure space.

Lemma 3.5.5. *If $N_h^U = \chi^U \mathbb{R}$ for any $U \in \mathcal{U}_h$, then*

(1) *$\boldsymbol{V}_h \times (M_h \cap \Sigma_{U \in \mathcal{U}_h} N_h^U)$ is stable for $k > 1$, and*
(2) *$\boldsymbol{V}_h \times (M_h \cap \Sigma_{U \in \mathcal{U}_h} N_h^U)$ is stable for $k = 1$ if the intersection of any pair of nondisjoint macroelements in $\mathcal{U}_h$ is either a single vertex or a connected set of at least two edges in $\mathcal{T}_h$.*

Proof. We consider statement (1) first. Define

$$\begin{aligned} \boldsymbol{V}_1 &:= \mathring{\boldsymbol{M}}_0^k, \\ P_1 &:= M_{-1}^0. \end{aligned}$$

It is well known that $\boldsymbol{V}_1 \times P_1$ is stable for $k > 1$. Since

$$M_h \bigcap \sum_{U \in \mathcal{U}_h} N_h^U \subset M_{-1}^0 \quad \text{and} \quad \boldsymbol{V}_h \supset \boldsymbol{V}_1,$$

we have $\boldsymbol{V}_h \times (M_h \cap \Sigma_{U \in \mathcal{U}_h} N_h^U)$ is stable for $k > 1$.

For the statement (2), we need to consider the stability of the finite element $\boldsymbol{V}_1 \times P_1$ on the macroelement partition $\mathcal{U}_h$, where

$$\begin{aligned} \boldsymbol{V}_1 &:= \mathring{\boldsymbol{M}}_0^k(\mathcal{U}_h), \\ P_1 &:= M_{-1}^0(\mathcal{U}_h). \end{aligned}$$

Because of the special property of the macroelement partition, it is easy to show that $\boldsymbol{V}_1 \times P_1$ is stable (see Stenberg [24] and [25]). This proves that $\boldsymbol{V}_h \times (M_h \cap \Sigma_{U \in \mathcal{U}_h} N_h^U)$ is stable for $k = 1$. $\square$

Chapter 4

STABILITY AND APPROXIMATION PROPERTIES OF THE $\mathcal{P}^2$–$\mathcal{P}^1$ ELEMENT

In this chapter, we discuss some theoretical results on the $\mathcal{P}^2$–$\mathcal{P}^1$ element for the Stokes equations. The $\mathcal{P}^2$–$\mathcal{P}^1$ element is defined by

$$\boldsymbol{V}_h = \mathring{\boldsymbol{M}}_0^2(\mathcal{T}_h) \quad \text{and} \quad P_h = M_{-1}^1(\mathcal{T}_h).$$

As we mentioned before, the stability and approximability of this element depend on the mesh configuration. Namely, the element is stable for some mesh family but unstable for others.

The main issue in this chapter is the analysis of the performance of this element on different mesh families. In Section 1, we introduce some known results on this element—a negative result due to de Boor and Höllig for diagonal meshes and a positive one due to Mercier for crisscross meshes. In Section 2, we analyze the spurious pressure modes on diagonal and crisscross mesh structures and display them explicitly. Studying spurious pressure modes is a crucial step in understanding the reduced stability and the approximation properties of the reduced pressure space of a finite element. We study the stability and approximation properties of the finite element on irregular crisscross meshes in Section 3. As we will see, the rate of convergence for both velocity and pressure is optimal on this mesh family.

In Section 4, we deal with a mixed mesh family—a mixture of diagonal and crisscross structures. On these meshes we prove that the reduced inf–sup constant can be bounded away from zero by a positive number (independent of h) as long as there is a nonvanishing proportion of crisscross structures uniformly distributed throughout the mesh.

In Sections 5 and 6, we discuss two mesh families with no singular vertices. On these two families the $\mathcal{P}^2$–$\mathcal{P}^1$ element is completely stable, so both velocity and pressure have optimal rates of convergence.

4.1. Known Results

In this section, we present two known results on the $\mathcal{P}^2$–$\mathcal{P}^1$ element. One is a negative result which shows, by an example, that the numerical solution for velocity has at most suboptimal rate of convergence on a type of mesh, and the other one is positive stating that the rate of convergence of the numerical solution for velocity is optimal on another mesh family.

4.1.1. A Negative Result: Diagonal Meshes

Let the domain Ω be the unit square. Let the triangulation $\mathcal{T}_h$ of Ω be formed by dividing the unit square into h^{-2} ($h = 1/n$, n is a positive integer) small squares where each of them is partitioned by its positively sloped diagonal, see Figure 4.1. The mesh $\mathcal{T}_h$ is called a diagonal mesh.

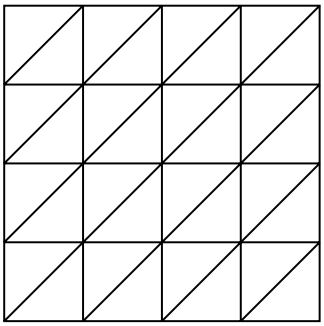

Figure 4.1. Diagonal mesh of the unit square ($h = 1/4$).

On diagonal meshes, a negative result can be deduced from the work of de Boor and Höllig [5], see also de Boor and Devore [4]. They showed that the space of C^1 piecewise cubic polynomials has approximation properties which are one order suboptimal. This implies that the rate of convergence of $\boldsymbol{u}_h$ to $\boldsymbol{u}$ is suboptimal. (The norms considered by de Boor and Höllig are not exactly those pertinent to this discussion. However, their argument can be adapted. Cf. Babuška and Suri [1].)

Theorem 4.1.1 (C. de Boor, 1990). *Let $\mathcal{T}_h$ be a diagonal mesh on the unit square Ω. For $f \in H^4(\Omega)$, we have*

$$\inf_{w \in M_1^3} \|f - w\|_{0,\Omega} \leq C\, h^3 \|f\|_{4,\Omega}.$$

Moreover, there exists a function $g \in C^\infty$ such that

$$\inf_{w \in M_1^3} \|g - w\|_{0,\Omega} \geq C\, h^3.$$

Here C is a constant independent of h.

This result implies that the rate of convergence of finite element solution for the velocity of the Stokes equations with traction boundary conditions is one order less than the optimal. Moreover, the result cannot be improved. It is believed that the poor approximation property of the element on the diagonal mesh is caused by the special mesh structures—only three types of lines appear in $\mathcal{T}_h$.

For the Stokes squations with Dirichlet boundary conditions, we cannot expect a better result than the one offered by Theorem 4.1.1. Essentially, the rate of convergence of the finite element solution for the velocity is no better than suboptimal. We will give some numerical evidence in Chapter 5.

The above theorem does not say anything about the approximation property of the finite element solution for pressure. However, from Theorem 2.2.1 we can infer that the reduced inf–sup constant is at least as small as $O(h)$. Therefore, no meaningful error estimate for the pressure can be obtained by using Theorem 2.2.1.

4.1.2. A Positive Result: Irregular Crisscross Meshes

Mercier [17] has proved a positive result on irregular crisscross meshes for the $\mathcal{P}^2$–$\mathcal{P}^1$ element by using the Fraeijs de Veubeke-Sander elements [10].

Let Ω be any polygonal domain. Let $\mathcal{T}_h$ be the triangulation of Ω that results from partitioning Ω into quadrilaterals and then dividing each quadrilateral by its two diagonals, see Figure 4.2. This type of mesh is called an irregular crisscross mesh.

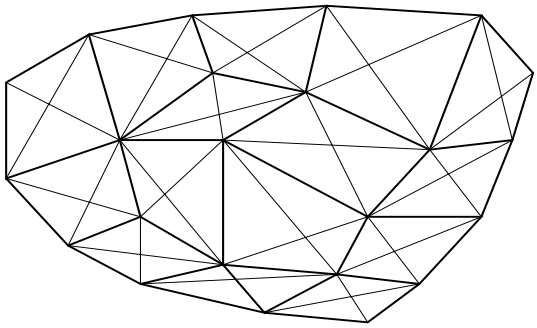

Figure 4.2. Irregular crisscross mesh.

Theorem 4.1.2 (Mercier, 1978). *Let $\mathcal{T}_h$ be an irregular crisscross mesh on Ω. If $\boldsymbol{u} \in \mathring{\boldsymbol{H}}^3$, then we have*

$$\inf_{\boldsymbol{v} \in \boldsymbol{Z}_h} \|\boldsymbol{u} - \boldsymbol{v}\|_{1,\Omega} \leq Ch^2 \|\boldsymbol{u}\|_{3,\Omega},$$

where C is a constant independent of h and $\boldsymbol{Z}_h$ is the space of all the divergence free functions in $\boldsymbol{V}_h$ $(:= \mathring{\boldsymbol{M}}_0^2(\mathcal{T}_h))$.

The proof of the theorem is based on the C^1 Fraeijs de Veubeke-Sander element.

On irregular crisscross meshes, Mercier's theorem guarantees that the solution for the velocity from the $\mathcal{P}^2$–$\mathcal{P}^1$ element converges optimally. However, there is no estimate for the pressure in the above theorem. Also, the theorem says nothing about the reduced stability of this element on irregular crisscross meshes.

We define a singular vertex as the intersection of exactly two segments in a triangulation $\mathcal{T}_h$. For example, in Figure 4.3, the vertex s is a singular vertex. It is believed that the $\mathcal{P}^2$–$\mathcal{P}^1$ element possesses good approximation properties on irregular crisscross meshes due to the presence of the singular vertices. The more singular vertices a mesh possesses, the more divergence-free functions are there in $\boldsymbol{V}_h$. This can be seen from the following lemma.

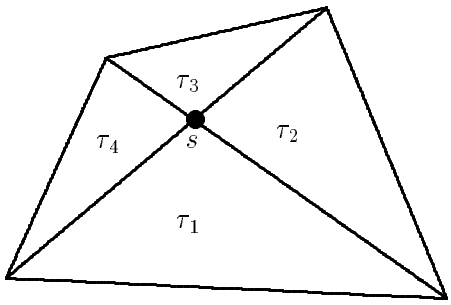

Figure 4.3. Singular vertex.

Lemma 4.1.1. *Let $\boldsymbol{u} = (u, v)$ be a function on the quadrilateral which is*

(1) *continuous on the quadrilateral shown in Figure 4.3. and*
(2) *differentiable on each triangle τ_i for $i = 1, 2, 3, 4$.*

Then we have

$$\sum_{i=1}^{4} (-1)^i (\operatorname{div} \boldsymbol{u}|_{\tau_i})(s) = 0. \tag{4.1.1}$$

Proof. Let $\boldsymbol{n}_1 = (n_{11}, n_{12})$ and $\boldsymbol{n}_2 = (n_{21}, n_{22})$ denote the two unit vectors which are parallel to the diagonals of the quadrilateral in Figure 4.3 respectively. For convenience, we denote $\boldsymbol{u}$ on each triangle τ_i by $\boldsymbol{u}_i = (u_i, v_i)$.

Simple calculations show that

$$a := \frac{\partial u_1}{\partial \boldsymbol{n}_1}(s) = \frac{\partial u_4}{\partial \boldsymbol{n}_1}(s), \quad b := \frac{\partial u_1}{\partial \boldsymbol{n}_2}(s) = \frac{\partial u_2}{\partial \boldsymbol{n}_2}(s),$$
$$c := \frac{\partial u_2}{\partial \boldsymbol{n}_1}(s) = \frac{\partial u_3}{\partial \boldsymbol{n}_1}(s), \quad d := \frac{\partial u_3}{\partial \boldsymbol{n}_2}(s) = \frac{\partial u_4}{\partial \boldsymbol{n}_2}(s).$$

We define matrix D by

$$D = \begin{pmatrix} \boldsymbol{n}_1 \\ \boldsymbol{n}_2 \end{pmatrix}.$$

Therefore, we have

$$\begin{pmatrix} \frac{\partial u_1}{\partial x}(s) \\ \frac{\partial u_1}{\partial y}(s) \end{pmatrix} = \frac{1}{|D|}\begin{pmatrix} n_{22}a - n_{12}b \\ n_{21}a + n_{11}b \end{pmatrix}, \quad \begin{pmatrix} \frac{\partial u_2}{\partial x}(s) \\ \frac{\partial u_2}{\partial y}(s) \end{pmatrix} = \frac{1}{|D|}\begin{pmatrix} n_{22}c - n_{12}b \\ n_{21}c + n_{11}b \end{pmatrix},$$
$$\begin{pmatrix} \frac{\partial u_3}{\partial x}(s) \\ \frac{\partial u_3}{\partial y}(s) \end{pmatrix} = \frac{1}{|D|}\begin{pmatrix} n_{22}c - n_{12}d \\ n_{21}c + n_{11}d \end{pmatrix}, \quad \begin{pmatrix} \frac{\partial u_4}{\partial x}(s) \\ \frac{\partial u_4}{\partial y}(s) \end{pmatrix} = \frac{1}{|D|}\begin{pmatrix} n_{22}a - n_{12}d \\ n_{21}a + n_{11}d \end{pmatrix}.$$

Clearly,

$$\sum_{i=1}^{4}(-1)^i \frac{\partial u_j}{\partial x}(s) = 0 \quad \text{and} \quad \sum_{i=1}^{4}(-1)^i \frac{\partial u_j}{\partial y}(s) = 0, \tag{4.1.2}$$

hold for $j = 1, 2$. Similar arguments show that the equalities (4.1.2) hold if we replace u by v. Finally we have

$$\sum_{i=1}^{4}(-1)^i (\operatorname{div} \boldsymbol{u}|_{\tau_i})(s) = 0. \quad \square$$

Since $\operatorname{div} \boldsymbol{u}$ automatically satisfies the equation (4.1.1) at each singular vertex, the dimension of the space $\boldsymbol{Z}_h$ is increased by one wherever there is a singular vertex in the triangulation $\mathcal{T}_h$. Hence, conclude that the approximation properties of $\boldsymbol{Z}_h$ improve with any increase of the number of singular vertices in $\mathcal{T}_h$.

4.2. Spurious Pressure Modes

In this section, we display explicitly the spurious pressure modes for the diagonal and irregular crisscross mesh families. We study spurious pressure modes to determine the rate of convergence of the finite element solution from the space $\boldsymbol{V}_h \times P_h$. Specifically, in order to determine the approximation properties of M_h and the stability of $\boldsymbol{V}_h \times M_h$ we need to know the spurious pressure modes.

4.2.1. Spurious Modes on Diagonal Meshes

Consider a diagonal mesh $\mathcal{T}_h$ of the unit square ($h = \frac{1}{n}$, integer $n \geq 2$). Let $K_{i,j}$, $1 \leq i, j \leq n$, denote the $(i,j)^{th}$ square in this mesh (Figure 4.4). Let each $K_{i,j}$ be bisected by its positively sloped diagonal (see Figure 4.4).

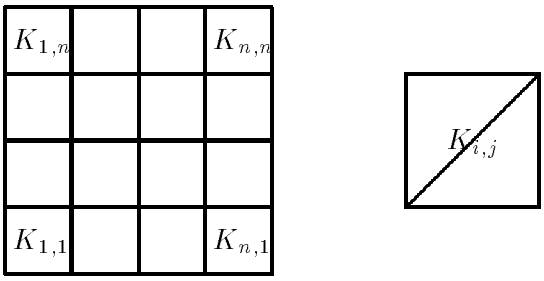

Figure 4.4. Diagonal mesh.

The following lemma (see Chui and Schumaker and Wang [8] and Scott and Vogelius [22]) gives the dimension of the space N_h for the diagonal mesh family.

Lemma 4.2.1. *On the diagonal mesh $\mathcal{T}_h$ ($n = 1/h$, $n \geq 2$) of the unit square, we have*

$$\dim N_h = 6.$$

Before we explicitly show that N_h has 6 independent functions, we introduce some notations. For any pressure function p in P_h (see Figure 4.5), we denote the values of p at the vertices of $K_{i,j}$ by $p_{i,j}^{(1)}$, $p_{i,j}^{(2)}$, $p_{i,j}^{(3)}$, $q_{i,j}^{(1)}$, $q_{i,j}^{(2)}$, and $q_{i,j}^{(3)}$. For convenience, on square $K_{i,j}$ we define 5 functions Φ_1, Φ_2, Φ_3, Φ_4, and Φ_5 (Figure 4.6).

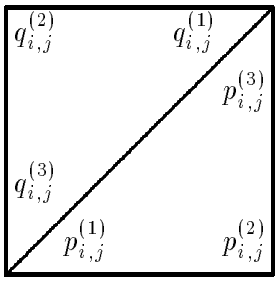

Figure 4.5. Values of p.

Theorem 4.2.1. *On the diagonal mesh $\mathcal{T}_h$, we define*

$$\begin{aligned}
&\Psi_l|_{K_{i,j}} = \Phi_l, \quad \forall K_{i,j}, \text{ for } l = 1,2,3,\\
&\Psi_4|_{K_{i,j}} = \begin{cases} \Phi_4, & K_{1,n} \\ 0, & \text{otherwise,} \end{cases}\\
&\Psi_5|_{K_{i,j}} = \begin{cases} \Phi_5, & K_{n,1} \\ 0, & \text{otherwise, and} \end{cases}\\
&\Psi_6|_{K_{i,j}} = \Phi_5 + 4(i-1)(\Phi_1 - \Phi_2) + 4(j-1)(\Phi_2 - \Phi_3), \quad \forall K_{i,j}.
\end{aligned}$$

For $n \geq 2$, the functions Ψ_i, $i = 1,2,\ldots,6$ form a basis of N_h.

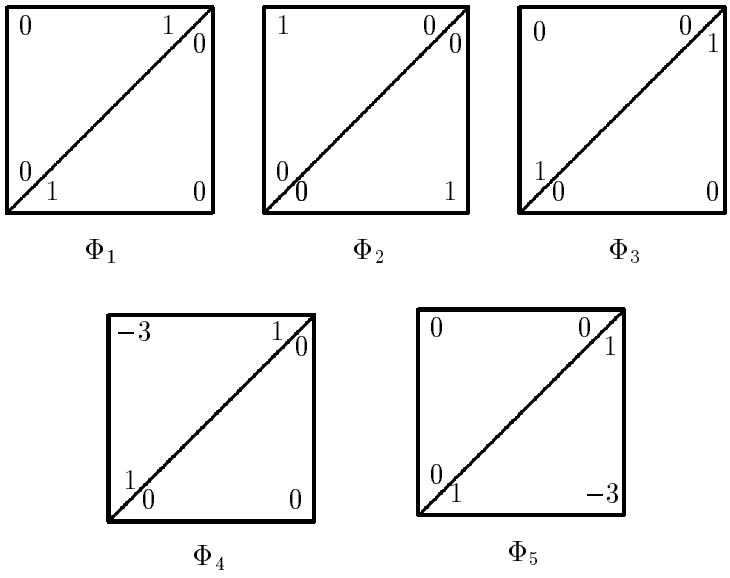

Figure 4.6. Definition of Φ_i.

Proof. We prove the independence of Ψ_i for $i = 1, 2, \ldots, 6$ first. Assume there are constants α_i, for $i = 1, \ldots, 6$, such that

$$\sum_{i=1}^{6} \alpha_i \Psi_i = 0, \text{ on } \mathcal{T}_h. \tag{4.2.1}$$

We need to show that $\alpha_i = 0$ for $i = 1, \ldots, 6$. By considering (4.2.1) on $K_{n,1}$, we get a system of linear equations:

$$\begin{aligned}
\alpha_1 &= 0, \\
\alpha_2 + (4n-4)\alpha_6 &= 0, \\
\alpha_3 - (4n+4)\alpha_6 &= 0, \\
\alpha_1 + \alpha_5 + \alpha_6 &= 0, \\
\alpha_2 - 3\alpha_5 + (4n-7)\alpha_6 &= 0, \\
\alpha_3 + \alpha_5 - (4n-2)\alpha_6 &= 0.
\end{aligned}$$

Solving the above system, we get

$$\alpha_1 = \alpha_2 = \alpha_3 = \alpha_5 = \alpha_6 = 0.$$

On the other hand, considering (4.2.1) on $K_{1,n}$, we have

$$\alpha_1 = \alpha_2 = \alpha_3 = \alpha_4 = \alpha_6 = 0.$$

The above two results combine to complete the proof for the independence of $\{\Psi_i\}_{i=1}^{6}$.

We now show that each Ψ_i belongs to N_h. For the space $\mathring{M}_0^2$, there are 4 types of basis functions. One is piecewise linears on six triangles (first figure of Figure 4.7) and the remaining three types are all piecewise quadratics on the shaded triangles in the rest of the figures of Figure 4.7. For convenience, we denote these four basis functions by ϕ_a, ϕ_b, ϕ_c, and ϕ_d respectively. If we can prove that the first order derivatives of these basis functions with respect to x and y are orthogonal to all Ψ_i, then we are done.

Because of the special shape of $\mathrm{spt}\{\phi_a\}$, $\mathrm{spt}\{\phi_b\}$, and $\mathrm{spt}\{\phi_d\}$, it is easy to show that

$$\int_{\mathrm{spt}\{\phi_l\}} \frac{\partial \phi_l}{\partial x}\Psi_k = 0 \quad \text{and} \quad \int_{\mathrm{spt}\{\phi_l\}} \frac{\partial \phi_l}{\partial y}\Psi_k = 0,$$

for $l = a, b, d$ and for $k = 4, 5$.

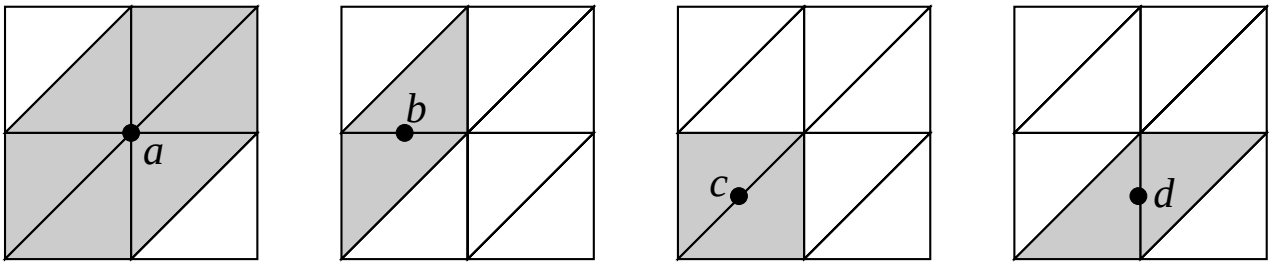

Figure 4.7. Supports of basis functions.

Since $\phi_c = -4(x-1)yn^2$ in $\mathrm{spt}\{\Psi_5\} \cap K_{n,1}$ and $\phi_c = -4x(y-1)n^2$ in $\mathrm{spt}\{\Psi_6\} \cap K_{1,n}$, simple calculations show that

$$\int_{\mathrm{spt}\ \Psi_k} \frac{\partial \phi_c}{\partial x}\Psi_k = 0 \quad \text{and} \quad \int_{\mathrm{spt}\ \Psi_k} \frac{\partial \phi_c}{\partial y}\Psi_k = 0,$$

for $k = 4, 5$. Thus, we have shown that Ψ_4 and Ψ_5 are in N_h.

Since constants are always in N_h, we only need to show that Ψ_1, Ψ_2, and Ψ_6 are in N_h.

Let the macroelement U be formed by four small squares $K_{i,j}$, $K_{i+1,j}$, $K_{i,j+1}$, and $K_{i+1,j+1}$. If we can prove

$$\int_U \frac{\partial \phi_l}{\partial x}\Psi_k = 0 \quad \text{and} \quad \int_U \frac{\partial \phi_l}{\partial y}\Psi_k = 0,$$

for $l = a, b, c, d$ and $k = 1, 2, 6$, then we are done.

On U we define

$$v := a\phi_a + b\phi_b + c\phi_c + d\phi_d.$$

For any $p \in P_h$, we have

$$\begin{aligned}
\frac{1}{6n}\int_U \frac{\partial v}{\partial x}p = &\big(-p^{(1)}_{i,j} - p^{(2)}_{i,j} - 2p^{(3)}_{i,j} + q^{(1)}_{i,j} + q^{(2)}_{i,j} + 2q^{(3)}_{i,j}\big)c + \\
&\big(p^{(1)}_{i,j} + p^{(2)}_{i,j} + 2p^{(3)}_{i,j} - q^{(1)}_{i+1,j} - q^{(2)}_{i+1,j} - 2q^{(3)}_{i+1,j}\big)d + \\
&\big(p^{(1)}_{i,j+1} - p^{(2)}_{i,j+1} - q^{(1)}_{i,j} + q^{(2)}_{i,j}\big)b + \\
&\big(p^{(1)}_{i,j+1} + p^{(2)}_{i,j+1} + p^{(3)}_{i,j+1} - p^{(1)}_{i+1,j+1} - p^{(2)}_{i+1,j+1} - p^{(3)}_{i+1,j+1} + \\
&q^{(1)}_{i,j} + q^{(2)}_{i,j} + q^{(3)}_{i,j} - q^{(1)}_{i+1,j} - q^{(2)}_{i+1,j} - q^{(3)}_{i+1,j}\big)a,
\end{aligned} \tag{4.2.2}$$

and

$$\begin{aligned}
\frac{1}{6n}\int_U \frac{\partial v}{\partial y}p = &\big(2p^{(1)}_{i,j} + p^{(2)}_{i,j} + p^{(3)}_{i,j} - 2q^{(1)}_{i,j} - q^{(2)}_{i,j} - q^{(3)}_{i,j}\big)c + \\
&\big(p^{(2)}_{i,j} - p^{(3)}_{i,j} - q^{(2)}_{i+1,j} + q^{(3)}_{i+1,j}\big)d + \\
&\big(-2p^{(1)}_{i,j+1} - p^{(2)}_{i,j+1} - p^{(3)}_{i,j+1} + 2q^{(1)}_{i,j} + q^{(2)}_{i,j} + q^{(3)}_{i,j}\big)b + \\
&\big(p^{(1)}_{i,j} + p^{(2)}_{i,j} + p^{(3)}_{i,j} - p^{(1)}_{i,j+1} - p^{(2)}_{i,j+1} - p^{(3)}_{i,j+1} + \\
&q^{(1)}_{i+1,j} + q^{(2)}_{i+1,j} + q^{(3)}_{i+1,j} - q^{(1)}_{i+1,j+1} - q^{(2)}_{i+1,j+1} - q^{(3)}_{i+1,j+1}\big)a.
\end{aligned} \tag{4.2.3}$$

Taking v to be equal to Φ_1 or Φ_2 in either (4.2.2) or (4.2.3), we get zero for any choice of a, b, c, and d. Therefore, Ψ_1 and Ψ_2 are in N_h.

The values of Ψ_6 in U are

$$\begin{array}{lll}
p^{(1)}_{i,j} = 4i-3, & p^{(2)}_{i,j} = 4(j-i)-3, & p^{(3)}_{i,j} = -4j+5, \\
q^{(1)}_{i,j} = 4i-4, & q^{(2)}_{i,j} = 4(j-i), & q^{(3)}_{i,j} = -4j+4, \\
p^{(1)}_{i+1,j} = 4i+1, & p^{(2)}_{i+1,j} = 4(j-i)-7, & p^{(3)}_{i+1,j} = -4j+5, \\
q^{(1)}_{i+1,j} = 4i, & q^{(2)}_{i+1,j} = 4(j-i)-4, & q^{(3)}_{i+1,j} = -4j+4, \\
p^{(1)}_{i,j+1} = 4i-3, & p^{(2)}_{i,j+1} = 4(j-i)+1, & p^{(3)}_{i,j+1} = -4j+1, \\
q^{(1)}_{i,j+1} = 4i-4, & q^{(2)}_{i,j+1} = 4(j-i)+4, & q^{(3)}_{i,j+1} = -4j, \\
p^{(1)}_{i+1,j+1} = 4i+1, & p^{(2)}_{i+1,j+1} = 4(j-i)-3, & p^{(3)}_{i+1,j+1} = -4j+1, \\
q^{(1)}_{i+1,j+1} = 4i, & q^{(2)}_{i+1,j+1} = 4(j-i), & q^{(3)}_{i+1,j+1} = -4j.
\end{array}$$

Plugging Ψ_6 for v into (4.2.2) and (4.2.3), we find that both (4.2.2) and (4.2.3) are zeros. Therefore Ψ_6 is in N_h.

Thus, we have shown that $\Psi_1, \ldots, \Psi_6$ are in N_h and are independent. Since the dimension of N_h is 6 (by Lemma 4.2.1), $\{\Psi_i\}_{i=1}^6$ forms a basis for N_h. $\square$

The spurious modes Ψ_1, Ψ_2, Ψ_3, and Ψ_6 all have $\mathcal{T}_h$ as their support. The modes Ψ_4 and Ψ_5 have a small local support if we consider P_h as the pressure space. On the other hand, they are globally supported if $\hat{P}_h$ is considered.

There are 6 independent pressure modes in N_h associated with the Stokes equations with Dirichlet boundary conditions. Since the Stokes equations with traction boundary conditions has the velocity space $\boldsymbol{M}_0^2(\mathcal{T}_h)$, all the 6 pressure modes are wiped out by the presence of $\boldsymbol{M}_0^2(\mathcal{T}_h)$. Hence, for the Stokes equations with traction boundary conditions, N_h only contains the zero function. Since there is no spurious pressure mode for the traction boundary condition problems, the inf–sup constant is positive on diagonal meshes. However, the element is unstable (see Theorem 4.1.1).

4.2.2. Spurious Modes Around a Singular Vertex

In this subsection, we prove that there is a locally supported spurious pressure mode associated with each singular vertex. More general results on irregular crisscross meshes appear in the next section.

We first consider the spurious pressure modes supported on a macroelement U, which is an arbitrary quadrilateral divided by its two diagonals (the first figure in Figure 4.8). Let a, b, c, and d denote the lengths of the interior edges of U. Without loss of generality, we assume that one diagonal of U lies on the x-axis (since rotations and translations do not change the dimension of N_h^U). This assumption simplifies the computations. If we denote the directions of the two diagonals by $\boldsymbol{n}_1 = (1,0)$ and $\boldsymbol{n}_2 = (n_1, n_2)$, then the coordinates of the four vertices of the quadrilateral U are given by

$$(a,0), \quad (bn_1, bn_2), \quad (-c,0), \text{ and } \quad (-dn_1, -dn_2).$$

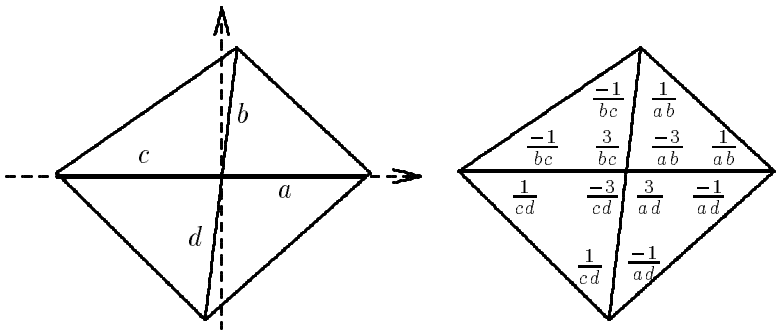

Figure 4.8. Macroelement U and spurious mode δ^U.

The following result is due to Morgan and Scott [19].

Lemma 4.2.2. *Let*

$$N_h(U) := \{p \in M_{-1}^{l-1}(U) \mid b(\boldsymbol{v}, p) = 0, \forall \boldsymbol{v} \in \boldsymbol{M}_0^l(U)\}.$$

Then for $l \geq 1$, $\dim N_h(U) = 1$.

For the $\mathcal{P}^2$–$\mathcal{P}^1$ element, we number all the vertices of U in a manner shown in the first figure of Figure 4.9. Any $\boldsymbol{u} \in \boldsymbol{M}_0^2(U)$ can be expressed as

$$\boldsymbol{u} = \sum_{i=1}^{13} (u_i, v_i)\phi_i,$$

where $(u_i, v_i) \in \mathbb{R}^2$, for $i = 1, 2, \ldots, 13$, and $\{\phi_i\}_{i=1}^{13}$ is the set of nodal basis functions. Let $p \in M_{-1}^1(U)$ be such that its values at the vertices of the four triangles of U are as shown in the second figure of Figure 4.9.

Our objective is to obtain a linear system of equations from $\int_U p \operatorname{div} \boldsymbol{u} = 0$ for any $\boldsymbol{u} \in \boldsymbol{M}_0^2(U)$. Obviously, the solutions of the system are the spurious pressure modes. This is a system of 26 equations in 12 unknowns and it has 6 parameters. It is difficult to find solutions of the system in this form. To this end, we first solve a subsystem corresponding to $\int_U p \operatorname{div} \boldsymbol{u} = 0$ for any $\boldsymbol{u} \in \mathring{\boldsymbol{M}}_0^2(U)$. Then, we substitute the solutions obtained from the subsystem into the system to find the solutions we want.

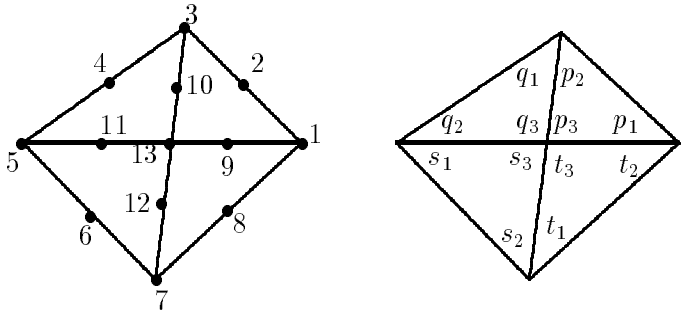

Figure 4.9. Vertices in $\mathcal{T}_h^U$ and values of p.

We set

$$0 = 6 \int_U p \operatorname{div} \boldsymbol{u} =: I_1 + I_2, \tag{4.2.4}$$

for any $\boldsymbol{u}_i = (u_i, v_i)$ for $i = 9, 10, \ldots, 13$, with

$$\begin{aligned} I_1 =& n_2(bp_1 - bp_3 + dt_2 - dt_3)u_9 + \\ & n_2(bp_1 + 2bp_2 + bp_3 - 2bq_1 - bq_2 - bq_3)u_{10} + \\ & n_2(-bq_2 + bq_3 - ds_1 + ds_3)u_{11} + \\ & n_2(-ds_1 - 2ds_2 - ds_3 + 2dt_1 + dt_2 + dt_3)u_{12} + \\ & n_2(bp_1 + bp_2 + bp_3 - bq_1 - bq_2 - bq_3 - ds_1 - ds_2 - ds_3 + dt_1 + dt_2 + dt_3)u_{13}, \end{aligned}$$

and

$$\begin{aligned} I_2 =& (2ap_1 + ap_2 + ap_3 - at_1 - 2at_2 - at_3 - n_1(bp_1 - bp_3 + dt_2 - dt_3))v_9 + \\ & (ap_2 - ap_3 + cq_1 - cq_3 - n_1(bp_1 + 2bp_2 + bp_3 - 2bq_1 - bq_2 - bq_3))v_{10} + \\ & (cq_1 + 2cq_2 + cq_3 - 2cs_1 - cs_2 - cs_3 - n_1(-bq_2 + bq_3 - ds_1 + ds_3))v_{11} + \\ & (-cs_2 + cs_3 - at_1 + at_3 - n_1(-ds_1 - 2ds_2 - ds_3 + 2dt_1 + dt_2 + dt_3))v_{12} + \\ & (ap_1 + ap_2 + ap_3 + cq_1 + cq_2 + cq_3 - cs_1 + -cs_2 - cs_3 - at_1 - at_2 - at_3 \\ & - n_1(bp_1 + bp_2 + bp_3 - bq_1 - bq_2 - bq_3 - ds_1 - ds_2 - ds_3 + dt_1 + dt_2 + dt_3))v_{13}. \end{aligned}$$

Since $n_2 \neq 0$, so the equations obtained from I_1 do not depend on n_2. Since each equation from I_2 contains a multiple of an equation from I_1 as a part, we can eliminate this part in each equation from I_2. Eventually, (4.2.4) implies that the system of equations obtained from I_1 and I_2 are independent of n_1 and n_2. This subsystem consists of 10 equations in 12 unknowns and it has 4 parameters, a, b, c, and d.

Solving the subsystem, we obtain two independent solutions. One is the constant vector 1, and the other, called δ^U, is shown in the second figure of Figure 4.8.

For some nonzero $\boldsymbol{u} \in \boldsymbol{M}_0^2(U)$, $\int_U \operatorname{div} \boldsymbol{u} \neq 0$. For all $\boldsymbol{u} \in \boldsymbol{M}_0^2(U)$, we have $\int_U \delta^U \operatorname{div} \boldsymbol{u} = 0$. Therefore, there is only one independent spurious pressure mode δ^U on U. The previous discussion proves the following theorem.

Theorem 4.2.2. *For any marcoelement U (see Figure 4.8), δ^U is a basis function for the space of spurious pressure modes supported by U.*

If a singular vertex lies on the boundary of a triangulation $\mathcal{T}_h$, it has to fall in one of the cases shown in Figure 4.10. The dark lines indicate the boundary edges. We call any singular vertices on the mesh boundary a boundary singular vertex. A boundary singular vertex contributes to spurious pressure modes if and only if any function in $\boldsymbol{V}_h$ vanishes on the two boundary edges which meet at the boundary singular vertex. Spurious pressure modes associated with a boundary singular vertex are multiples of the cut off of the mode shown in Figure 4.8.

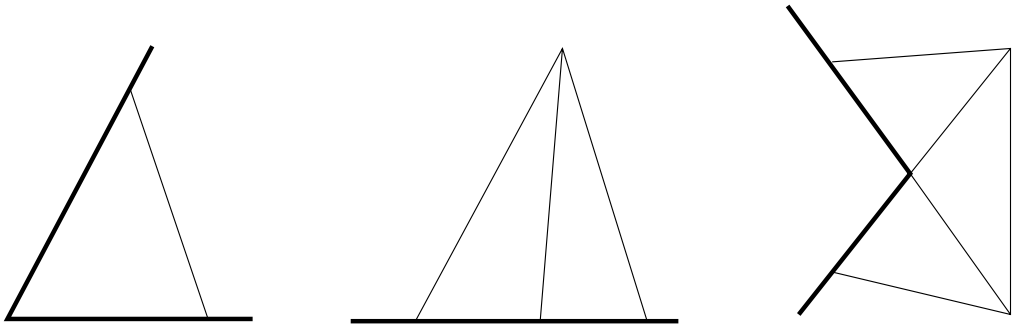

Figure 4.10. Different boundary singular vertices.

4.3. Stability and Approximability on Irregular Crisscross Meshes

In this section, we analyze the stability and approximation properties of the $\mathcal{P}^2$–$\mathcal{P}^1$ element on the irregular crisscross meshes. By Mercier's result, the finite element solution for velocity converges with optimal order to the true solution on this type of mesh. We show here that the $\mathcal{P}^2$–$\mathcal{P}^1$ element is reduced-stable on the irregular crisscross mesh and that the pressure can be recovered. This recovered pressure has an optimal rate of convergence.

Let Ω be a polygonal domain and $\mathcal{T}_h$ be a irregular crisscross mesh on Ω satisfying the regularity assumption (2.3.2) (see Figure 4.2). Singular vertices appear in every quadrilateral in $\mathcal{T}_h$. For convenience, we let σ denote the number of singular vertices in $\mathcal{T}_h$.

Theorem 4.3.1. *Let $\boldsymbol{V}_h := \mathring{\boldsymbol{M}}_0^2(\mathcal{T}_h)$ and $P_h := M_{-1}^1(\mathcal{T}_h)$. Then we have the following:*

(1) $\dim N_h = \sigma + 1$,

(2) *Consider a regular family of irregular crisscross meshes parametrized by h tending to zero. Then the reduced inf–sup constant $\bar{\gamma}_h \geq \alpha > 0$ with α independent of h.*

(3) *If $(\boldsymbol{u}_h, p_h)$ and $(\boldsymbol{u}_h, \bar{p}_h)$ are the numerical solutions from $\boldsymbol{V}_h \times P_h$ and $\boldsymbol{V}_h \times M_h$ respectively, then*

$$\|\boldsymbol{u} - \boldsymbol{u}_h\|_1 + \|p - \bar{p}_h\|_0 \leq Ch^2(\|\boldsymbol{u}\|_3 + \|p\|_2).$$

Here we assume $(\boldsymbol{u}, p) \in \boldsymbol{H}^3(\Omega) \times H^2(\Omega)$ is the solution of (2.1.1).

Proof. Let $\mathcal{U}_h$ denote a macroelement partition of $\mathcal{T}_h$ such that each macro U in $\mathcal{U}_h$ is a quadrilateral formed by four triangles of $\mathcal{T}_h$ and the only interior vertex of U is a singular vertex.

By Theorem 4.2.2, for each macroelement U in $\mathcal{U}_h$ there is a spurious pressure mode $\delta^U \in N_h$ with $\operatorname{spt} \delta^U = U$. Therefore, $\dim N_h \geq \sigma$. Since the global constant 1 is in N_h, we have

$$\dim N_h \geq \sigma + 1.$$

In order to prove (1), we need to show that, any $p \in N_h$ must be a linear combination of the constant function 1 and δ^U for some $U \in \mathcal{U}_h$. Let $p \in N_h$ be arbitrary. Since $\chi^U p \in N_h^U$, for each $U \in \mathcal{U}_h$, we have

$$\chi^U p = \beta_1^U \delta^U + \beta_2^U \chi^U.$$

Here β_1^U and β_2^U are two constants. Since δ^U is in N_h for each $U \in \mathcal{U}_h$, we need to show that $p - \sum_{U \in \mathcal{U}_h} \beta_1^U \delta^U = \sum_{U \in \mathcal{U}_h} \beta_2^U \chi^U$ is a constant. Namely, we need to prove that $\boldsymbol{V}_h \times M_{-1}^0(\mathcal{U}_h)$ has no spurious pressure modes. This is true since $\boldsymbol{V}_h \times M_{-1}^0(\mathcal{T}_h)$ is a stable finite element. This proves that any $p \in N_h$ is a linear combination of the constant function 1 and δ^U for some $U \in \mathcal{U}_h$. Hence, $\dim N_h = \sigma + 1$.

Since the mesh family is regular, all meshes of the family must satisfy the shape constraint (2.3.2) for some positive number θ independet of h. Let S_θ denote the set of all the macroelements of all $\mathcal{U}_h$'s for the meshes of the mesh family. Let the vertices of a macroelement $U \in S_\theta$ be numbered $u_1, \ldots, u_5$ such that u_5 is the singular vertex (see Figure 4.11). Since translations or dilations leave the reduced inf–sup constant unchanged, we assume $u_5 = (0, 0)$ and $\max_{\tau \in U}\{h_\tau\} = 1$ for any U in S_θ. Define

$$W = \{(u_1, \ldots, u_5) \mid U \in S_\theta)\},$$

then it is a closed set in $\mathbb{R}^{10}$.

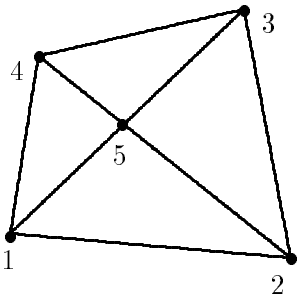

Figure 4.11. Macroelement U.

By Theorem 4.2.2, for any two macroelements U and $\hat{U}$ in S_θ, we have

$$\begin{aligned}
\dim \boldsymbol{V}_h^{\hat{U}} &= \dim \boldsymbol{V}_h^U = 10, \\
\dim N_h^{\hat{U}} &= \dim N_h^U = 2, \\
\dim P_h^{\hat{U}} &= \dim P_h^U = 12, \text{ and} \\
\dim M_h^{\hat{U}} &= \dim M_h^U = 10.
\end{aligned}$$

Therefore,

$$\bar{\gamma}_h^U(u_1, \ldots, u_5) = \sqrt{\lambda_3\big(M_U^{-1/2} B_U A_U^{-1} B_U^t M_U^{-1/2}\big)},$$

for any $U \in S_\theta$ (please see the relevant sections of Chapter 5). Since the entries of matrices M_U, A_U, and B_U depend continuously on vertices $u_1, \ldots, u_5$ of U, the reduced inf–sup constant $\bar{\gamma}^U$ must continuously depend on the vertices of U. Since W is a bounded closed domain, there is a positive number $\bar{\alpha}$ independent of h such that

$$\bar{\gamma}^U \geq \bar{\alpha}, \ \forall U \in S_\theta.$$

Since

$$Q_h = M_h \bigcap \sum_{U \in \mathcal{U}_h} N_h^U \subset M_{-1}^0(\mathcal{U}_h) \subset M_{-1}^0(\mathcal{T}_h),$$

and $\boldsymbol{V}_h \times M_{-1}^0(\mathcal{T}_h)$ is stable, there exists a $\beta > 0$ independent of h such that the inf–sup constant from $\boldsymbol{V}_h \times Q_h$ is greater than or equal to β. Let $\alpha = \min(\bar{\alpha}, \beta)$, then (2) follows by using the macroelement partition theorem.

By Theorem 2.2.1, we get

$$\|\boldsymbol{u} - \boldsymbol{u}_h\|_{1,\Omega} + \|p - \bar{p}_h\|_{0,\Omega} \leq C\big(\inf_{\boldsymbol{v} \in \boldsymbol{V}_h} \|\boldsymbol{u} - \boldsymbol{v}\|_{1,\Omega} + \inf_{q \in M_h} \|p - q\|_{0,\Omega}\big).$$

Now we analyze the approximation properties of the spaces M_h and $\boldsymbol{V}_h$. Obviously, $\boldsymbol{V}_h$ has optimal approximation properties. Since $M_{-1}^1(\mathcal{U}_h) \subset M_h$, M_h also has optimal approximation properties. If we assume that the solution $(\boldsymbol{u}, p)$ of (2.1.1) is in $\boldsymbol{H}^3(\Omega) \times H^2(\Omega)$, then (3) follows. $\square$

For irregular crisscross meshes it is also easy to compute $\bar{p}_h$ once a represent for p_h, which is determined modulo N_h, is known. This is done on each macroelement U by the formula

$$\bar{p}_h = p_h - \lambda^U \delta^U, \qquad \lambda^U = \frac{\int_U p_h \delta^U}{\int_U (\delta^U)^2}, \tag{4.3.1}$$

assuming that p_h has already been normalized to have mean value zero.

It is easy to see that for the Stokes equations with traction boundary conditions on irregular crisscross meshes $\dim N_h = \sigma$. By Theorem 3.4.3, Theorem 4.3.1 also holds for traction boundary condition problems with $\dim N_h = \sigma$.

4.4. Stability and Approximability on a Mixed Type of Meshes

We have seen that singular vertices play an important role in the approximation properties of numerical solutions. On the diagonal mesh (with no singular vertex except those at the two corners), the velocity has only suboptimal rate of convergence. On the other hand, for the crisscross mesh, the numerical solution is optimal for both the velocity and the pressure. In this section, we investigate the intermediate situation.

For convenience, we assume the domain Ω to be the unit square in this section. However, similar arguments can be carried out for more general domains.

We only consider a particular class of triangulations of the unit square Ω. Let $\mathcal{Q}_h$ denote the partition of Ω into n^2 equal subsquares of length $h = 1/n$ (with $n > 2$ an integer). The meshes $\mathcal{T}_h$ considered in this section are obtained from $\mathcal{Q}_h$ by subdividing each of the squares by some of their diagonals. Specifically, we assume that each square is either subdivided into two triangles by its positively sloped diagonal, which we will call a diagonal subdivision, or into four triangles by both its diagonals, a crisscross subdivision (see Figure 4.12). A mixed mesh is a mesh of diagonal and crisscross subdivisions.

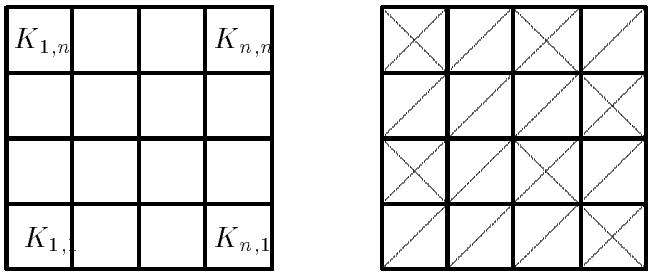

Figure 4.12. Mesh mixed with diagonals and crisscrosses.

If every square is subject to a diagonal subdivision, then N_h has dimension 6. From the work of de Boor and Höllig cited in subsection 4.1.1, we can deduce that even after eliminating the modes of N_h, the method is unstable. However, if every square is subdivided by two diagonals, then we have seen that the method is stable after the pressure modes associated with the singular vertices have been removed.

We now consider the case of mixed meshes. Our main result is that the $\mathcal{P}^2$–$\mathcal{P}^1$ method is stable on mixed mesh family after the removal of local pressure modes associated with the singular vertices, as long as the proportion of crisscross subdivisions is not vanishingly small in any part of the domain.

Let us call a macroelement from the triangulation $\mathcal{T}_h$ a k-square if it is a square of side kh. Thus, $\mathcal{Q}_h$ is the set of all 1-squares. Note that there must always be at least two singular vertices in the triangulation, since either the upper left and lower right corners are singular vertices, or the 1-squares containing them are crisscross subdivided and therefore contain singular vertices.

Again, we assume $\boldsymbol{V}_h := \mathring{\boldsymbol{M}}_0^2(\mathcal{T}_h)$ and $P_h := M_{-1}^1(\mathcal{T}_h)$. For convenience, we define

$$\mathcal{T}_h^D := \text{the diagonal mesh of the unit square, and}$$
$$\mathcal{T}_h^C := \text{the crisscross mesh of the unit square.}$$

Theorem 4.4.1. *Let $\mathcal{T}_h$ be a mixed mesh of the unit square. Let σ denote the number of singular vertices in $\mathcal{T}_h$.*

(1) *If $\sigma \geq 3$, then $\dim N_h = \sigma + 1$, and N_h is spanned by the constant function 1 and the locally supported pressure modes associated with the singular vertices.*

(2) *Consider a family of mixed meshes $\mathcal{T}_h$ parametrized by h tending to zero. Suppose that there exists a number k such that every k-square contains at least one 1-square which is crisscross subdivided. Then there exists a positive constant γ depending only on k such that $\bar{\gamma}_h \geq \gamma$.*

Proof. Let $U_1, U_2, \ldots, U_m$ denote all the $K_{i,j}$ of $\mathcal{Q}_h$ which have exactly one interior singular vertex, and let δ^{U_i} represent the spurious pressure modes on U_i for $i = 1, 2, \ldots, m$.

Let $p \in N_h$ be arbitrary. Define

$$\bar{p} := p - \sum_{i=1}^{k} \lambda^{U_i} \delta^{U_i},$$

where

$$\lambda^{U_i} = \frac{\int_{U_i} p\delta^{U_i}}{\int_{U_i} (\delta^{U_i})^2},$$

for $i = 1, 2, \ldots, m$. Clearly, $\bar{p}$ is in N_h.

Since $\chi^{U_i}\bar{p} \in N_h^{U_i}$, $\chi^{U_i}\bar{p} = \chi^{U_i} c_i$, for $i = 1, 2, \ldots, m$, with c_i a constant. Obviously,

$$\bar{p} \in N_h(\mathcal{T}_h^D).$$

Therefore,

$$\bar{p} = \sum_{i=1}^{6} \alpha_i \Psi_i,$$

where $\{\Psi_i\}_{i=1}^6$, defined in Theorem 4.2.1, is a basis for $N_h(\mathcal{T}_h^D)$.

Since there are at least three singular vertices in $\mathcal{T}_h$, we can assume that $U_1 = K_{i,j}$ with $(i,j) \neq (1,n)$ and $(i,j) \neq (n,1)$. On U_1, we have

$$c_1 = \alpha_1\Psi_1 + \alpha_2\Psi_2 + \alpha_3\Psi_3 + \alpha_6\Psi_6.$$

By the definitions of the Ψ_i, the above equation implies that $\alpha_1 = \alpha_2 = \alpha_3 = c_1$, and $\alpha_6 = 0$. That is,

$$\bar{p} = \alpha_4\Psi_4 + \alpha_5\Psi_5 + c_1.$$

Regarding the structure of $K_{1,n}$ or $K_{n,1}$, we have the following two cases.

Case 1. Neither of $K_{1,n}$ and $K_{n,1}$ contains an interior singular vertex.

In this case,

$$p = \alpha_4\Psi_4 + \alpha_5\Psi_5 + c_1 + \sum_{i=1}^{m} \lambda^{U_i}\delta^{U_i}.$$

Case 2. At least one of $K_{1,n}$ and $K_{n,1}$ contains an interior singular vertex.

Assume that only $U_2 = K_{1,n}$ is a crisscross subdivision. On U_2, we have

$$c_2 = \alpha_4 \Psi_4 + c_1,$$

which gives $c_2 = c_1$, and $\alpha_4 = 0$. Now we can conclude that

$$p = \alpha_5 \Psi_5 + c_1 + \sum_{i=1}^{m} \lambda^{U_i} \delta^{U_i}.$$

Similarly, if $K_{n,1}$ is a crisscross subdivision, then we have

$$p = \alpha_4 \Psi_4 + c_1 + \sum_{i=1}^{m} \lambda^{U_i} \delta^{U_i}.$$

If both $K_{1,n}$ and $K_{n,1}$ are crisscross subdivisions, then clearly we have

$$p = c_1 + \sum_{i=1}^{k} \lambda^{U_i} \delta^{U_i}.$$

Combining the cases 1 and 2, we proved (1).

The proof of the second part is based on the macroelement covering theorem with a slightly complicated choice of macroelements. We associate a macroelement U to each $(k+2)$-square S as follows. The vertices on the boundary of S are never singular, except possibly the vertices at the upper left and lower right corners of S, which are singular or not depending on whether a diagonal or crisscross subdivision is applied to the 1-square in S which contains them. If neither corner vertex is singular then we take $U = S$. If both corner vertices are singular we take $U = S \setminus (\tau_1 \cup \tau_2)$ where τ_1 and τ_2 are the triangles of $\mathcal{T}_h$ in S which contain these corners. If only one corner vertex is singular we only excise the corresponding triangle from S. But however for $K_{1,n}$ and $K_{n,1}$, we always keep them in U if S contains them. In this way we obtain a macroelement covering $\mathcal{U}_h$ which satisfies the overlap property. Figure 4.13 displays several macroelement configurations which may arise for $k = 2$.

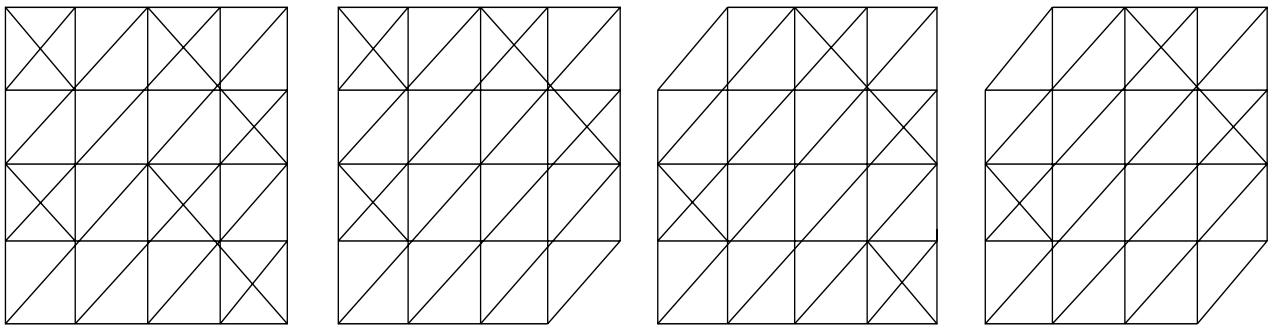

Figure 4.13. Different macroelement configurations.

Macroelements constructed in this way may differ due to which corners are excised and the particular pattern of diagonal and crisscross subdivisions. However, since k is a fixed integer, there is a fixed finite number of macroelement configurations such that every macroelement in $\mathcal{U}_h$, for any h, is obtained by dilation and translation from one of these. Since $\bar{\gamma}_h^U$ is invariant under dilation and translation, we can bound it from below by a positive number independent of h.

It remains to verify hypothesis (3.3.2) of the macroelement covering theorem. Every macroelement $U \in \mathcal{U}_h$ contains a k-square in its interior, and hence, by hypothesis, contains an interior 1-square which is crisscross subdivided. Reasoning as in the proof of the first part of the theorem, we find that N_h^U is spanned by χ^U and the locally supported pressure modes from the singular vertices. Thus hypothesis (3.3.2) holds. $\square$

Combining Theorem 4.4.1 and Theorem 2.2.1, we have the following theorem.

Theorem 4.4.2. *Let $(\boldsymbol{u}, p) \in \boldsymbol{H}^3(\Omega) \times H^2(\Omega)$ solve (2.1.1). Under the assumptions of Theorem 4.4.1, we have*

$$\|\boldsymbol{u} - \boldsymbol{u}_h\|_{1,\Omega} \leq C \inf_{\boldsymbol{v} \in \boldsymbol{V}_h} \|\boldsymbol{u} - \boldsymbol{v}\|_{1,\Omega} \leq Ch^2 \|\boldsymbol{u}\|_{3,\Omega}, \tag{4.4.1}$$

$$\|p - \bar{p}_h\|_{0,\Omega} \leq Ch^2 \|\boldsymbol{u}\|_{3,\Omega} + C \inf_{q \in M_h} \|p - q\|_{0,\Omega}. \tag{4.4.2}$$

Moreover, if $K_{1,n}$ and $K_{n,1}$ are crisscross subdivisions, then

$$\|p - \bar{p}_h\|_{0,\Omega} \leq Ch^2 (\|\boldsymbol{u}\|_{3,\Omega} + \|p\|_{2,\Omega}). \tag{4.4.3}$$

If $K_{1,n}$ and $K_{n,1}$ are crisscross subdivisions, then $M_{-1}^1(\mathcal{Q}_h) \subset M_h$, and we can obtain (4.4.3) from (4.4.2). If p is orthogonal to the spurious pressure modes associated with the boundary singular vertices in $\mathcal{T}_h$, then p can again be approximated by $\bar{p}_h \in M_h$ with an optimal order. We do not know the approximation properties of $\bar{p}_h$ if p is not orthogonal to the spurious pressure modes associated with the boundary singular vertices in $\mathcal{T}_h$,

The recovery of the pressure is completely similar to that for irregular crisscross meshes. Therefore, $\bar{p}_h$ can be computed from p_h by an inexpensive postprocess.

For this mixed mesh family, the finite element velocity space for the Stokes equations with traction boundary conditions makes the spurious modes around the boundary singular vertices and the global constant functions in N_h disappear. Therefore, the dimension of the kernel of the discrete gradient operator is equal to the number of all the interior singular vertices in $\mathcal{T}_h$. Applying the subspace theorem a few times and combining the results in Theorem 4.4.1 and 4.4.2, we have the following theorem for the Stokes equations with traction boundary conditions.

Theorem 4.4.3. *Assume $\boldsymbol{V}_h := \boldsymbol{M}_0^2(\mathcal{T}_h)$ and $P_h := M_{-1}^1(\mathcal{T}_h)$. Suppose that the $\mathcal{T}_h$ is a mixed mesh on the unit square, and that $(\boldsymbol{u}, p) \in \boldsymbol{H}^3(\Omega) \times H^2(\Omega)$ solves (2.1.1). Then we have,*

(1) $\dim N_h$ *is the number of all interior singular vertices in $\mathcal{T}_h$.*

(2) *Consider a family of mixed mesh $\mathcal{T}_h$, parametrized by h tending to zero, on the unit square. Suppose that there exists a number k such that every k-square contains at least one 1-square which is crisscross subdivided. Then the element is reduced stable for this mesh family, and furthermore,*

$$\|\boldsymbol{u} - \boldsymbol{u}_h\|_{1,\Omega} + \|p - \bar{p}_h\|_{0,\Omega} \leq Ch^2 (\|\boldsymbol{u}\|_{3,\Omega} + \|p\|_{2,\Omega}).$$

4.5. Stability and Approximability on Distorted Crisscross Meshes

It might appear that singular vertices are responsible for the good performance of the $\mathcal{P}^2$–$\mathcal{P}^1$ finite element method on the crisscross mesh family. However, this is not the whole story. In this section, we will display a sequence of distorted crisscross meshes for the unit square such that the

$\mathcal{P}^2$–$\mathcal{P}^1$ element is stable and has optimal rate of convergence for both the velocity and the pressure. These meshes have no singular vertices.

Let $\mathcal{Q}_h$ denote the partition of the unit square Ω into $n \times n$ ($h = 1/n$) equal small squares. Let $\mathcal{T}_h$ be obtained from $\mathcal{Q}_h$ by dividing each small square of $\mathcal{Q}_h$ into 4 triangles as shown in the first figure of Figure 4.14. This is equivalent to moving the interior vertex of a crisscross subdivision vertically down a fixed distance, for instance $h/4$. A small square with such a division is called a distorted crisscross subdivision.

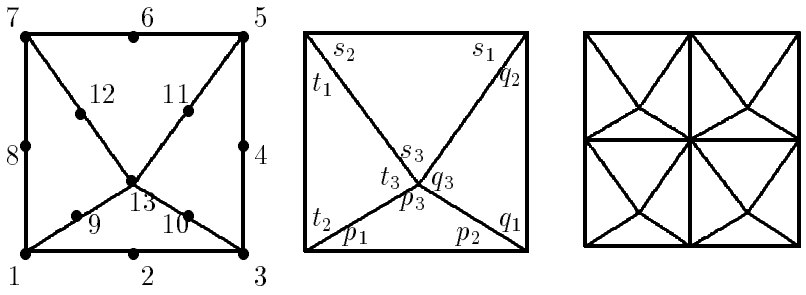

Figure 4.14. Macroelement.

Let $\mathcal{U}_h$ be a macroelement covering of $\mathcal{T}_h$ such that any 2×2 distorted crisscross subdivisions (four small squares) of $\mathcal{T}_h$ form a macroelement in $\mathcal{U}_h$ (see the third figure of Figure 4.14). We will prove that $\boldsymbol{V}_h \times P_h$ is stable and that $\dim N_h = 1$.

In order to prove that $\dim N_h = 1$, we first show that N_h^U only contains constant functions for any U in $\mathcal{U}_h$. If this is the case, then we have, for any p in N_h, $\chi^U p$ is a constant for any U in $\mathcal{U}_h$. Since $\mathcal{U}_h$ is a macroelement covering satisfying the overlap property, p must be a constant on the whole domain.

We figure out the spurious pressure modes on a single distorted crisscross subdivided square S first. We assume that the vertices in S have coordinates $(0,0)$, $(1,0)$, $(1,1)$, $(0,1)$, and $(0.5,t)$. Let $\boldsymbol{u} \in \boldsymbol{V}_h^S$ be expressed as

$$\boldsymbol{u} = \sum_{i=9}^{13} (u_i, v_i)\phi_i$$

and $p \in P_h^S$ in the manner shown in the second figure of Figure 4.14. Set

$$\begin{aligned}
6\int_S p \operatorname{div} \boldsymbol{u} = {} & (-tp_1 - tp_2 - 2tp_3 + tt_1 + t_2 + tt_2 - t_3 + 2tt_3)u_9 + \\
& (tp_1 + tp_2 + 2tp_3 - q_1 - tq_1 - tq_2 + q_3 - 2tq_3)u_{10} + \\
& (-q_1 + tq_1 - 2q_2 + tq_2 - q_3 + 2tq_3 + s_1 - ts_1 + s_2 - ts_2 + 2s_3 - 2ts_3)u_{11} + \\
& (-s_1 + ts_1 - s_2 + ts_2 - 2s_3 + 2ts_3 + 2t_1 - tt_1 + t_2 - tt_2 + t_3 - 2tt_3)u_{12} + \\
& (-q_1 - q_2 - q_3 + t_1 + t_2 + t_3)u_{13} + \\
& (3p_1 + p_2 - t_1 - t_2 - 2t_3)v_9/2 + \\
& (p_1 + 3p_2 - q_1 - q_2 - 2q_3)v_{10}/2 + \\
& (q_1 + q_2 + 2q_3 - 3s_1 - s_2)v_{11}/2 + \\
& (-s_1 - 3s_2 + t_1 + t_2 + 2t_3)v_{12}/2 + \\
& (p_1 + p_2 + p_3 - s_1 - s_2 - s_3)v_{13} = 0,
\end{aligned}$$

for any (u_i, v_i) for $i = 9, 10, 11, 12, 13$. Solving the system that results from the above equality, we find two independent solutions. One is $p_1^S = 1$ and the other one is p_2^S with

$$\begin{array}{lll} p_1 = 1-3t, & p_2 = 1-3t, & p_3 = 3-3t, \\ q_1 = t, & q_2 = 4-7t, & q_3 = -3t, \\ s_1 = 1-3t, & s_2 = 1-3t, & s_3 = 3-3t, \\ t_1 = 4-7t, & t_2 = t, & t_3 = -3t, \end{array}$$

where $0 < t < 1/2$ or $1/2 < t < 1$.

For any $p \in N_h$, $\chi^S p$ is a linear combination of p_1^S and p_2^S. Moreover, for any $U \in \mathcal{U}_h$, $\chi^U p$ is a linear combination of 8 functions. By some algebraic manipulations, we can verify that $\chi^U p$ must be a constant.

Thus we have proved that $\dim N_h^U = 1$ for any $U \in \mathcal{U}_h$. Consequently, we have $\dim N_h = 1$.

Theorem 4.5.1.

(1) *Suppose that the triangulation $\mathcal{T}_h$ is obtained from $\mathcal{Q}_h$ by partition each small square in $\mathcal{Q}_h$ with a same distorted crisscross subdivision. Then N_h only contains constant functions.*

(2) *Consider a family of such triangulations $\mathcal{T}_h$ parametrized by h tending to zero. Then $\boldsymbol{V}_h \times P_h$ is stable and*

$$\|\boldsymbol{u} - \boldsymbol{u}_h\|_{1,\Omega} + \|p - p_h\|_{0,\Omega} \le Ch^2(\|\boldsymbol{u}\|_{3,\Omega} + \|p\|_{2,\Omega}).$$

Here we assume $(\boldsymbol{u}, p) \in \boldsymbol{H}^3(\Omega) \times H^2(\Omega)$ is the solution of (2.1.1).

Proof. Since all the macroelements in $\mathcal{U}_h$ are translations or dilations of a distorted crisscross subdivision for all meshes $\mathcal{T}_h$, we have a common positive lower bound independent of h for all the local reduced inf–sup constants. Further, since $\boldsymbol{V}_h$ contains $\mathring{\boldsymbol{M}}_0^1$, all the conditions in the macroelement covering theorem hold. This proves that $\boldsymbol{V}_h \times P_h$ is stable and

$$\|\boldsymbol{u} - \boldsymbol{u}_h\|_{1,\Omega} + \|p - p_h\|_{0,\Omega} \le Ch^2(\|\boldsymbol{u}\|_{3,\Omega} + \|p\|_{2,\Omega}). \quad \square$$

Remark 4.5.1. *Let $\mathcal{T}_h$ be a distorted crisscross mesh obtained from a crisscross mesh by distorting each square of the crisscross mesh in exactly the same way. Then we can prove that the element is stable on $\mathcal{T}_h$ and has optimal rates of convergence for the velocity and the pressure.*

Distorted crisscross meshes are better than crisscross meshes in the sense of stability. Both types of meshes have exactly the same topological structure, but one has a lot of spurious pressure modes, while the other one doesn't have any. We conclude that spurious pressure modes can be removed by distorting the mesh.

4.6. Stability and Approximability on Barycentric Trisected Meshes

In this section, we examine the $\mathcal{P}^2$–$\mathcal{P}1$ finite element method on barycentric trisected triangulations. We show that there are no spurious pressure modes on this type of mesh, and moreover, the method is stable. Consequently, the rates of convergence for velocity and pressure are both optimal.

A barycentric trisected triangulation $\mathcal{T}_h$ is obtained from a arbitrary triangulation $\mathcal{S}_h$ of a polygonal domain Ω by connecting the three vertices of each triangle in $\mathcal{S}_h$ to its barycenter (see the third figure in Figure 4.15).

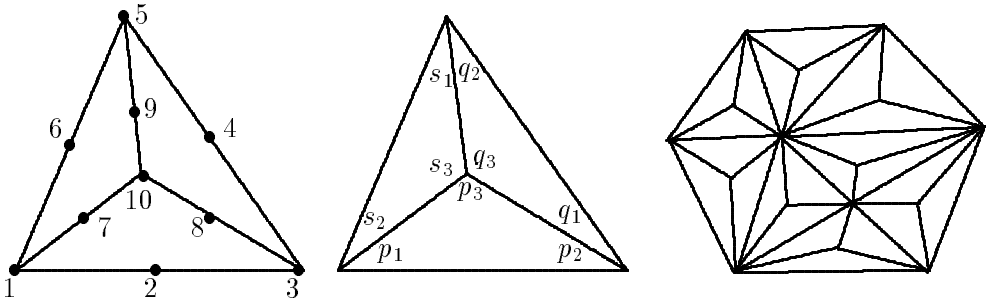

Figure 4.15. Barycentric trisected partition.

We will prove the stability and approximability of the $\mathcal{P}^2$–$\mathcal{P}^1$ element on this barycentric trisected mesh family by using the macroelement partition theorem. Let $\mathcal{U}_h$ be a macroelement partition of $\mathcal{T}_h$ such that each macroelement U in $\mathcal{U}_h$ is a triangle in $\mathcal{S}_h$. In order to use the macroelement partition theorem, we first need to show that there is a common positive lower bound independent of h for the local inf–sup constant $\bar{\gamma}_h^U$ for all U in $\mathcal{U}_h$, and secondly to prove that the inf–sup constant for $\boldsymbol{V}_h \times (M_h \cap \Sigma_{U\in\mathcal{U}_h} N_h^U)$ is bounded away from 0.

Pick any U in $\mathcal{U}_h$, and let the vertices of U be numbered in the manner shown in the first figure of Figure 4.15. Any $\boldsymbol{u} \in \boldsymbol{V}_h^U$ can be expressed as

$$\boldsymbol{u} = \sum_{i=7}^{10} (u_i, v_i)\phi_i,$$

where ϕ_i, $i = 7, 8, 9, 10$, are nodal basis functions.

We denote the values of p in P_h^U at the vertices of the triangles of U in the manner shown in the second figure of Figure 4.15.

It is clear that $\mathcal{U}_h \subset E(U, F)$, where F is the set of all invertible linear mappings. Without loss of generality, we assume that the vertices 1, 2, and 3 of U have coordinates $(0,0)$, $(1,0)$, and $(0,1)$ respectively.

If $\mathcal{T}_h$ satisfies (2.3.2), then by Lemma 3.5.4 there is a positive lower bound α^U independent of h, such that

$$\bar{\gamma}_h^{\hat{U}} \geq \alpha^U, \quad \forall \hat{U} \in E_\theta(U, F).$$

Let $p \in N_h^U$ be arbitrary. For any $\boldsymbol{u} \in \boldsymbol{V}_h^U$, we have

$$\begin{aligned} 18 \int_U p \operatorname{div} \boldsymbol{u} =& (-p_1 - p_2 - 2p_3 + s_1 + 4s_2 - s_3)u_7 + \\ & (p_1 + p_2 + 2p_3 - 4q_1 - q_2 + q_3)u_8 + \\ & (-2q_1 - 5q_2 - q_3 + 5s_1 + 2s_2 + s_3)u_9 + \\ & (-3q_1 - 3q_2 - 3q_3 + 3s_1 + 3s_2 + 3s_3)u_{10} + \\ & (4p_1 + p_2 - p_3 - s_1 - s_2 - 2s_3)v_7 + \\ & (2p_1 + 5p_2 + p_3 - 5q_1 - 2q_2 - q_3)v_8 + \\ & (-q_1 - 4q_2 + q_3 + s_1 + s_2 + 2s_3)v_9 + \\ & (3p_1 + 3p_2 + 3p_3 - 3q_1 - 3q_2 - 3q_3)v_{10} = 0. \end{aligned} \tag{4.6.1}$$

Solving the linear system obtained from (4.6.1), we have

$$p_1 = p_2 = p_3 = q_1 = q_2 = q_3 = s_1 = s_2 = s_3.$$

Hence, N_h^U is the one dimensional space of constant functions. By Lemma 3.5.1, we know that for any $\hat{U}$ in $\mathcal{U}_h$, $N_h^{\hat{U}}$ contains only the constant functions. If p is in N_h, then p is in $N_h(\mathcal{U}_h)$ since $\chi^{\hat{U}} p \in Nh^{\hat{U}}$ is a constant for $\hat{U}$ in $\mathcal{U}_h$. Since $\boldsymbol{V}_h \times M_{-1}^0(\mathcal{T}_h)$ is stable, $\boldsymbol{V}_h \times M_{-1}^0(\mathcal{U}_h)$ is stable, and therefore $N_h(\mathcal{U}_h)$ contains only the constant functions. We know that

$$\boldsymbol{V}_h \times (M_h \bigcap \sum_{U \in \mathcal{U}_h} N_h^U) = \boldsymbol{V}_h \times (\hat{P}_h \bigcap \sum_{U \in \mathcal{U}_h} N_h^U) = \boldsymbol{V}_h \times \hat{M}_{-1}^0(\mathcal{U}_h),$$

and therefore $\boldsymbol{V}_h \times (M_h \cap \Sigma_{U \in \mathcal{U}_h} N_h^U)$ is stable.

From the above discussions, we have that $\boldsymbol{V}_h \times P_h$ is stable on $\mathcal{T}_h$. Furthermore, since the finite element space $\boldsymbol{V}_h \times P_h$ has optimal approximation properties, the following theorem holds.

Theorem 4.6.1.

(1) *If the mesh $\mathcal{T}_h$ is a barycentric trisected triangulation, then N_h only consists of constant functions.*

(2) *Consider a regular family of barycentric trisected meshes $\mathcal{T}_h$ parametrized by h tending to zero. Then $\boldsymbol{V}_h \times P_h$ is stable and*

$$\begin{aligned} \|\boldsymbol{u} - \boldsymbol{u}_h\|_{1,\Omega} &\leq C \inf_{\boldsymbol{v} \in \boldsymbol{V}_h} \|\boldsymbol{u} - \boldsymbol{v}\|_{1,\Omega} \leq Ch^2 \|\boldsymbol{u}\|_{3,\Omega}, \\ \|p - p_h\|_{0,\Omega} &\leq Ch^2 \|\boldsymbol{u}\|_{3,\Omega} + C \inf_{q \in M_h} \|p - q\|_{0,\Omega} \leq Ch^2 (\|\boldsymbol{u}\|_{3,\Omega} + \|p\|_{2,\Omega}). \end{aligned}$$

Here we assume $(\boldsymbol{u}, p) \in \boldsymbol{H}^3(\Omega) \times H^2(\Omega)$ is the solution of (2.1.1).

Remark 4.6.1. *Actually, we can prove similar results by almost the same arguments as we used in this section for any triangulation $\mathcal{T}_h$ formed by connecting the three vertices of each triangle of $\mathcal{S}_h$ to any interior point such that $\mathcal{T}_h$ satisfies the condition (2.3.2).*

Remark 4.6.2. *Following the idea in the Section 4, we consider a mixed type of meshes of the unit square from the square partition $\mathcal{Q}_h$ (see the definition in the Section 4) by refining each square of $\mathcal{Q}_h$ with either a diagonal subdivision or a barycentric trisected subdivision. A barycentric trisected subdivision is the barycentric trisected parttition of a diagonal subdivision. Then the only spurious pressure modes are from the corner verices. We can prove similar results as stated in Theorem 4.4.1, Theorem 4.4.2, and Theorem 4.4.3 for this type of meshes.*

Chapter 5

NUMERICAL COMPUTATIONS ON THE $\mathcal{P}^2$–$\mathcal{P}^1$ ELEMENT

This chapter contains two classes of numerical computations on the $\mathcal{P}^2$–$\mathcal{P}^1$ element for the Stokes equations. One class is on the stability (or reduced stability) of the $\mathcal{P}^2$–$\mathcal{P}^1$ element, and the other is on rates of convergence of numerical solutions.

Supporting the theoretical analysis of the $\mathcal{P}^2$–$\mathcal{P}^1$ element in Chapter 4, numerical results presented in this chapter reflect that the performance of the element depends on mesh configurations. We do numerical computations not only on the meshes for which we understand theoretically, but also on some meshes for which we do not have theoretical results.

In Section 1, we introduce an eigenproblem and its variations associated with the inf–sup constant of a mixed finite element. In Section 2, we discuss some properties of the eigenproblem on both the continuous and the discrete level. In Section 3, we present a model problem to be employed in our numerical computations for testing rates of convergence of numerical solutions. Finally, we present some analysis, tables, and figures for different mesh configurations in Section 4.

5.1. An Eigenproblem Associated with the inf–sup Condition

The stability of a mixed finite element method for the Stokes equations can be studied by investigating some eigenvalues of an associated eigenproblem. In this section, we will show that the inf–sup or reduced inf–sup constant is equal to the square root of a certain eigenvalue of an eigenproblem.

As usual, we denote the finite element velocity space by $\boldsymbol{V}_h$ and the pressure space by P_h. Spaces N_h and M_h are defined as in (2.4.1). Let $\{\boldsymbol{\psi}_i\}_{i=1}^n$ be a basis of $\boldsymbol{V}_h$, $\{\phi_i\}_{i=1}^l$ be a basis of N_h, and $\{\phi_i\}_{i=l+1}^m$ be a basis of M_h. For convenience, we set $k = m - l$, and make the following definitions.

$$
\begin{aligned}
A &:= \Big(\int_\Omega \nabla\boldsymbol{\psi}_i : \nabla\boldsymbol{\psi}_j + \int_\Omega \boldsymbol{\psi}_i \cdot \boldsymbol{\psi}_j\Big)_{1\le i,j\le n},\\
B_N^t &:= \Big(\int_\Omega \phi_i \operatorname{div}\boldsymbol{\psi}_j\Big)_{\substack{1\le j\le n\\ 1\le i\le l}} = 0_{n\times l},\\
B_M^t &:= \Big(\int_\Omega \phi_{i+l} \operatorname{div}\boldsymbol{\psi}_j\Big)_{\substack{1\le j\le n\\ 1\le i\le k}},\\
M_N &:= \Big(\int_\Omega \phi_i\phi_j\Big)_{1\le i,j\le l},\\
M_M &:= \Big(\int_\Omega \phi_{i+l}\phi_{j+l}\Big)_{1\le i,j\le k},\\
B^t &:= \begin{pmatrix} B_N^t & B_M^t \end{pmatrix},\\
M &:= \begin{pmatrix} M_N & 0\\ 0 & M_M \end{pmatrix}.
\end{aligned}
\tag{5.1.1}
$$

Clearly, matrices A, M_N, and M_M are symmetric positive definite, and matrix B_M^t has a full column rank. The following lemma describes a relation between the reduced inf–sup constant and the minimum eigenvalue of a matrix.

Lemma 5.1.1. *Using the definitions* (5.1.1), *we have*

$$
\bar{\gamma}_h := \inf_{0\neq p\in M_h}\sup_{0\neq \boldsymbol{v}\in \boldsymbol{V}_h} \frac{\int_\Omega p \operatorname{div}\boldsymbol{v}}{\|\boldsymbol{v}\|_{1,\Omega}\|p\|_{0,\Omega}} = \sqrt{\lambda_{\min}(M_M^{-\frac{1}{2}} B_M A^{-1} B_M^t M_M^{-\frac{1}{2}})},
$$

where $M_M^{-\frac{1}{2}} M_M^{-\frac{1}{2}} =: M_M^{-1}$ *and* $\lambda_{min}(M_M^{-\frac{1}{2}} B_M A^{-1} B_M^t M_M^{-\frac{1}{2}})$ *denotes the smallest eigenvalue of the matrix.*

Proof. By the definition of $\bar{\gamma}_h$, we have

$$\begin{aligned}
\bar{\gamma}_h &= \inf_{0\neq\beta\in\mathbb{R}^k} \sup_{0\neq\alpha\in\mathbb{R}^n} \frac{(\alpha, B_M^t\beta)}{(A\alpha,\alpha)^{1/2}(M_M\beta,\beta)^{1/2}} \\
&= \inf_{0\neq\beta\in\mathbb{R}^k} \sup_{0\neq\bar{\alpha}=A^{1/2}\alpha\in\mathbb{R}^n} \frac{(\bar{\alpha}, A^{-1/2}B_M^t\beta)}{(\bar{\alpha},\bar{\alpha})^{1/2}(M_M\beta,\beta)^{1/2}} \\
&= \inf_{0\neq\beta\in\mathbb{R}^k} \frac{(A^{-1/2}B_M^t\beta, A^{-1/2}B_M^t\beta)^{1/2}}{(M_M\beta,\beta)^{1/2}} \\
&= \inf_{0\neq\bar{\beta}=M_M^{1/2}\beta\in\mathbb{R}^k} \frac{(A^{-1/2}B_M^tM_M^{-1/2}\bar{\beta}, A^{-1/2}B_M^tM_M^{-1/2}\bar{\beta})^{1/2}}{(\bar{\beta},\bar{\beta})^{1/2}} \\
&= \sqrt{\lambda_{\min}(M_M^{-\frac{1}{2}}B_MA^{-1}B_M^tM_M^{-\frac{1}{2}})}. \quad \square
\end{aligned}$$

It is difficult to figure out the structure of the spaces N_h and M_h in most cases. Fortunately, the reduced inf–sup constant can be computed directly from the matrices A, B, and M.

Theorem 5.1.1. *Let $\lambda_1 \le \lambda_2 \le \cdots \le \lambda_m$ denote all the eigenvalues of the matrix $M^{-\frac{1}{2}}BA^{-1}B^tM^{-\frac{1}{2}}$. Then $\lambda_1 = \lambda_2 = \cdots = \lambda_l = 0$ and*

$$\bar{\gamma}_h = \sqrt{\lambda_{l+1}} > 0.$$

Proof. Simple calculations show that the generalized eigenproblem

$$\begin{pmatrix} A & B^t \\ B & 0 \end{pmatrix}\begin{pmatrix} u \\ p \end{pmatrix} = \lambda\begin{pmatrix} 0 & 0 \\ 0 & -M \end{pmatrix}\begin{pmatrix} u \\ p \end{pmatrix}, \tag{5.1.2}$$

and the eigenproblem

$$M^{-\frac{1}{2}}BA^{-1}B^tM^{-\frac{1}{2}}p = \lambda p, \tag{5.1.3}$$

have exactly the same set of eigenvalues. Similar calculations show that the eigenvalues from

$$\begin{pmatrix} A & B_M^t \\ B_M & 0 \end{pmatrix}\begin{pmatrix} u \\ \bar{p} \end{pmatrix} = \lambda\begin{pmatrix} 0 & 0 \\ 0 & -M_M \end{pmatrix}\begin{pmatrix} u \\ \bar{p} \end{pmatrix}, \tag{5.1.4}$$

and the eigenvalues from

$$M_M^{-\frac{1}{2}}B_MA^{-1}B_M^tM_M^{-\frac{1}{2}}\bar{p} = \lambda\bar{p}, \tag{5.1.5}$$

are the same. Moreover, neither (5.1.4) or (5.1.5) has zero eigenvalues.

By definitions of B and M, if we set

$$p := \begin{pmatrix} p_N \\ p_M \end{pmatrix},$$

then eigenproblem (5.1.2) is equivalent to

$$\begin{pmatrix} Au + B_M^tp_M \\ 0 \\ B_Mu \end{pmatrix} = \lambda\begin{pmatrix} 0 \\ -M_Np_N \\ -M_Mp_M \end{pmatrix}.$$

Clearly, eigenproblems (5.1.2) and (5.1.4) have the same nonzero eigenvalues. That is, eigenproblems (5.1.3) and (5.1.5) have the same nonzero eigenvalues. Since $\dim N_h = l$, eigenproblem (5.1.3) has exactly l zero eigenvalues. The above arguments show that

$$\lambda_{l+1} = \lambda_{\min}(M_M^{-\frac{1}{2}} B_M A^{-1} B_M^t M_M^{-\frac{1}{2}}),$$

where

$$\lambda_1 = \lambda_2 = \cdots = \lambda_l = 0.$$

By Lemma 5.1.1, the proof is complete. □

For any invertible matrices $T \in \mathbb{R}^{m\times m}$ and $Q \in \mathbb{R}^{n\times n}$, since

$$\begin{aligned}
M^{-\frac{1}{2}} B A^{-1} B^t M^{-\frac{1}{2}} p &= \lambda p \\
&\Longleftrightarrow B A^{-1} B^t \bar{p} = \lambda M \bar{p} && \text{with } \bar{p} = M^{-\frac{1}{2}} p \\
&\Longleftrightarrow B A^{-1} B^t T \tilde{p} = \lambda M T \tilde{p} && \text{with } \tilde{p} = T^{-1} \bar{p} \\
&\Longleftrightarrow T^t B A^{-1} B^t T \tilde{p} = \lambda T^t M T \tilde{p} \\
&\Longleftrightarrow (T^t B Q)(Q^t A Q)^{-1}(Q^t B^t T)\tilde{p} = \lambda (T^t M T)\tilde{p},
\end{aligned}$$

the statement of Theorem 5.1.1 holds for any choice of basis functions for $\boldsymbol{V}_h$ or P_h.

The following statements are useful in practical computations.

Lemma 5.1.2. *Using the definitions, the nonzero eigenvalue of the following eigenproblems are equal.*

(1) $M^{-\frac{1}{2}} B A^{-1} B^t M^{-\frac{1}{2}} p = \lambda p$.
(2) $A^{-\frac{1}{2}} B^t M^{-1} B A^{-\frac{1}{2}} u = \lambda u$.
(3) $B A^{-1} B^t p = \lambda M p$.
(4) $B^t M^{-1} B u = \lambda A u$.
(5)
$$\begin{pmatrix} A & B^t \\ B & 0 \end{pmatrix} \begin{pmatrix} u \\ p \end{pmatrix} = \lambda \begin{pmatrix} 0 & 0 \\ 0 & -M \end{pmatrix} \begin{pmatrix} u \\ p \end{pmatrix}.$$
(6)
$$\begin{pmatrix} A & B^t \\ B & \alpha M \end{pmatrix} \begin{pmatrix} u \\ p \end{pmatrix} = (\lambda - \alpha) \begin{pmatrix} 0 & 0 \\ 0 & -M \end{pmatrix} \begin{pmatrix} u \\ p \end{pmatrix},$$
with $\alpha > 0$ such that
$$\begin{pmatrix} A & B^t \\ B & \alpha M \end{pmatrix}$$
is symmetric positive definite.

Proof. (1)$\Longleftrightarrow$(3), (2)$\Longleftrightarrow$(4), (5)$\Longleftrightarrow$(6), (3)$\Longleftrightarrow$(5), and (4)$\Longleftrightarrow$(5) are immediate. This proves the lemma. □

The eigenproblems (1), (2), (3), and (4) in the above lemma involve inverses of matrices, but the size of each problem is small. In contrast, (5) and (6) do not contain the inverse of any matrix, but their size is large.

In our computations, we used LAPACK to solve the generalized eigenproblem

$$B A^{-1} B^t p = \lambda M p, \tag{5.1.6}$$

from the $\mathcal{P}^2$–$\mathcal{P}^1$ element on the unit square. Two velocity spaces $\boldsymbol{V}_h := \mathring{\boldsymbol{M}}_0^2(\mathcal{T}_h)$ and $\boldsymbol{V}_h := \boldsymbol{M}_0^2(\mathcal{T}_h)$ were tested on various mesh configurations.

If the finite element velocity space $\boldsymbol{V}_h$ is a subspace of $\mathring{\boldsymbol{H}}^1(\Omega)$, then we use $|\cdot|_{1,\Omega}$ as the norm in the analysis. Therefore, the corresponding reduced inf–sup constant is defined by

$$\bar{\gamma}_h = \inf_{0\neq p\in M_h} \sup_{0\neq \boldsymbol{v}\in \boldsymbol{V}_h} \frac{\int_\Omega p \operatorname{div} \boldsymbol{v}}{|\boldsymbol{v}|_{1,\Omega}\|p\|_{0,\Omega}},$$

and the matrix A is defined by

$$A = \Big(\int_\Omega \nabla \boldsymbol{\psi}_i : \nabla \boldsymbol{\psi}_j\Big)_{1\le i,j\le n}. \tag{5.1.7}$$

5.2. Properties of an Eigenproblem

In this section, we discuss some properties of the eigenproblem

$$\begin{pmatrix} A & B^t \\ B & 0 \end{pmatrix}\begin{pmatrix} u \\ p \end{pmatrix} = \lambda \begin{pmatrix} 0 & 0 \\ 0 & -M \end{pmatrix}\begin{pmatrix} u \\ p \end{pmatrix}, \tag{5.2.1}$$

which is associated with the inf–sup constant of a finite element $\boldsymbol{V}_h \times P_h$. Here $\boldsymbol{V}_h$ is a subspace of $\mathring{\boldsymbol{H}}^1(\Omega)$ and the matrix A is defined as in (5.1.7). These properties are not essential to the stability analysis or to the numerical computations in this thesis, but we include them here for integrity.

On the discrete level, (5.2.1) corresponds to

$$\begin{aligned} a(\boldsymbol{u},\boldsymbol{v}) + b(\boldsymbol{v},p) &= 0 \quad \forall \boldsymbol{v}\in \boldsymbol{V}_h, \\ b(\boldsymbol{u},q) &= -\lambda(p,q) \quad \forall q \in P_h. \end{aligned} \tag{5.2.2}$$

On the continuous level, we have

$$\begin{aligned} \Delta \boldsymbol{u} + \nabla p &= 0, \\ \operatorname{div} \boldsymbol{u} &= -\lambda p, \\ \boldsymbol{u}|_{\partial\Omega} &= 0. \end{aligned} \tag{5.2.3}$$

Here $\boldsymbol{u} \in \boldsymbol{V} := \mathring{\boldsymbol{H}}^1(\Omega)$ and $p \in \mathcal{P} := L^2(\Omega)$. If $\lambda = 0$ in (5.2.3), then $\operatorname{div} \boldsymbol{u} = 0$. Therefore, divergence free functions are eigenfunctions of (5.2.3) corresponding to $\lambda = 0$. The following theorem describes some properties of the eigenproblem (5.2.3).

Theorem 5.2.1. *If λ is an eigenvalue of* (5.2.3)*, then*

(1) $1-\lambda$ *is a slso an eigenvalue, and moreover,*
(2) $\lambda \in [0,1]$.

Proof. We only need to show that (1) holds for $\lambda \neq 0$. The eigenproblem (5.2.3) is equivalent to

$$\begin{aligned} a(\boldsymbol{u},\boldsymbol{v}) + b(\boldsymbol{v},p) &= 0, \quad \forall \boldsymbol{v}\in \boldsymbol{V}, \\ b(\boldsymbol{u},q) &= -\lambda(p,q), \quad \forall q \in \mathcal{P}. \end{aligned} \tag{5.2.4}$$

Since $\operatorname{div} \boldsymbol{V} \subset \mathcal{P}$, there is a function $p \in \mathcal{P}$ such that

$$p = -\frac{1}{\lambda}\operatorname{div} \boldsymbol{u},$$

if $\lambda \neq 0$. Putting p into the first equation of (5.2.4), we have

$$-\lambda a(\boldsymbol{u}, \boldsymbol{v}) + (\operatorname{div} \boldsymbol{u}, \operatorname{div} \boldsymbol{v}) = 0, \quad \forall \boldsymbol{v} \in \boldsymbol{V}. \tag{5.2.5}$$

Simple calculations show that if $\{\lambda, \boldsymbol{u} = (u_1, u_2)\}$ is an eigenpair of

$$-\lambda a(\boldsymbol{u}, \boldsymbol{v}) + (\operatorname{div} \boldsymbol{u}, \operatorname{div} \boldsymbol{v}) = 0, \quad \forall \boldsymbol{v} = (v_1, v_2) \in \boldsymbol{V},$$

then $\{1 - \lambda, \bar{\boldsymbol{u}} = (-u_2, u_1)\}$ satisfies

$$-(1 - \lambda) a(\bar{\boldsymbol{u}}, \bar{\boldsymbol{v}}) + (\operatorname{div} \bar{\boldsymbol{u}}, \operatorname{div} \bar{\boldsymbol{v}}) = 0,$$

for all $\bar{\boldsymbol{v}} = (v_2, -v_1) \in \boldsymbol{V}$. Hence, (1) follows.

Obviously, (5.2.4) implies $\lambda \geq 0$. Combining with (1), we prove (2). That is, if λ is an eigenvalue of (5.2.3), then $\lambda \in [0, 1]$. □

The following theorem is due to Mikhlin [18].

Theorem 5.2.2. *The eigenvalues of the eigensystem* (5.2.3) *are situated on the interval* $[0, 1]$ *and can condense only at the points* 0, 1/2, *and* 1. *Furthermore,* 0 *and* 1 *are eigenvalues of infinite multiplicity.*

On the discrete level, the properties of the eigenvalues in Theorem 5.2.1 are preserved if the divergence of any function in the velocity space $\boldsymbol{V}_h$ is a function in the pressure space P_h. We have the following analogue of Theorem 5.2.1.

Theorem 5.2.3. *Let* (5.2.2) *be considered in the finite element space* $\boldsymbol{V}_h \times P_h$ *such that* $\operatorname{div} \boldsymbol{V}_h \subset P_h$. *If* λ *is an eigenvalue of the eigenproblem* (5.2.2), *then*

(1) $1 - \lambda$ *is a also an eigenvalue of* (5.2.2), *and moreover,*
(2) $\lambda \in [0, 1]$.

Proof. This theorem is proved analogously to the proof of Theorem 5.2.1. □

5.3. The Problem for Numerical Tests

We test the $\mathcal{P}^2$–$\mathcal{P}^1$ element on a penalized system of the Stokes equations:

$$\begin{aligned} -\Delta \boldsymbol{u} + \nabla p &= \boldsymbol{f}, \qquad \text{on } \Omega \\ \operatorname{div} \boldsymbol{u} &= \epsilon p, \qquad \text{on } \Omega \\ \boldsymbol{u}|_{\partial\Omega} &= 0, \end{aligned} \tag{5.3.1}$$

with $\Omega = [0, 1] \times [0, 1]$, where ϵ is a small positive number.

The exact solution $(\boldsymbol{u}, p)$ of (5.3.1) and the forcing function $\boldsymbol{f}$ are taken to be:

$$\begin{aligned} \boldsymbol{u} &= -\begin{pmatrix} \phi_y \\ -\phi_x \end{pmatrix} - \epsilon(x - x^2)(y - y^2)\begin{pmatrix} 1 \\ 1 \end{pmatrix}, \\ p &= x - x^2 + y - 4xy + 2x^2 y - y^2 + 2xy^2, \\ \boldsymbol{f} &= \begin{pmatrix} f_1 \\ f_2 \end{pmatrix}. \end{aligned}$$

Here

$$\begin{aligned}
\phi =&(x-x^2)^2(y-y^2)^2,\\
f_1 =&1-2x-12x^2+24x^3-12x^4-20xy+48x^2y-48x^3y+24x^4y-10y^2+\\
&72xy^2-72x^2y^2+8y^3-48xy^3+48x^2y^3-2y\epsilon+2y^2\epsilon,\\
f_2 =&1-8x+14x^2-8x^3-2y+28xy-72x^2y+48x^3y+12y^2-48xy^2+72x^2y^2-\\
&48x^3y^2-24y^3+48xy^3+12y^4-24xy^4-2x\epsilon+2x^2\epsilon.
\end{aligned}$$

We can see that the velocity $\boldsymbol{u}$ is divergence free when $\epsilon = 0$.

The finite element formulation of (5.3.1) is

$$\begin{aligned}
a(\boldsymbol{u}_h,\boldsymbol{v})-b(\boldsymbol{v},p_h)&=(\boldsymbol{f},\boldsymbol{v}),\quad \forall \boldsymbol{v}\in \boldsymbol{V}_h,\\
b(\boldsymbol{u}_h,q)&=\epsilon(p_h,q),\quad \forall q\in P_h.
\end{aligned}\tag{5.3.2}$$

An advantage of using (5.3.2) is that the pressure p_h is automatically in M_h. Therefore, we do not need to filter out spurious pressure modes from the numerical solution for the pressure.

5.4. Numerical Computations

We will present some numerical results for the $\mathcal{P}^2$–$\mathcal{P}^1$ element in this section. As we mentioned before, the numerical tests focus on the inf–sup (or reduced inf–sup constant) and rates of convergence of numerical solutions on different mesh configurations.

We do tests on the stability of the $\mathcal{P}^2$–$\mathcal{P}^1$ element for both Dirichlet and traction boundary conditions. Namely, the velocity space $\boldsymbol{V}_h$ is taken to be $\boldsymbol{M}_0^2$ and $\mathring{\boldsymbol{M}}_0^2$ are considered in numerical computations. All the spurious pressure modes corresponding to $\boldsymbol{V}_h = \boldsymbol{M}_0^2$ are locally supported.

The tests on rates of convergence of the numerical solutions are carried out by computing the penalized system (5.3.1) of the Stokes equations. We choose different values for ϵ such as 0.002, 0.0002, and 0.00002 in our numerical experiments. Since the second equation of (5.3.2) keeps p_h in M_h, the pressure p_h from (5.3.2) can be regarded as $\bar{p}_h$ of (2.4.3) as ϵ tends to 0. If ϵ is small, the second equation of (5.3.1) forces $\boldsymbol{u}_h$ to be an almost divergence free function. The behavior of the numerical solution of (2.4.3) is reflected by the behavior of $\boldsymbol{u}_h$ and p_h from (5.3.2).

This section is organized as follows. In each subsection, we discuss one mesh configuration. For each mesh configuration, supported tables and figures are organized in the following way: first, we give a table of the reduced inf–sup constants for the Stokes equations with either the Dirichlet or the traction boundary conditions. Secondly, we list four diagrams of the distributions of inf–sup eigenvalues of (5.1.6), for $h = 1/2$, $1/4$, $1/6$, and $1/8$ (Dirichlet boundary condition only). Finally, we display rates of convergence of numerical solutions for different ϵ in three tables (Dirichlet boundary condition only).

In Figure 5.1, we list only a basic $2h \times 2h$ pattern for each mesh $\mathcal{T}_h$ of the unit square. $\mathcal{T}_h$ is formed by translating this pattern around, therefore $\mathcal{T}_h$ is a periodic mesh. For example, the diagonal mesh $\mathcal{T}_h$, $h = 1/4$, is formed by four submeshes which are congruent to pattern 1.

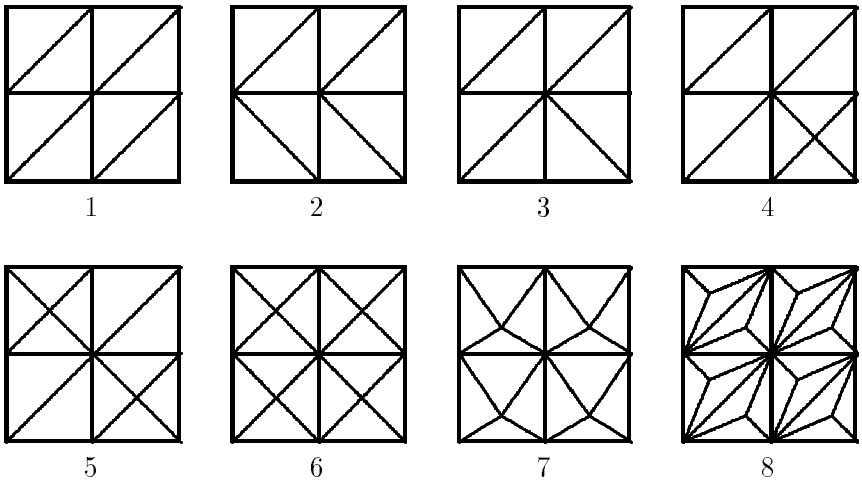

Figure 5.1. Different $2h \times 2h$ mesh patterns.

5.4.1. Mesh 1

For this diagonal mesh, Table 5.4 shows that the reduced inf–sup constant is about $O(h)$ for both Dirichlet and traction conditions. Furthermore, all spurious pressure modes are globally supported for Dirichlet boundary conditions. The number of independent spurious pressure modes remains unchanged as h goes to zero. The eigenvalues are in $[0, 1]$ and they are distributed symmetrically as told by Theorem 5.2.3.

As ϵ becomes smaller and smaller, the rate of convergence of the solution becomes worse and worse. It is quite clear that the rate of convergence is 2 for the velocity in the H^1 norm and no convergence at all for the pressure in the L^2 norm.

5.4.2. Mesh 2

On this mesh, the behavior is quite similar to that on the diagonal mesh. The reduced inf–sup constant is about $O(h)$, the velocity converges suboptimally, and there is no convergence for the pressure. However, the number of spurious pressure modes grows in the order of $O(h^{-1})$ and all of them are globally supported. This indicates that the number of globally supported spurious pressure modes is not always fixed as h goes to zero.

5.4.3. Mesh 3

The reduced inf–sup constant is about $O(h)$ for both boundary conditions. However, the velocity space $\boldsymbol{Z}_h \subset \mathring{\boldsymbol{M}}_0^2$ has optimal approximation properties. Since the reduced inf–sup constant is about $O(h)$, by Theorem 2.2.1, only suboptimal rate of convergence of the numerical solution for the velocity can be expected. This mesh clearly shows that the inf–sup condition can not tell the whole story about approximation properties of finite element solutions. The numerical solution for the pressure converges in a suboptimal fashion, and this agrees with estimates in Theorem 2.2.1 if we assume that the numerical solution for the velocity has an optimal rate of convergence.

5.4.4. Mesh 4

The reduced inf–sup constant is independent of h and the numerical solution converges optimally as predicted by Theorem 4.4.1 and 4.4.2. It is hard to see the jump between the zero eigenvalues and the one corresponding to the inf–sup constant in Figure 5.5. However, Table 5.13 shows that the reduced inf–sup constant is bounded away from zero by a positive number as h goes to zero.

5.4.5. Mesh 5

Like mesh 4, the reduced inf–sup constant is independent of h and the numerical solution converges optimally as predicted by Theorem 4.4.1 and 4.4.2. There is a sharp jump between zero eigenvalues and the the first nonzero eigenvalue which is the square of the reduced inf–sup constant.

5.4.6. Mesh 6

This is the crisscross mesh. The reduced inf–sup constant is independent of h and the numerical solution converges optimally. The strange behavior of the rate of convergence for the pressure shown in Table 5.24 is due to the effect of the locally supported spurious pressure modes. The second equation of (5.3.2) definitely guarantees that the velocity $\boldsymbol{u}_h$ is almost divergence free if ϵ is small. However, in numerical computations, it is difficult to remove spurious pressure modes completely from p_h when ϵ is very small.

5.4.7. Mesh 7

Theorem 4.5.1 guarantees everything is fine for this mesh. Although the element is stable on this mesh, the inf–sup constant is smaller than the reduced inf–sup constant for crisscross meshes, and the error is also larger for this mesh. This mesh is a distortion of the crisscross mesh. All the zero eigenvalues of the crisscross mesh, except for the first one, are shifted away from zero for this mesh.

5.4.8. Mesh 8

Theorem 4.6.1 guarantees everything is fine for this mesh. The jump between the first and the second eigenvalue is quite significant.

Table 5.1. Mesh 1

	$\boldsymbol{V}_h = \mathring{\boldsymbol{M}}_0^2$			$\boldsymbol{V}_h = \boldsymbol{M}_0^2$		
$1/h$	$\bar{\gamma}_h$	α $(\bar{\gamma}_h = Ch^\alpha)$	$dim(N_h)$	$\bar{\gamma}_h$	α $(\bar{\gamma}_h = Ch^\alpha)$	$dim(N_h)$
2	0.13093082		6	0.32807883		0
4	0.07811972	0.745046	6	0.15713876	1.062003	0
6	0.05302801	0.955501	6	0.10402865	1.017259	0
8	0.04004810	0.975866	6	0.07787991	1.006313	0
10	0.03214701	0.984845	6	0.06226484	1.002813	0
12	0.02684083	0.989434	6	0.05187360	1.001456	0
14	0.02303584	0.991710	6	0.04445796	1.000748	0
16	0.02017052	0.994740	6	0.03889871	1.000384	0

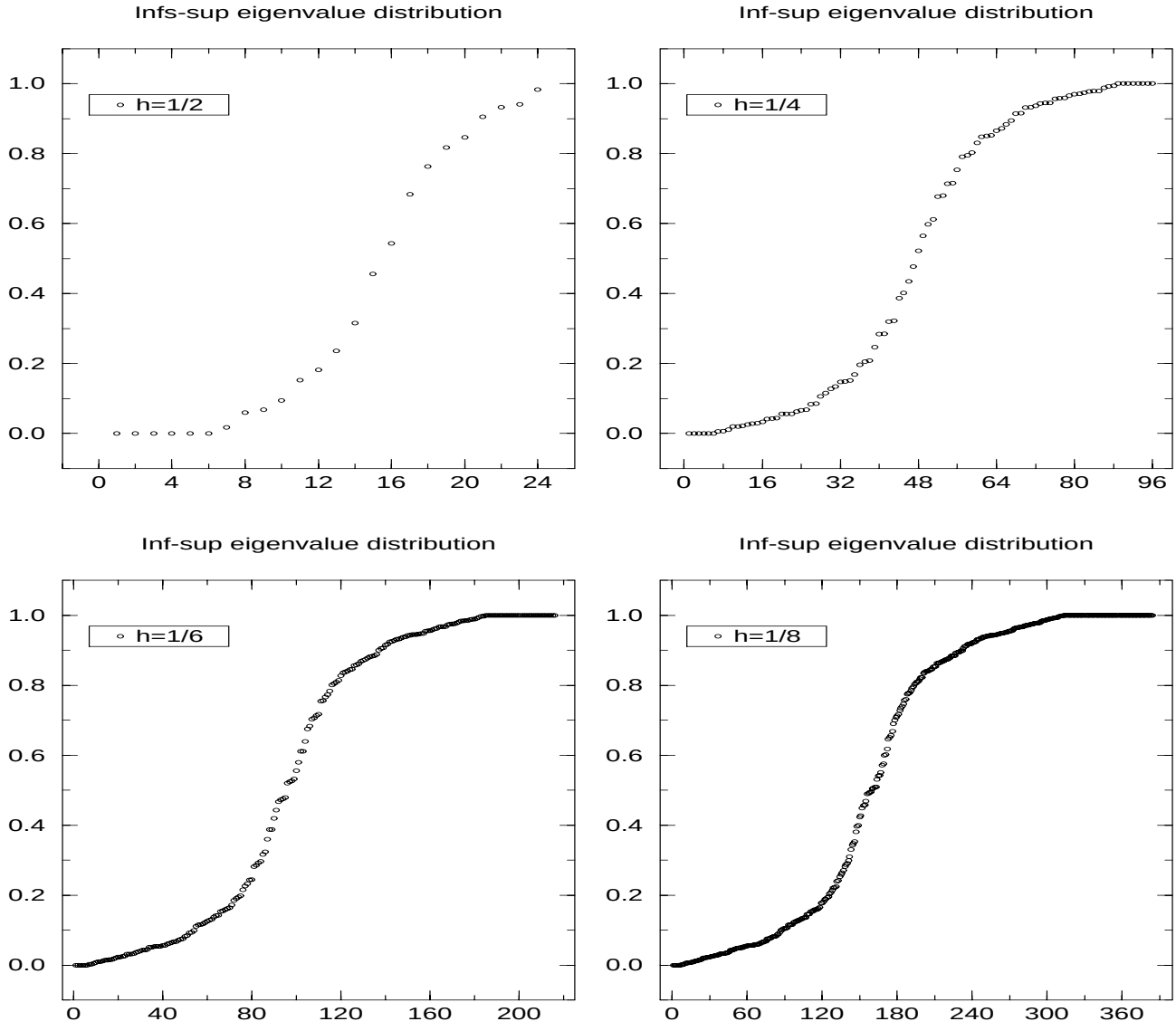

Figure 5.2. Mesh 1

Table 5.2. Mesh 1, $\epsilon = 0.002$

$1/h$	$L^2 : \boldsymbol{u} - \boldsymbol{u}_h$	Rate	$\boldsymbol{H}^1 : \boldsymbol{u} - \boldsymbol{u}_h$	Rate	$L^2 : p - p_h$	Rate
2	0.7768649E-02	0.0000	0.5514695E-01	0.0000	0.2120587E+00	0.0000
4	0.2574038E-02	1.5936	0.3011311E-01	0.8729	0.1587661E+00	0.4176
6	0.1075027E-02	2.1534	0.1874462E-01	1.1692	0.1373761E+00	0.3569
8	0.5634911E-03	2.2454	0.1306806E-01	1.2539	0.1240383E+00	0.3550
10	0.3339049E-03	2.3451	0.9652103E-02	1.3578	0.1122738E+00	0.4466
12	0.2136238E-03	2.4497	0.7387039E-02	1.4669	0.1012928E+00	0.5645
14	0.1441573E-03	2.5515	0.5797876E-02	1.5714	0.9111821E-01	0.6867
16	0.1012507E-03	2.6459	0.4641168E-02	1.6665	0.8185191E-01	0.8032
18	0.7339893E-04	2.7312	0.3776486E-02	1.7504	0.7353794E-01	0.9094
20	0.5460377E-04	2.8076	0.3116297E-02	1.8237	0.6615707E-01	1.0039

Table 5.3. Mesh 1, $\epsilon = 0.0002$

$1/h$	$L^2 : \boldsymbol{u} - \boldsymbol{u}_h$	Rate	$\boldsymbol{H}^1 : \boldsymbol{u} - \boldsymbol{u}_h$	Rate	$L^2 : p - p_h$	Rate
2	0.7951619E-02	0.0000	0.5641579E-01	0.0000	0.2183801E+00	0.0000
4	0.2695047E-02	1.5609	0.3159246E-01	0.8365	0.1674108E+00	0.3834
6	0.1172162E-02	2.0534	0.2053628E-01	1.0623	0.1520498E+00	0.2374
8	0.6485122E-03	2.0576	0.1515959E-01	1.0552	0.1465195E+00	0.1288
10	0.4092134E-03	2.0634	0.1196239E-01	1.0615	0.1431243E+00	0.1051
12	0.2802384E-03	2.0765	0.9830597E-02	1.0765	0.1403170E+00	0.1087
14	0.2028898E-03	2.0952	0.8300850E-02	1.0972	0.1376360E+00	0.1251
16	0.1529061E-03	2.1181	0.7145656E-02	1.1222	0.1349172E+00	0.1494
18	0.1187770E-03	2.1444	0.6240096E-02	1.1505	0.1321037E+00	0.1789
20	0.9446839E-04	2.1733	0.5509801E-02	1.1813	0.1291789E+00	0.2125

Table 5.4. Mesh 1, $\epsilon = 0.00002$

$1/h$	$L^2 : \boldsymbol{u} - \boldsymbol{u}_h$	Rate	$\boldsymbol{H}^1 : \boldsymbol{u} - \boldsymbol{u}_h$	Rate	$L^2 : p - p_h$	Rate
2	0.7970498E-02	0.0000	0.5654720E-01	0.0000	0.2190493E+00	0.0000
4	0.2707860E-02	1.5575	0.3174966E-01	0.8327	0.1683506E+00	0.3798
6	0.1183031E-02	2.0423	0.2073784E-01	1.0505	0.1537239E+00	0.2242
8	0.6587578E-03	2.0352	0.1541369E-01	1.0314	0.1492804E+00	0.1020
10	0.4191188E-03	2.0265	0.1226977E-01	1.0223	0.1472468E+00	0.0615
12	0.2898892E-03	2.0220	0.1019000E-01	1.0187	0.1460850E+00	0.0434
14	0.2123130E-03	2.0203	0.8710130E-02	1.0180	0.1452750E+00	0.0361
16	0.1621077E-03	2.0205	0.7602139E-02	1.0189	0.1446619E+00	0.0317
18	0.1277545E-03	2.0219	0.6740761E-02	1.0210	0.1440946E+00	0.0334
20	0.1032163E-03	2.0243	0.6051404E-02	1.0239	0.1435860E+00	0.0336

Table 5.5. Mesh 2

	$\boldsymbol{V}_h = \mathring{\boldsymbol{M}}_0^2$			$\boldsymbol{V}_h = \boldsymbol{M}_0^2$		
$1/h$	$\bar{\gamma}_h$	$\alpha\ (\bar{\gamma}_h = Ch^\alpha)$	$dim(N_h)$	$\bar{\gamma}_h$	$\alpha\ (\bar{\gamma}_h = Ch^\alpha)$	$dim(N_h)$
2	0.20795310		6	0.30566117		0
4	0.05863438	1.826440	8	0.15138448	1.013716	0
6	0.03991015	0.948764	10	0.10156855	0.984274	0
8	0.03010133	0.980462	12	0.07633846	0.992613	0
10	0.02413752	0.989505	14	0.06110630	0.997393	0
12	0.02013604	0.994158	16	0.05092200	0.999991	0
14	0.01727165	0.995419	18	0.04364023	1.001069	0
16	0.01511787	0.997436	20	0.03817525	1.001952	0

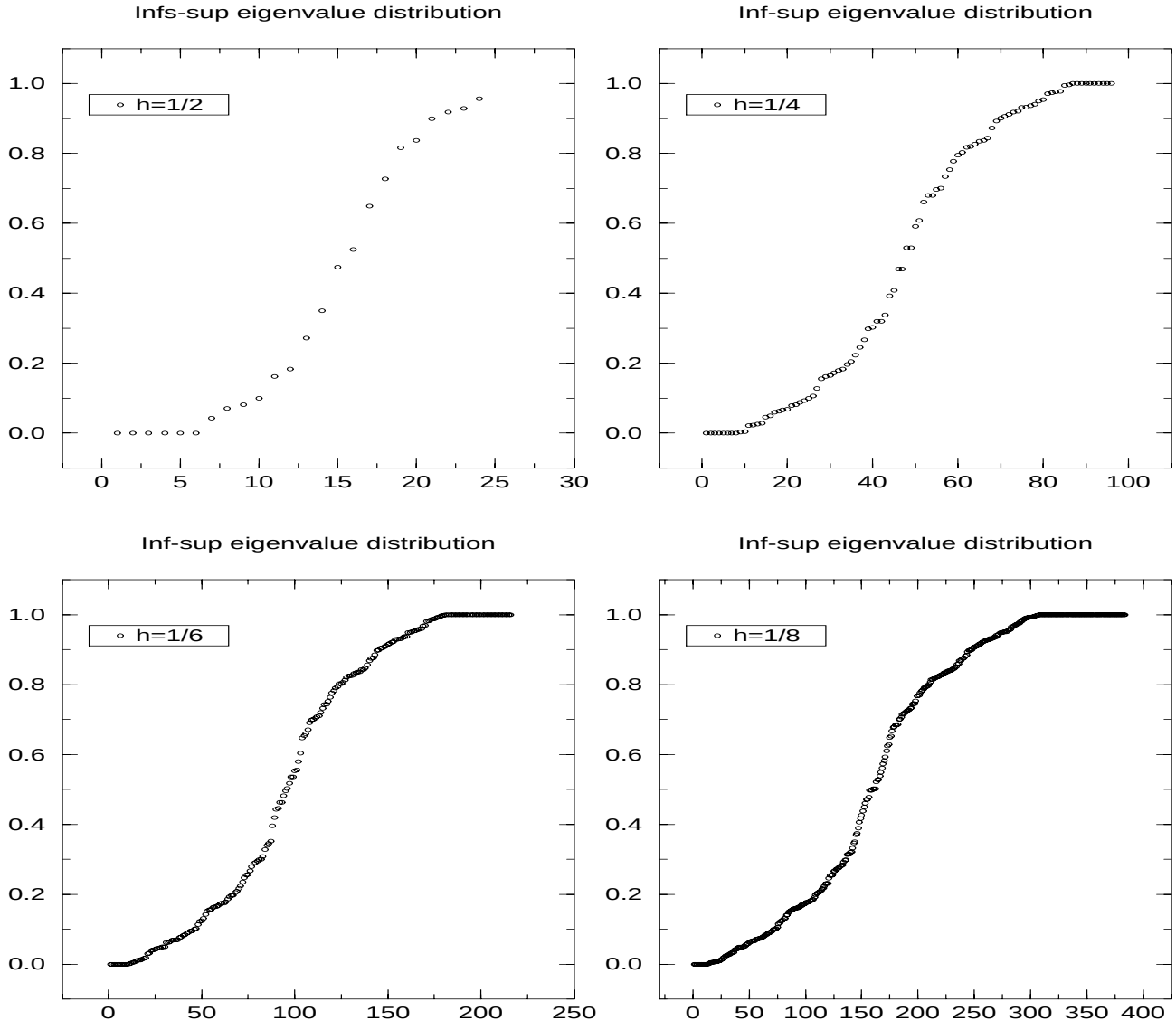

Figure 5.3. Mesh 2

Table 5.6. Mesh 2, $\epsilon = 0.002$

$1/h$	$L^2 : \boldsymbol{u} - \boldsymbol{u}_h$	Rate	$\boldsymbol{H}^1 : \boldsymbol{u} - \boldsymbol{u}_h$	Rate	$L^2 : p - p_h$	Rate
2	0.7827469E-02	0.0000	0.5553850E-01	0.0000	0.1814816E+00	0.0000
4	0.2276989E-02	1.7814	0.2821522E-01	0.9770	0.1545140E+00	0.2321
6	0.9323356E-03	2.2022	0.1719538E-01	1.2214	0.1355382E+00	0.3232
8	0.4719867E-03	2.3663	0.1165177E-01	1.3528	0.1209970E+00	0.3945
10	0.2704707E-03	2.4952	0.8377875E-02	1.4783	0.1078016E+00	0.5175
12	0.1678418E-03	2.6170	0.6253839E-02	1.6038	0.9566816E-01	0.6549
14	0.1101634E-03	2.7315	0.4795010E-02	1.7231	0.8470728E-01	0.7894
16	0.7543446E-04	2.8360	0.3754478E-02	1.8320	0.7497856E-01	0.9136
18	0.5342020E-04	2.9298	0.2991550E-02	1.9286	0.6645087E-01	1.0251
20	0.3889089E-04	3.0128	0.2419819E-02	2.0131	0.5903328E-01	1.1234

Table 5.7. Mesh 2, $\epsilon = 0.0002$

$1/h$	$L^2 : \boldsymbol{u} - \boldsymbol{u}_h$	Rate	$\boldsymbol{H}^1 : \boldsymbol{u} - \boldsymbol{u}_h$	Rate	$L^2 : p - p_h$	Rate
2	0.7957833E-02	0.0000	0.5645769E-01	0.0000	0.1843129E+00	0.0000
4	0.2400072E-02	1.7293	0.2971926E-01	0.9258	0.1647176E+00	0.1622
6	0.1034219E-02	2.0763	0.1910097E-01	1.0902	0.1540154E+00	0.1657
8	0.5602323E-03	2.1310	0.1388588E-01	1.1084	0.1491634E+00	0.1113
10	0.3472561E-03	2.1434	0.1082731E-01	1.1150	0.1456732E+00	0.1061
12	0.2344187E-03	2.1553	0.8813224E-02	1.1289	0.1424343E+00	0.1233
14	0.1676939E-03	2.1730	0.7380946E-02	1.1505	0.1391470E+00	0.1515
16	0.1250617E-03	2.1967	0.6306360E-02	1.1783	0.1357333E+00	0.1860
18	0.9622360E-04	2.2256	0.5468131E-02	1.2109	0.1321834E+00	0.2250
20	0.7584801E-04	2.2584	0.4794873E-02	1.2470	0.1285143E+00	0.2672

Table 5.8. Mesh 2, $\epsilon = 0.00002$

$1/h$	$L^2 : \boldsymbol{u} - \boldsymbol{u}_h$	Rate	$\boldsymbol{H}^1 : \boldsymbol{u} - \boldsymbol{u}_h$	Rate	$L^2 : p - p_h$	Rate
2	0.7971123E-02	0.0000	0.5655142E-01	0.0000	0.1846018E+00	0.0000
4	0.2413400E-02	1.7237	0.2988210E-01	0.9203	0.1658870E+00	0.1542
6	0.1046080E-02	2.0618	0.1932363E-01	1.0751	0.1562713E+00	0.1473
8	0.5715279E-03	2.1013	0.1417355E-01	1.0774	0.1529677E+00	0.0743
10	0.3582082E-03	2.0937	0.1117922E-01	1.0635	0.1513855E+00	0.0466
12	0.2450786E-03	2.0817	0.9226363E-02	1.0530	0.1503879E+00	0.0363
14	0.1780667E-03	2.0721	0.7851361E-02	1.0469	0.1496183E+00	0.0333
16	0.1351399E-03	2.0658	0.6829650E-02	1.0441	0.1489601E+00	0.0330
18	0.1059971E-03	2.0623	0.6039662E-02	1.0437	0.1483084E+00	0.0372
20	0.8530750E-04	2.0610	0.5409928E-02	1.0451	0.1476816E+00	0.0402

Table 5.9. Mesh 3

	$\boldsymbol{V}_h = \mathring{\boldsymbol{M}}_0^2$			$\boldsymbol{V}_h = \boldsymbol{M}_0^2$		
$1/h$	$\bar{\gamma}_h$	$\alpha\ (\bar{\gamma}_h = Ch^\alpha)$	$dim(N_h)$	$\bar{\gamma}_h$	$\alpha\ (\bar{\gamma}_h = Ch^\alpha)$	$dim(N_h)$
2	0.18856362		6	0.36897215		0
4	0.04583754	2.040450	7	0.12790970	1.528386	0
6	0.03773950	0.479440	9	0.08733081	0.941194	0
8	0.03315796	0.449888	11	0.06553816	0.997875	0
10	0.02940221	0.538724	13	0.05230870	1.010425	0
12	0.02610038	0.653351	15	0.04348080	1.013831	0
14	0.02324586	0.751362	17	0.03718494	1.014693	0
16	0.02083267	0.820816	19	0.03247599	1.014015	0
18	0.01880611	0.868888	21			

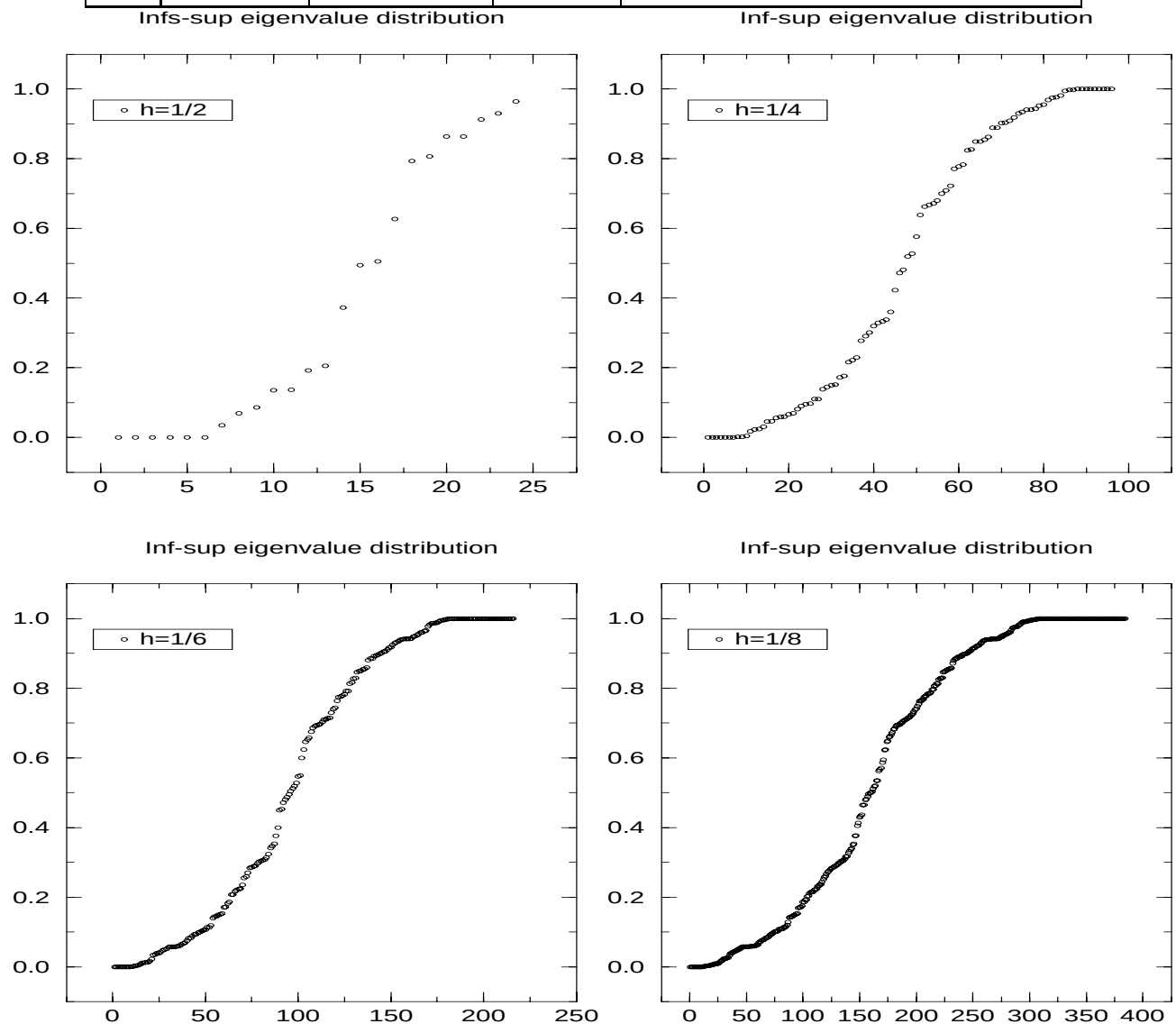

Figure 5.4. Mesh 3

Table 5.10. Mesh 3, $\epsilon = 0.002$

$1/h$	$L^2 : \boldsymbol{u} - \boldsymbol{u}_h$	Rate	$\boldsymbol{H}^1 : \boldsymbol{u} - \boldsymbol{u}_h$	Rate	$L^2 : p - p_h$	Rate
2	0.7806727E-02	0.0000	0.5538587E-01	0.0000	0.1885378E+00	0.0000
4	0.1710856E-02	2.1900	0.2199915E-01	1.3321	0.1316194E+00	0.5185
6	0.7921602E-03	1.8990	0.1472190E-01	0.9906	0.1039612E+00	0.5818
8	0.3981966E-03	2.3909	0.9953791E-02	1.3605	0.8496312E-01	0.7015
10	0.2191918E-03	2.6754	0.7029048E-02	1.5591	0.6772022E-01	1.0165
12	0.1303492E-03	2.8506	0.5169715E-02	1.6851	0.5378526E-01	1.2636
14	0.8260550E-04	2.9591	0.3936732E-02	1.7675	0.4310016E-01	1.4367
16	0.5513345E-04	3.0279	0.3085865E-02	1.8237	0.3501082E-01	1.5567
18	0.3838965E-04	3.0732	0.2477647E-02	1.8638	0.2885602E-01	1.6415
20	0.2768175E-04	3.1038	0.2029509E-02	1.8936	0.2411611E-01	1.7031

Table 5.11. Mesh 3, $\epsilon = 0.0002$

$1/h$	$L^2 : \boldsymbol{u} - \boldsymbol{u}_h$	Rate	$\boldsymbol{H}^1 : \boldsymbol{u} - \boldsymbol{u}_h$	Rate	$L^2 : p - p_h$	Rate
2	0.7955532E-02	0.0000	0.5644056E-01	0.0000	0.1928962E+00	0.0000
4	0.1828947E-02	2.1209	0.2342794E-01	1.2685	0.1608916E+00	0.2617
6	0.8616662E-03	1.8562	0.1604169E-01	0.9341	0.1189821E+00	0.7442
8	0.4492187E-03	2.2642	0.1125326E-01	1.2324	0.9962953E-01	0.6170
10	0.2554750E-03	2.5292	0.8196958E-02	1.4201	0.8238935E-01	0.8515
12	0.1559943E-03	2.7057	0.6171928E-02	1.5563	0.6779845E-01	1.0691
14	0.1009821E-03	2.8211	0.4783021E-02	1.6538	0.5610603E-01	1.2280
16	0.6858462E-04	2.8973	0.3799526E-02	1.7239	0.4691476E-01	1.3398
18	0.4846204E-04	2.9485	0.3082648E-02	1.7752	0.3969507E-01	1.4188
20	0.3538980E-04	2.9836	0.2546495E-02	1.8135	0.3398434E-01	1.4742

Table 5.12. Mesh 3, $\epsilon = 0.00002$

$1/h$	$L^2 : \boldsymbol{u} - \boldsymbol{u}_h$	Rate	$\boldsymbol{H}^1 : \boldsymbol{u} - \boldsymbol{u}_h$	Rate	$L^2 : p - p_h$	Rate
2	0.7970891E-02	0.0000	0.5654969E-01	0.0000	0.1933527E+00	0.0000
4	0.1845137E-02	2.1110	0.2362248E-01	1.2594	0.1663078E+00	0.2174
6	0.8699926E-03	1.8542	0.1620007E-01	0.9302	0.1214737E+00	0.7748
8	0.4554328E-03	2.2498	0.1141209E-01	1.2178	0.1017890E+00	0.6146
10	0.2601162E-03	2.5101	0.8346248E-02	1.4021	0.8459875E-01	0.8290
12	0.1594605E-03	2.6839	0.6306374E-02	1.5371	0.7012081E-01	1.0295
14	0.1036076E-03	2.7972	0.4902056E-02	1.6342	0.5853946E-01	1.1711
16	0.7061293E-04	2.8712	0.3904550E-02	1.7038	0.4948074E-01	1.2590
18	0.5006136E-04	2.9203	0.3175580E-02	1.7545	0.4236105E-01	1.3190
20	0.3667562E-04	2.9531	0.2629206E-02	1.7920	0.3675297E-01	1.3479

Table 5.13. Mesh 4

	$\boldsymbol{V}_h = \mathring{\boldsymbol{M}}_0^2$			$\boldsymbol{V}_h = \boldsymbol{M}_0^2$		
$1/h$	$\bar{\gamma}_h$	α $(\bar{\gamma}_h = Ch^\alpha)$	$dim(N_h)$	$\bar{\gamma}_h$	α $(\bar{\gamma}_h = Ch^\alpha)$	$dim(N_h)$
2	0.08401291		4	0.36827590		1
4	0.06252127	0.426263	6	0.19808347	0.894679	4
6	0.06942132	-0.258190	11	0.16842156	0.400080	9
8	0.07152600	-0.103819	18	0.15660271	0.252911	16
10	0.07220782	-0.042516	27	0.14925967	0.215218	25
12	0.07242354	-0.016361	38	0.14513215	0.153810	36
14	0.07248848	-0.005813	51	0.14258373	0.114922	49

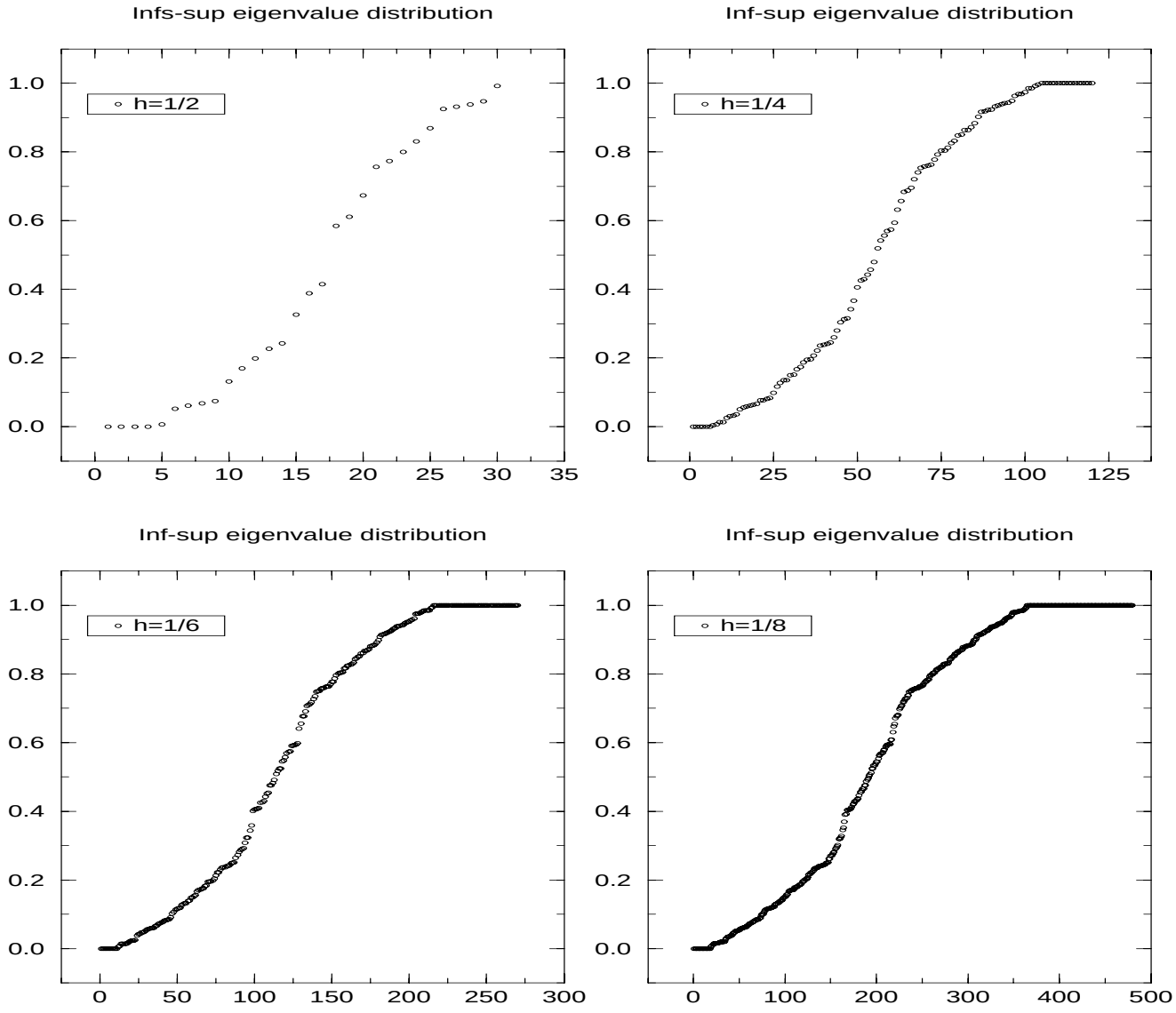

Figure 5.5. Mesh 4

Table 5.14. Mesh 4, $\epsilon = 0.002$

$1/h$	$L^2 : \boldsymbol{u} - \boldsymbol{u}_h$	Rate	$\boldsymbol{H}^1 : \boldsymbol{u} - \boldsymbol{u}_h$	Rate	$L^2 : p - p_h$	Rate
2	0.7653364E-02	0.0000	0.5460609E-01	0.0000	0.2803161E+00	0.0000
4	0.1661853E-02	2.2033	0.2159634E-01	1.3383	0.1118130E+00	1.3260
6	0.6736845E-03	2.2269	0.1309262E-01	1.2343	0.8138313E-01	0.7834
8	0.3097648E-03	2.7007	0.8445776E-02	1.5238	0.5857912E-01	1.1429
10	0.1607243E-03	2.9404	0.5795396E-02	1.6877	0.4248801E-01	1.4392
12	0.9184545E-04	3.0692	0.4186577E-02	1.7836	0.3164466E-01	1.6161
14	0.5655427E-04	3.1457	0.3150115E-02	1.8452	0.2424870E-01	1.7269
16	0.3692376E-04	3.1928	0.2448133E-02	1.8880	0.1906022E-01	1.8030
18	0.2526652E-04	3.2210	0.1952824E-02	1.9192	0.1531155E-01	1.8593
20	0.1796713E-04	3.2359	0.1591391E-02	1.9425	0.1253006E-01	1.9028

Table 5.15. Mesh 4, $\epsilon = 0.0002$

$1/h$	$L^2 : \boldsymbol{u} - \boldsymbol{u}_h$	Rate	$\boldsymbol{H}^1 : \boldsymbol{u} - \boldsymbol{u}_h$	Rate	$L^2 : p - p_h$	Rate
2	0.7960191E-02	0.0000	0.5664472E-01	0.0000	0.3149452E+00	0.0000
4	0.1739691E-02	2.1940	0.2261937E-01	1.3244	0.1189032E+00	1.4053
6	0.7189004E-03	2.1796	0.1399218E-01	1.1846	0.8777856E-01	0.7485
8	0.3354605E-03	2.6495	0.9168235E-02	1.4695	0.6429613E-01	1.0822
10	0.1756276E-03	2.9001	0.6348980E-02	1.6467	0.4712652E-01	1.3922
12	0.1009580E-03	3.0367	0.4611497E-02	1.7537	0.3531675E-01	1.5823
14	0.6242348E-04	3.1188	0.3481649E-02	1.8232	0.2716695E-01	1.7019
16	0.4087388E-04	3.1712	0.2711687E-02	1.8717	0.2140868E-01	1.7839
18	0.2802395E-04	3.2045	0.2166046E-02	1.9075	0.1722844E-01	1.8444
20	0.1995220E-04	3.2244	0.1766625E-02	1.9346	0.1411512E-01	1.8917

Table 5.16. Mesh 4, $\epsilon = 0.00002$

$1/h$	$L^2 : \boldsymbol{u} - \boldsymbol{u}_h$	Rate	$\boldsymbol{H}^1 : \boldsymbol{u} - \boldsymbol{u}_h$	Rate	$L^2 : p - p_h$	Rate
2	0.7995464E-02	0.0000	0.5688633E-01	0.0000	0.3194573E+00	0.0000
4	0.1747998E-02	2.1935	0.2272968E-01	1.3235	0.1197054E+00	1.4161
6	0.7238222E-03	2.1745	0.1409049E-01	1.1793	0.8848563E-01	0.7453
8	0.3383146E-03	2.6438	0.9248827E-02	1.4634	0.6494617E-01	1.0751
10	0.1773027E-03	2.8955	0.6411504E-02	1.6420	0.4765370E-01	1.3874
12	0.1019896E-03	3.0330	0.4659840E-02	1.7503	0.3574128E-01	1.5777
14	0.6309136E-04	3.1157	0.3519540E-02	1.8206	0.2750012E-01	1.7004
16	0.4132517E-04	3.1686	0.2741901E-02	1.8698	0.2169446E-01	1.7759
18	0.2833992E-04	3.2025	0.2190544E-02	1.9061	0.1745635E-01	1.8454
20	0.2018017E-04	3.2229	0.1786788E-02	1.9336	0.1430210E-01	1.8916

Table 5.17. Mesh 5

	$\boldsymbol{V}_h = \mathring{\boldsymbol{M}}_0^2$			$\boldsymbol{V}_h = \boldsymbol{M}_0^2$		
$1/h$	$\bar{\gamma}_h$	$\alpha\ (\bar{\gamma}_h = Ch^\alpha)$	$dim(N_h)$	$\bar{\gamma}_h$	$\alpha\ (\bar{\gamma}_h = Ch^\alpha)$	$dim(N_h)$
2	0.20811636		3	0.49430817		2
4	0.23235417	-0.158935	9	0.32119961	0.621941	8
6	0.23346135	-0.011724	19	0.31458925	0.051287	18
8	0.23352492	-0.000946	33	0.31238342	0.024459	32
10	0.23354274	-0.000342	51	0.31133469	0.015070	50
12	0.23354745	-0.000111	73	0.31075441	0.010232	72

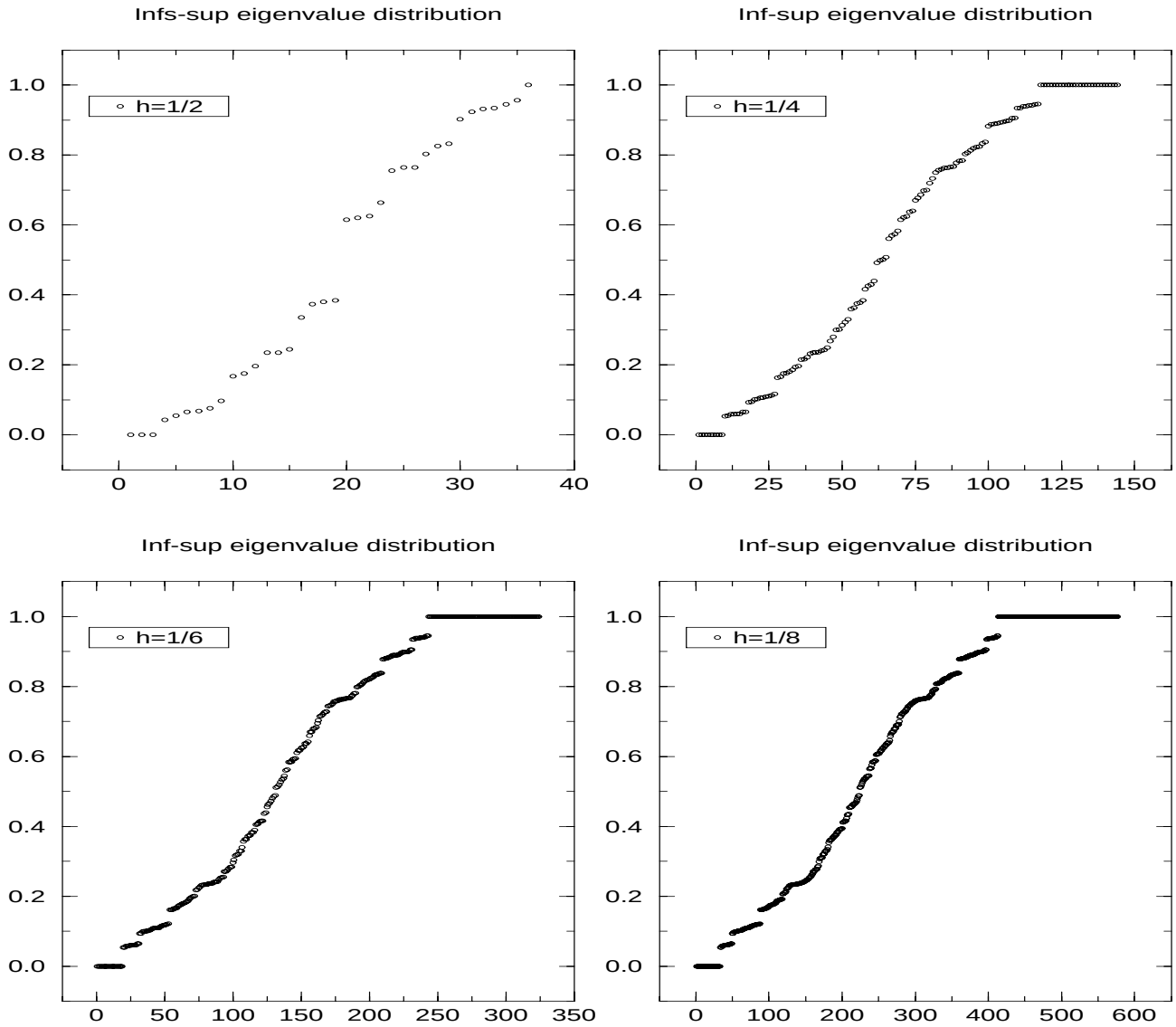

Figure 5.6. Mesh 5

Table 5.18. Mesh 5, $\epsilon = 0.002$

$1/h$	$L^2 : \boldsymbol{u} - \boldsymbol{u}_h$	Rate	$\boldsymbol{H}^1 : \boldsymbol{u} - \boldsymbol{u}_h$	Rate	$L^2 : p - p_h$	Rate
2	0.7723748E-02	0.0000	0.5535357E-01	0.0000	0.2611621E+00	0.0000
4	0.3272425E-03	4.5609	0.6767890E-02	3.0319	0.2201140E-01	3.5686
6	0.2050705E-03	1.1526	0.5239677E-02	0.6312	0.1643526E-01	0.7205
8	0.9538154E-04	2.6608	0.3264758E-02	1.6444	0.1034445E-01	1.6093
10	0.4943521E-04	2.9453	0.2147079E-02	1.8781	0.6772225E-02	1.8984
12	0.2836374E-04	3.0471	0.1498053E-02	1.9742	0.4674001E-02	2.0338
14	0.1760915E-04	3.0924	0.1096933E-02	2.0217	0.3377803E-02	2.1070
16	0.1161759E-04	3.1146	0.8345603E-03	2.0472	0.2535205E-02	2.1489
18	0.8039450E-05	3.1257	0.6546501E-03	2.0615	0.1962539E-02	2.1738
20	0.5780468E-05	3.1309	0.5264049E-03	2.0694	0.1558278E-02	2.1892

Table 5.19. Mesh 5, $\epsilon = 0.0002$

$1/h$	$L^2 : \boldsymbol{u} - \boldsymbol{u}_h$	Rate	$\boldsymbol{H}^1 : \boldsymbol{u} - \boldsymbol{u}_h$	Rate	$L^2 : p - p_h$	Rate
2	0.8016939E-02	0.0000	0.5738908E-01	0.0000	0.2709437E+00	0.0000
4	0.3324486E-03	4.5918	0.6869803E-02	3.0624	0.2238294E-01	3.5975
6	0.2086490E-03	1.1489	0.5325060E-02	0.6282	0.1676416E-01	0.7129
8	0.9712402E-04	2.6580	0.3319968E-02	1.6423	0.1056238E-01	1.6057
10	0.5033806E-04	2.9453	0.2183219E-02	1.8784	0.6916237E-02	1.8976
12	0.2887282E-04	3.0488	0.1522745E-02	1.9761	0.4772711E-02	2.0346
14	0.1791765E-04	3.0951	0.1114534E-02	2.0245	0.3447498E-02	2.1101
16	0.1181576E-04	3.1180	0.8475747E-03	2.0506	0.2586314E-02	2.1524
18	0.8172917E-05	3.1296	0.6645743E-03	2.0651	0.2001717E-02	2.1754
20	0.5873918E-05	3.1350	0.5341720E-03	2.0732	0.1588630E-02	2.1937

Table 5.20. Mesh 5, $\epsilon = 0.00002$

$1/h$	$L^2 : \boldsymbol{u} - \boldsymbol{u}_h$	Rate	$\boldsymbol{H}^1 : \boldsymbol{u} - \boldsymbol{u}_h$	Rate	$L^2 : p - p_h$	Rate
2	0.8047549E-02	0.0000	0.5760180E-01	0.0000	0.2719665E+00	0.0000
4	0.3329827E-03	4.5950	0.6880260E-02	3.0656	0.2242889E-01	3.6000
6	0.2090161E-03	1.1485	0.5333823E-02	0.6279	0.1681126E-01	0.7110
8	0.9730300E-04	2.6577	0.3325641E-02	1.6421	0.1060076E-01	1.6029
10	0.5043084E-04	2.9453	0.2186933E-02	1.8784	0.6932015E-02	1.9036
12	0.2892515E-04	3.0490	0.1525282E-02	1.9763	0.4811630E-02	2.0026
14	0.1794935E-04	3.0954	0.1116343E-02	2.0248	0.3456612E-02	2.1456
16	0.1183612E-04	3.1184	0.8489106E-03	2.0509	0.2661629E-02	1.9572
18	0.8186623E-05	3.1299	0.6655928E-03	2.0655	0.2132414E-02	1.8821
20	0.5883508E-05	3.1354	0.5349687E-03	2.0735	0.1630709E-02	2.5459

Table 5.21. Mesh 6

	$\boldsymbol{V}_h = \mathring{M}_0^2$			$\boldsymbol{V}_h = M_0^2$		
$1/h$	$\bar{\gamma}_h$	α $(\bar{\gamma}_h = Ch^\alpha)$	$dim(N_h)$	$\bar{\gamma}_h$	α $(\bar{\gamma}_h = Ch^\alpha)$	$dim(N_h)$
2	0.37842003		5	0.45842007		4
4	0.38287631	-0.016890	17	0.41892314	0.129985	16
6	0.38448853	-0.010363	37	0.40583929	0.078256	36
8	0.38505027	-0.005075	65	0.40073334	0.044011	64
10	0.38520295	-0.001777	101	0.39827226	0.027607	100

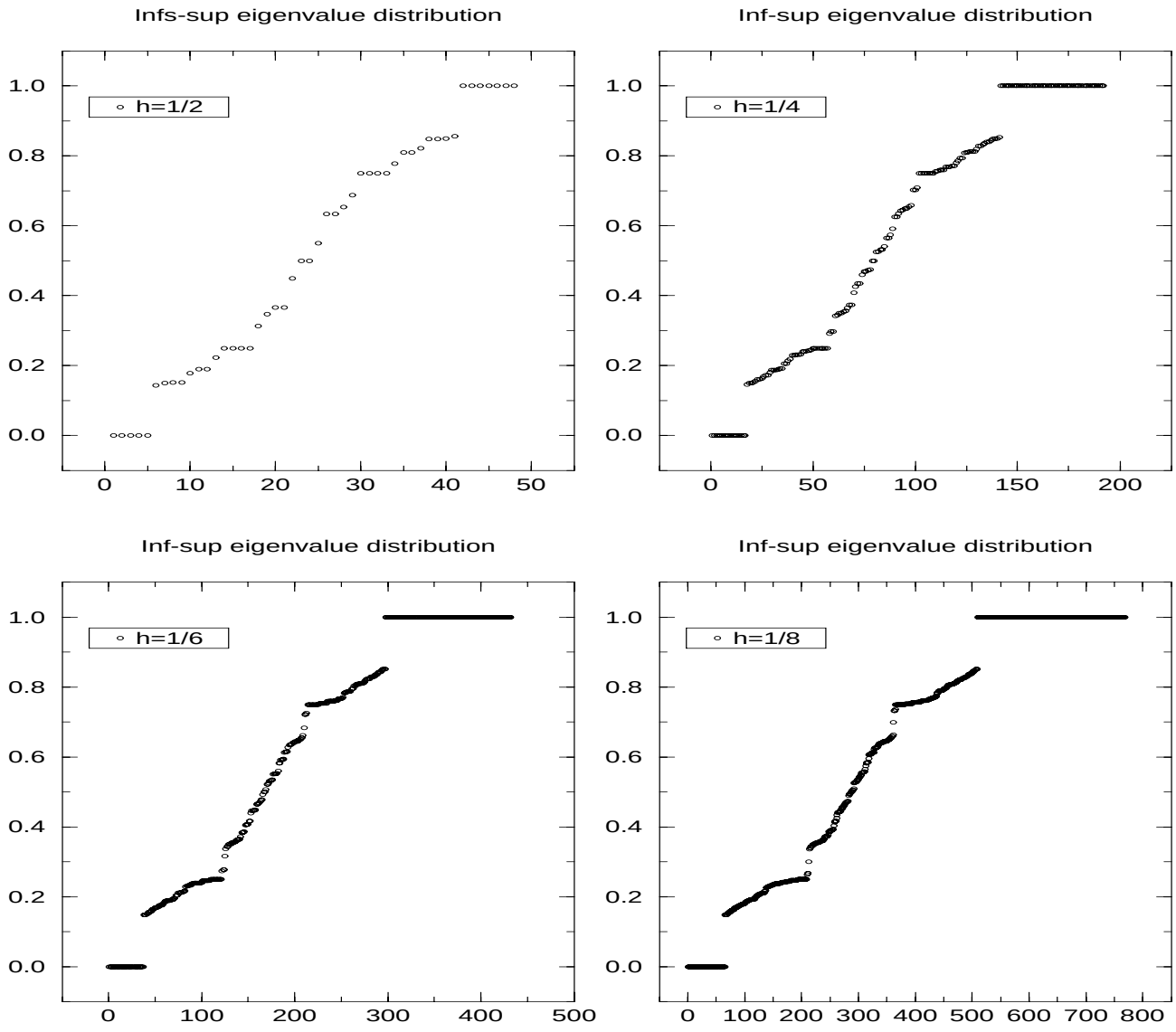

Figure 5.7. Mesh 6

Table 5.22. Mesh 6, $\epsilon = 0.002$

$1/h$	$L^2 : \boldsymbol{u} - \boldsymbol{u}_h$	Rate	$\boldsymbol{H}^1 : \boldsymbol{u} - \boldsymbol{u}_h$	Rate	$L^2 : p - p_h$	Rate
2	0.1005075E-02	0.0000	0.1320204E-01	0.0000	0.3322399E-01	0.0000
4	0.1506689E-03	2.7378	0.3935345E-02	1.7462	0.9595745E-02	1.7918
6	0.4438982E-04	3.0140	0.1779524E-02	1.9574	0.4179567E-02	2.0498
8	0.1853301E-04	3.0362	0.1004275E-02	1.9886	0.2316299E-02	2.0517
10	0.9426854E-05	3.0294	0.6433142E-03	1.9960	0.1470369E-02	2.0366
12	0.5433241E-05	3.0223	0.4468800E-03	1.9984	0.1016161E-02	2.0265
14	0.3412525E-05	3.0171	0.3283549E-03	1.9993	0.7446319E-03	2.0168
16	0.2282055E-05	3.0133	0.2514065E-03	1.9997	0.5691130E-03	2.0131
18	0.1600749E-05	3.0107	0.1986447E-03	1.9999	0.4492570E-03	2.0078
20	0.1165872E-05	3.0087	0.1609018E-03	2.0000	0.3633780E-03	2.0136

Table 5.23. Mesh 6, $\epsilon = 0.0002$

$1/h$	$L^2 : \boldsymbol{u} - \boldsymbol{u}_h$	Rate	$\boldsymbol{H}^1 : \boldsymbol{u} - \boldsymbol{u}_h$	Rate	$L^2 : p - p_h$	Rate
2	0.1010621E-02	0.0000	0.1329874E-01	0.0000	0.3341842E-01	0.0000
4	0.1518431E-03	2.7346	0.3966055E-02	1.7455	0.9658056E-02	1.7908
6	0.4471876E-04	3.0149	0.1792761E-02	1.9583	0.4205323E-02	2.0506
8	0.1866700E-04	3.0368	0.1011557E-02	1.9892	0.2330390E-02	2.0520
10	0.9494196E-05	3.0298	0.6479196E-03	1.9964	0.1477964E-02	2.0407
12	0.5471808E-05	3.0225	0.4500568E-03	1.9986	0.1022237E-02	2.0221
14	0.3436665E-05	3.0172	0.3306801E-03	1.9995	0.7507656E-03	2.0023
16	0.2298160E-05	3.0135	0.2531821E-03	1.9998	0.5739014E-03	2.0118
18	0.1612020E-05	3.0108	0.2000443E-03	2.0000	0.4544753E-03	1.9809
20	0.1174084E-05	3.0087	0.1620357E-03	2.0000	0.3676320E-03	2.0127

Table 5.24. Mesh 6, $\epsilon = 0.00002$

$1/h$	$L^2 : \boldsymbol{u} - \boldsymbol{u}_h$	Rate	$\boldsymbol{H}^1 : \boldsymbol{u} - \boldsymbol{u}_h$	Rate	$L^2 : p - p_h$	Rate
2	0.1011183E-02	0.0000	0.1330852E-01	0.0000	0.3343757E-01	0.0000
4	0.1519616E-03	2.7343	0.3969154E-02	1.7454	0.9664517E-02	1.7907
6	0.4475195E-04	3.0150	0.1794096E-02	1.9584	0.4213521E-02	2.0474
8	0.1868054E-04	3.0369	0.1012294E-02	1.9893	0.2350809E-02	2.0284
10	0.9500990E-05	3.0298	0.6483843E-03	1.9964	0.1503727E-02	2.0024
12	0.5475694E-05	3.0226	0.4503769E-03	1.9987	0.1187676E-02	1.2941
14	0.3439099E-05	3.0172	0.3309146E-03	1.9995	0.8064395E-03	2.5113
16	0.2299784E-05	3.0135	0.2533611E-03	1.9999	0.8506894E-03	-0.4000
18	0.1613162E-05	3.0108	0.2001861E-03	2.0000	0.1061703E-02	-1.8813
20	0.1174910E-05	3.0088	0.1621497E-03	2.0001	0.5771693E-03	5.7848

Table 5.25. Mesh 7

	$\boldsymbol{V}_h = \mathring{\boldsymbol{M}}_0^2$			$\boldsymbol{V}_h = \boldsymbol{M}_0^2$		
$1/h$	$\bar{\gamma}_h$	α $(\bar{\gamma}_h = Ch^\alpha)$	$dim(N_h)$	$\bar{\gamma}_h$	α $(\bar{\gamma}_h = Ch^\alpha)$	$dim(N_h)$
2	0.02971885		1	0.13656013		0
4	0.03317544	-0.158737	1	0.10915819	0.323116	0
6	0.03393715	-0.055986	1	0.10628716	0.065736	0
8	0.03431836	-0.038829	1	0.10549365	0.026049	0
10	0.03454750	-0.029823	1	0.10512783	0.015567	0

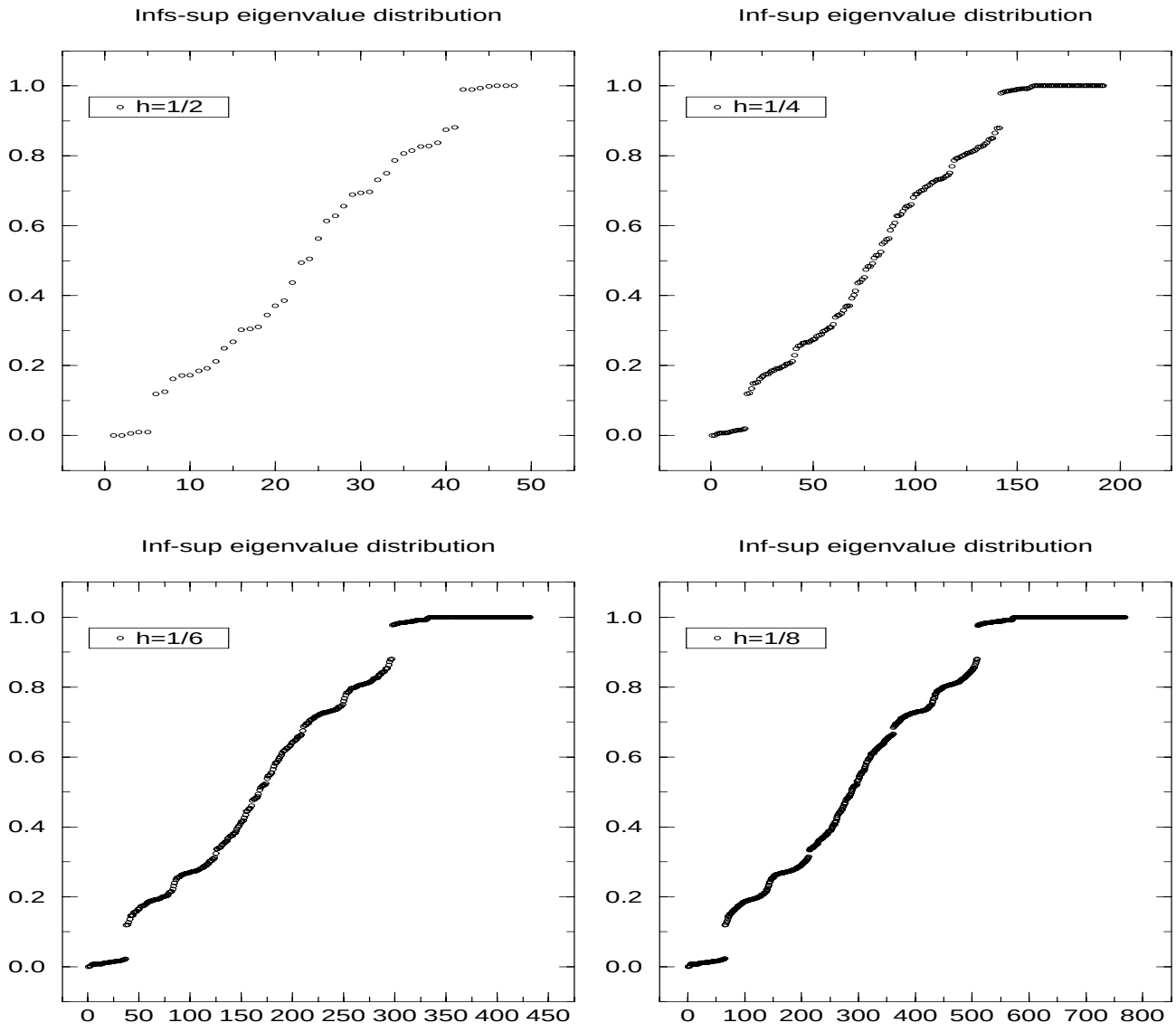

Figure 5.8. Mesh 7

Table 5.26. Mesh 7, $\epsilon = 0.002$

$1/h$	$L^2 : \boldsymbol{u} - \boldsymbol{u}_h$	Rate	$\boldsymbol{H}^1 : \boldsymbol{u} - \boldsymbol{u}_h$	Rate	$L^2 : p - p_h$	Rate
2	0.3014704E-02	0.0000	0.2476800E-01	0.0000	0.6090089E+00	0.0000
4	0.2905354E-03	3.3752	0.6779345E-02	1.8693	0.7403896E-01	3.0401
6	0.6802263E-04	3.5808	0.2724821E-02	2.2480	0.2118930E-01	3.0856
8	0.2590725E-04	3.3555	0.1449227E-02	2.1947	0.9473957E-02	2.7981
10	0.1257219E-04	3.2402	0.8966557E-03	2.1516	0.5341458E-02	2.5681
12	0.7042354E-05	3.1787	0.6088533E-03	2.1231	0.3437124E-02	2.4181
14	0.4338970E-05	3.1418	0.4402247E-03	2.1037	0.2403656E-02	2.3201
16	0.2861551E-05	3.1174	0.3330298E-03	2.0898	0.1778611E-02	2.2553
18	0.1986178E-05	3.1002	0.2606892E-03	2.0793	0.1371292E-02	2.2081
20	0.1434645E-05	3.0874	0.2095827E-03	2.0711	0.1089966E-02	2.1792

Table 5.27. Mesh 7, $\epsilon = 0.0002$

$1/h$	$L^2 : \boldsymbol{u} - \boldsymbol{u}_h$	Rate	$\boldsymbol{H}^1 : \boldsymbol{u} - \boldsymbol{u}_h$	Rate	$L^2 : p - p_h$	Rate
2	0.6719451E-02	0.0000	0.4848047E-01	0.0000	0.1517234E+01	0.0000
4	0.4051824E-03	4.0517	0.8356635E-02	2.5364	0.1391006E+00	3.4472
6	0.7959061E-04	4.0138	0.3030482E-02	2.5017	0.3272426E-01	3.5689
8	0.2835446E-04	3.5877	0.1556938E-02	2.3151	0.1268597E-01	3.2940
10	0.1340365E-04	3.3577	0.9494533E-03	2.2165	0.6571177E-02	2.9479
12	0.7418214E-05	3.2448	0.6400312E-03	2.1630	0.4027499E-02	2.6851
14	0.4541423E-05	3.1832	0.4608448E-03	2.1307	0.2738078E-02	2.5033
16	0.2983757E-05	3.1458	0.3477197E-03	2.1094	0.1990369E-02	2.3885
18	0.2065962E-05	3.1209	0.2717092E-03	2.0942	0.1516706E-02	2.3075
20	0.1489798E-05	3.1032	0.2181702E-03	2.0829	0.1197651E-02	2.2416

Table 5.28. Mesh 7, $\epsilon = 0.00002$

$1/h$	$L^2 : \boldsymbol{u} - \boldsymbol{u}_h$	Rate	$\boldsymbol{H}^1 : \boldsymbol{u} - \boldsymbol{u}_h$	Rate	$L^2 : p - p_h$	Rate
2	0.7901120E-02	0.0000	0.5652194E-01	0.0000	0.1809305E+01	0.0000
4	0.4402355E-03	4.1657	0.8777998E-02	2.6868	0.1577987E+00	3.5193
6	0.8285582E-04	4.1192	0.3094145E-02	2.5717	0.3596016E-01	3.6474
8	0.2892351E-04	3.6584	0.1574908E-02	2.3474	0.1354682E-01	3.3935
10	0.1356180E-04	3.3942	0.9570675E-03	2.2321	0.6873233E-02	3.0407
12	0.7479359E-05	3.2641	0.6441494E-03	2.1717	0.4168668E-02	2.7426
14	0.4570933E-05	3.1945	0.4634254E-03	2.1361	0.2828023E-02	2.5171
16	0.3000285E-05	3.1529	0.3494966E-03	2.1130	0.2118015E-02	2.1650
18	0.2076220E-05	3.1257	0.2730136E-03	2.0968	0.1723186E-02	1.7516
20	0.1496637E-05	3.1067	0.2191710E-03	2.0849	0.1304367E-02	2.6429

Table 5.29. Mesh 8

	$\boldsymbol{V}_h = \mathring{\boldsymbol{M}}_0^2$			$\boldsymbol{V}_h = \boldsymbol{M}_0^2$		
$1/h$	$\bar{\gamma}_h$	$\alpha\ (\bar{\gamma}_h = Ch^\alpha)$	$dim(N_h)$	$\bar{\gamma}_h$	$\alpha\ (\bar{\gamma}_h = Ch^\alpha)$	$dim(N_h)$
2	0.20795310		6	0.30566117		0
4	0.05863438	1.826440	8	0.15138448	1.013716	0
6	0.03991015	0.948764	10	0.10156855	0.984274	0
8	0.03010133	0.980462	12	0.07633846	0.992613	0
10	0.02413752	0.989505	14	0.06110630	0.997393	0
12	0.02013604	0.994158	16	0.05092200	0.999991	0
14	0.01727165	0.995419	18	0.04364023	1.001069	0
16	0.01511787	0.997436	20	0.03817525	1.001952	0

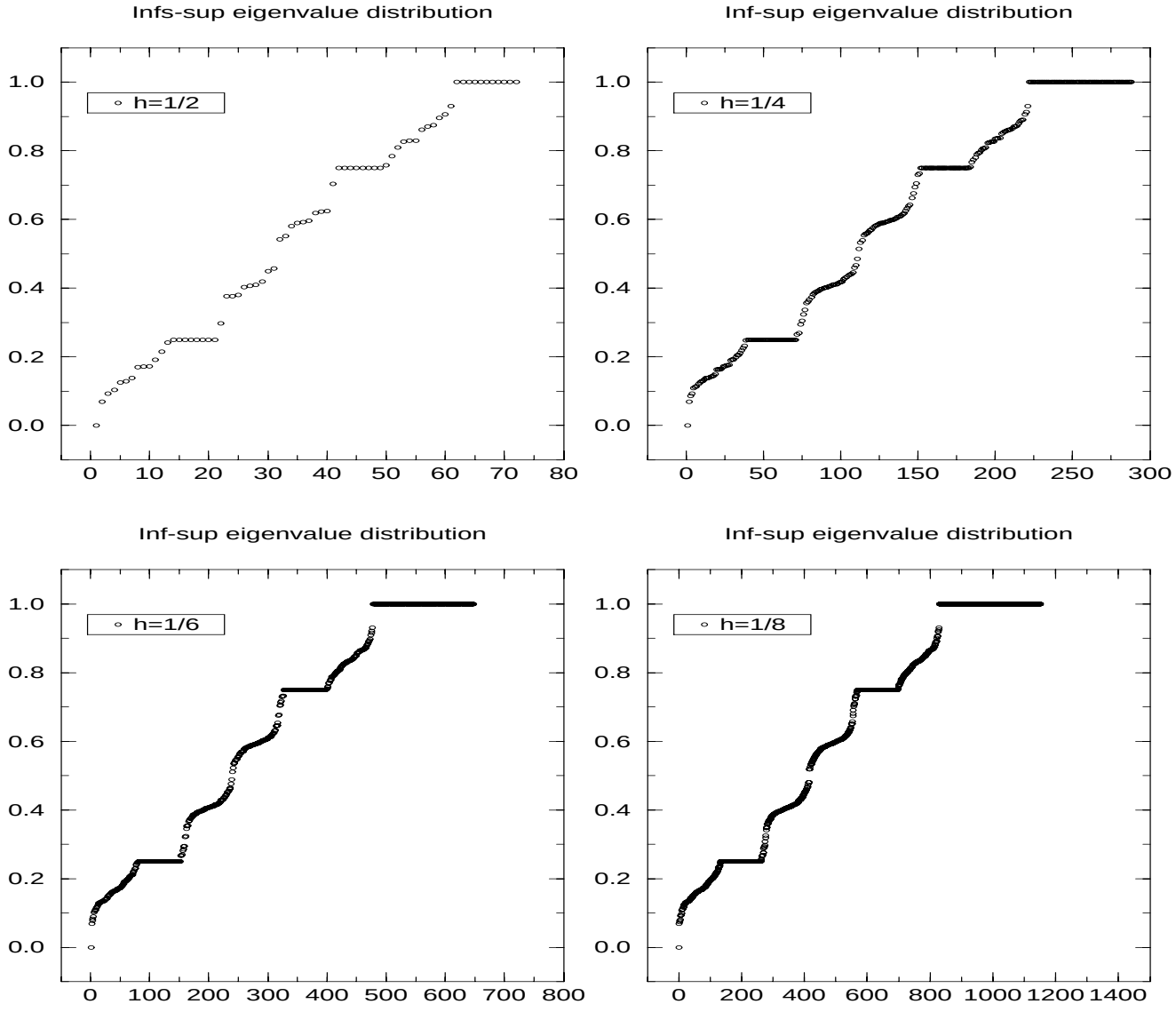

Figure 5.9. Mesh 8

Table 5.30. Mesh 8, $\epsilon = 0.002$

$1/h$	$L^2 : \boldsymbol{u} - \boldsymbol{u}_h$	Rate	$\boldsymbol{H}^1 : \boldsymbol{u} - \boldsymbol{u}_h$	Rate	$L^2 : p - p_h$	Rate
2	0.4924357E-02	0.0000	0.5574921E-01	0.0000	0.9184468E-01	0.0000
4	0.9057119E-03	2.4428	0.2039738E-01	1.4506	0.4609004E-01	0.9947
6	0.2872449E-03	2.8323	0.1052742E-01	1.6313	0.2705094E-01	1.3142
8	0.1213476E-03	2.9952	0.6406711E-02	1.7263	0.1763931E-01	1.4863
10	0.6104881E-04	3.0787	0.4302078E-02	1.7847	0.1236641E-01	1.5916
12	0.3452796E-04	3.1258	0.3084057E-02	1.8256	0.9129844E-02	1.6643
14	0.2124193E-04	3.1514	0.2316660E-02	1.8561	0.7004532E-02	1.7190
16	0.1392393E-04	3.1631	0.1802466E-02	1.8795	0.5536283E-02	1.7616
18	0.9590133E-05	3.1658	0.1441417E-02	1.8978	0.4481176E-02	1.7951
20	0.6872228E-05	3.1629	0.1178379E-02	1.9124	0.3698028E-02	1.8231

Table 5.31. Mesh 8, $\epsilon = 0.0002$

$1/h$	$L^2 : \boldsymbol{u} - \boldsymbol{u}_h$	Rate	$\boldsymbol{H}^1 : \boldsymbol{u} - \boldsymbol{u}_h$	Rate	$L^2 : p - p_h$	Rate
2	0.4957966E-02	0.0000	0.5603657E-01	0.0000	0.9267383E-01	0.0000
4	0.9164134E-03	2.4357	0.2060163E-01	1.4436	0.4678206E-01	0.9862
6	0.2913243E-03	2.8265	0.1066306E-01	1.6243	0.2754603E-01	1.3063
8	0.1232595E-03	2.9899	0.6501095E-02	1.7200	0.1799437E-01	1.4801
10	0.6208082E-04	3.0736	0.4370956E-02	1.7791	0.1262913E-01	1.5867
12	0.3514193E-04	3.1211	0.3136308E-02	1.8206	0.9330575E-02	1.6603
14	0.2163393E-04	3.1471	0.2357536E-02	1.8516	0.7163638E-02	1.7144
16	0.1418807E-04	3.1593	0.1835243E-02	1.8755	0.5664538E-02	1.7583
18	0.9775904E-05	3.1624	0.1468241E-02	1.8943	0.4586025E-02	1.7932
20	0.7007494E-05	3.1600	0.1200705E-02	1.9092	0.3789378E-02	1.8110

Table 5.32. Mesh 1, $\epsilon = 0.00002$

$1/h$	$L^2 : \boldsymbol{u} - \boldsymbol{u}_h$	Rate	$\boldsymbol{H}^1 : \boldsymbol{u} - \boldsymbol{u}_h$	Rate	$L^2 : p - p_h$	Rate
2	0.4961365E-02	0.0000	0.5606565E-01	0.0000	0.9275284E-01	0.0000
4	0.9175019E-03	2.4350	0.2062244E-01	1.4429	0.4686275E-01	0.9849
6	0.2917407E-03	2.8259	0.1067693E-01	1.6236	0.2763237E-01	1.3028
8	0.1234549E-03	2.9894	0.6510763E-02	1.7194	0.1807164E-01	1.4761
10	0.6218644E-04	3.0731	0.4378019E-02	1.7785	0.1266614E-01	1.5927
12	0.3520483E-04	3.1206	0.3141671E-02	1.8201	0.9411686E-02	1.6289
14	0.2167412E-04	3.1467	0.2361733E-02	1.8512	0.7293812E-02	1.6537
16	0.1421517E-04	3.1589	0.1838610E-02	1.8751	0.5799270E-02	1.7172
18	0.9794970E-05	3.1621	0.1470997E-02	1.8939	0.4792618E-02	1.6187
20	0.7021383E-05	3.1597	0.1202999E-02	1.9089	0.4020225E-02	1.6680

Chapter 6

STABILITY AND APPROXIMATION PROPERTIES OF THE $\mathcal{P}^3$–$\mathcal{P}^2$ ELEMENT

This chapter is devoted to the $\mathcal{P}^3$–$\mathcal{P}^2$ element for the Stokes equations. The $\mathcal{P}^3$–$\mathcal{P}^2$ element is defined for a polygonal domain $\Omega \subset \mathbb{R}^2$ as

$$\boldsymbol{V}_h = \mathring{\boldsymbol{M}}_0^3(\mathcal{T}_h) \quad \text{and} \quad P_h = M_{-1}^2(\mathcal{T}_h),$$

where $\mathcal{T}_h$ is a triangulation of Ω. The spaces M_h and N_h are defined accordingly for this element. With the many supporting evidences that will be displayed in this chapter, we will conclude that this element performs better than the $\mathcal{P}^2$–$\mathcal{P}^1$ element. For $n \geq 4$, the $\mathcal{P}^n$–$\mathcal{P}^{n-1}$ elements are stable on almost all meshes, see Scott and Vogelius [21].

To the best of our knowledge, there are only a few known results on the $\mathcal{P}^3$–$\mathcal{P}^2$ element. The work of Douglas and Dupont and Scott and Percell [14] implies that the $\mathcal{P}^3$–$\mathcal{P}^2$ element provides an optimal approximation for the velocity on irregular crisscross and barycentric trisected mesh families. In this chapter, we show that the numerical solution for the pressure can be optimally recovered as well on irregular crisscross meshes, and that the element is stable on the barycentric trisected mesh family.

In addition to the discussion on stability and approximation properties of the irregular crisscross and the barycentric trisected mesh families, we will study the element on mixed mesh family of diagonal and crisscross structures. It is shown that the $\mathcal{P}^3$–$\mathcal{P}^2$ element provides optimal approximations for both the velocity and the pressure on this mixed mesh family.

In the first section we introduce spurious pressure modes corresponding to diagonal and irregular crisscross meshes. As we will see, the number of independent pressure modes in N_h is 4 for the diagonal mesh. Therefore, the $\mathcal{P}^3$–$\mathcal{P}^2$ element also suffers from spurious pressure modes on these diagonal meshes. However, it is better than the $\mathcal{P}^2$–$\mathcal{P}^1$ element in that there are 6 independent pressure modes in N_h.

The technique used in this chapter is almost the same as the one used in Chapter 4. That is, we determine spurious pressure modes first, and then use the macroelement technique developed in Chapter 3 to determine the reduced stability of the finite element. Since all the results, proofs, and techniques of this chapter are similar to the ones in Chapter 4, we omit detailed discussions or proofs in order to keep this chapter shorter.

6.1. Spurious Pressure Modes

We shall determine spurious pressure modes of the $\mathcal{P}^3$–$\mathcal{P}^2$ element on the diagonal and the crisscross meshes in this section. On the diagonal mesh, there are four independent modes in N_h for the Stokes equations with Dirichlet boundary conditions. However, on an irregular crisscross mesh $\mathcal{T}_h$ there are $O(h^{-2})$ locally supported spurious pressure modes for the Stokes equations with either the Dirichlet or the traction boundary conditions.

6.1.1. Spurious Pressure Modes on a Diagonal Mesh

Let the unit square $\Omega = [0,1] \times [0,1]$ be partitioned into $n \times n$ equal small squares with n a positive integer and $h = 1/n$, and name each small square exactly in the way shown in Figure 4.4. Let $\mathcal{T}_h$ be the diagonal mesh of the unit square. Restricting any pressure function $p \in P_h$ on $K_{i,j}$, we can represent p by 12 real numbers $p_{i,j}^{(l)}$ and $q_{i,j}^{(l)}$, for $l = 1, 2, \cdots, 6$. Here $p_{i,j}^{(l)}$ are values of p at the vertices of the lower triangle of $K_{i,j}$, and $q_{i,j}^{(l)}$ are the values on the upper triangle of $K_{i.j}$ (see Figure 6.1). Let $\mathcal{U}_h$ be a macroelement covering of $\mathcal{T}_h$ such that any macroelement in $\mathcal{U}_h$ is formed by 2×2 small squares.

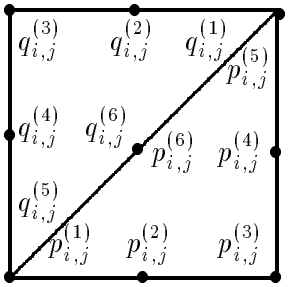

Figure 6.1. Values of p.

We will show that $\dim N_h$ equals 4 and display a basis for N_h explicitly in the following theorem. For convenience, we define 3 independent functions Φ_1,Φ_2, and Φ_3 of $P_h^{K_{i,j}} = M_{-1}^2(K_{i,j})$ (view $K_{i,j}$ as a macroelement) in the manner shown in Figure 6.2.

Theorem 6.1.1. *Define*

$$\Psi_1 = 1, \quad \forall K_{i,j},$$

$$\Psi_2|_{K_{i,j}} = \begin{cases} \Phi_1, & K_{1,n} \\ 0, & otherwise, \end{cases}$$

$$\Psi_3|_{K_{i,j}} = \begin{cases} \Phi_2, & K_{n,1} \\ 0, & otherwise, \end{cases}$$

$$\Psi_4|_{K_{i,j}} = \Phi_3, \quad \forall K_{i,j}.$$

Then Ψ_1, Ψ_2, Ψ_3, *and* Ψ_4 *form a basis for* N_h.

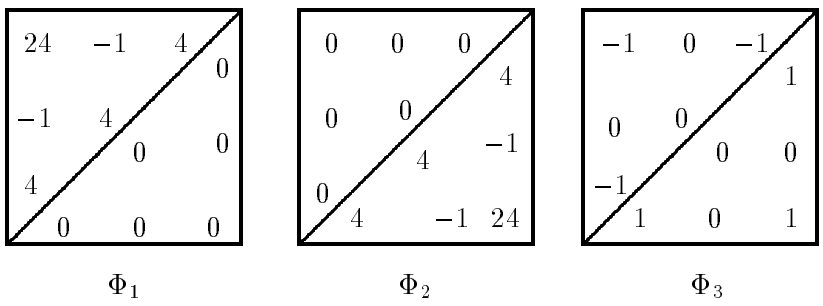

Figure 6.2. Definition of Φ_i.

Proof. Clearly, the functions Ψ_i are linearly independent. Therefore, we need to show that first any function in N_h must be a linear combination of the four functions, secondly these fouctions are in N_h.

Let $U_{i,j}$ be a macroelement formed by $K_{i,j}$, $K_{i+1,j}$, $K_{i,j+1}$, and $K_{i+1,j+1}$. Let $\boldsymbol{V}_h^{U_{i,j}} := \mathring{\boldsymbol{M}}_0^3(U_{i,j})$ and $P_h^{U_{i,j}} := M_{-1}^2(U_{i,j})$ be the velocity and the pressure space over $U_{i,j}$ respectively. Solving p from the system obtained by setting

$$\int_U p \operatorname{div} \boldsymbol{v} = 0, \quad \forall \boldsymbol{v} \in \boldsymbol{V}_h^{U_{i,j}},$$

we have $p \in N_h^{U_{i,j}}$ and p is a linear combination of following four pressure modes over $U_{i,j}$.

$$\begin{aligned}
p_1^{i,j} &= \begin{cases} \Phi_1, & K_{i,j+1} \\ 0, & \text{elsewhere in } U_{i,j}, \end{cases} \\
p_2^{i,j} &= \begin{cases} \Phi_2, & K_{i+1,j} \\ 0, & \text{elsewhere in } U_{i,j}, \end{cases} \\
p_3^{i,j} &= \Phi_3, \quad \forall K_{i,j} \in U_{i,j}, \\
p_4^{i,j} &= 1, \quad \forall K_{i,j} \in U_{i,j}.
\end{aligned}$$

Therefore, for any $p \in N_h$, p is a linear combination of $p_1^{i,j}$, $p_2^{i,j}$, $p_3^{i,j}$, and $p_4^{i,j}$ on any macroelement $U_{i,j}$ formed by 2×2 small squares. Since each macroelement overlaps with at least 3 other macroelements, the following argument is evident enough for us to conclude that p must be a linear combination of Ψ_1, Ψ_2, Ψ_3, and Ψ_4.

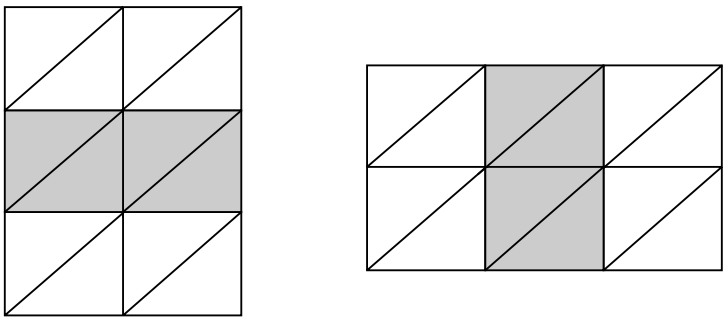

Figure 6.3. Overlaping macroelements.

We assume that the first submesh in Figure 6.3 is formed by two overlaping macroelements $U_{i,j}$ and $U_{i,j+1}$, and that the second one in Figure 6.3 by $U_{l,m}$ and $U_{l+1,m}$. The area of the overlap is shaded as indicated in Figure 6.3. For any $p \in N_h$, p satisfies

$$\begin{aligned}
p|_{U_{i,j}} &= \sum_{k=1}^{4} a_k^{i,j} p_k^{i,j}, \qquad p|_{U_{i,j+1}} = \sum_{k=1}^{4} a_k^{i,j+1} p_k^{i,j+1}, \\
p|_{U_{l,m}} &= \sum_{k=1}^{4} a_k^{l,m} p_k^{l,m}, \quad p|_{U_{l+1,m}} = \sum_{k=1}^{4} a_k^{l+1,m} p_k^{l+1,m}.
\end{aligned}$$

Since $U_{i,j}$ and $U_{i,j+1}$ are overlaping, simple calculations show that

$$a_1^{i,j} = 0, \quad a_3^{i,j} = a_3^{i,j+1}, \quad a_4^{i,j} = a_4^{i,j+1}, \quad \text{and} \quad a_2^{i,j+1} = 0.$$

Similarly, $U_{l,m}$ and $U_{l+1,m}$ gives

$$a_2^{l,m} = 0, \quad a_3^{l,m} = a_3^{l+1,m}, \quad a_4^{l,m} = a_4^{l+1,m}, \quad \text{and} \quad a_1^{l+1,m} = 0.$$

Repeatly applying the above arguments, we are able to show that any $p \in N_h$ must be a linear combination of Ψ_1, Ψ_2, Ψ_3, and Ψ_4.

It only remains to show that Ψ_i is in N_h, for $i = 1,2,3,4$. It is easy to see that $\Psi_i \in N_h$, for $i = 1,2,3$. For any nodal basis function in $\boldsymbol{V}_h$, its support is contained in some macroelement, so Ψ_4 is L^2 orthogonal to the divergence of any nodal basis function of $\boldsymbol{V}_h$. Therefore, Ψ_4 belongs to N_h. $\square$

It is interesting to see that the $\mathcal{P}^3$–$\mathcal{P}^2$ element has only 4 independent pressure modes in N_h on the diagonal mesh. As a matter of fact, only Ψ_4 affects the inf–sup constant and the rates of convergence of the numerical solutions. The function Ψ_1 equal to 1 globally does not hurt the stability and approximability of the element, neither do Ψ_2 and Ψ_3 (as long as the actual pressure is zero at these two corners). The functions Ψ_2 and Ψ_3 are induced by the two conner singular vertices of the triangulation $\mathcal{T}_h$.

It is easy to conclude that there are no spurious pressure modes for the Stokes equations with traction boundary conditions on the diagonal mesh family.

6.1.2. Spurious Pressure Modes around a Singular Vertex

Let U be a macroelement formed by partitioning a quadrilateral by its two diagonals (the first graph of Figure 6.4). Letters a, b, c, and d represent the lengths of the four interior edges of U.

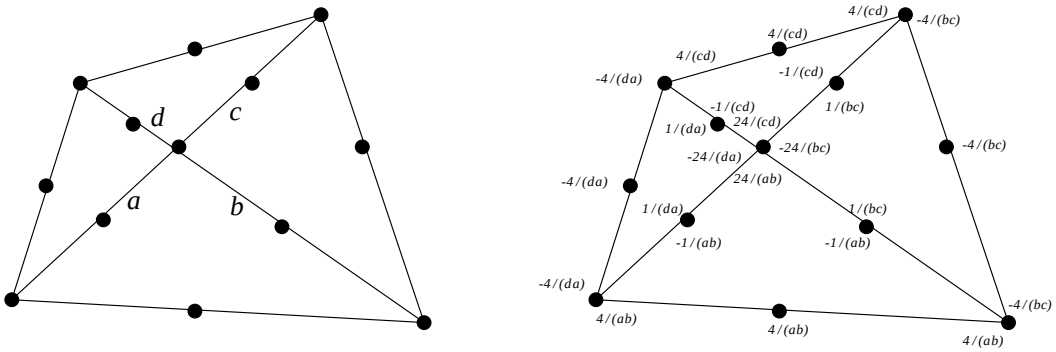

Figure 6.4. Macroelement U and spurious mode δ^U

Again, we solve a linear system obtained from

$$\int_U p \operatorname{div} \boldsymbol{v} = 0, \quad \forall \boldsymbol{v} \in \boldsymbol{V}_h^U := \mathring{\boldsymbol{M}}_0^3(U),$$

for the spurious pressure modes $p \in N_h^U$. With some calculations, we find that p is a linear combination of the constant function χ^U and δ^U. Here δ^U is displayed in the second gragh of Figure 6.4. In order to check whether p is in N_h, we put p into

$$\int_U p \operatorname{div} \boldsymbol{v},$$

and see if the integral equals zero for all $\boldsymbol{v} \in \boldsymbol{M}_0^3(U)$. The verification shows that only δ^U is in N_h.

Considering an irregular crisscross triangulation $\mathcal{T}_h$ of a polygonal domain Ω (see Figure 4.2), we find that for each singular vertex, there is a locally supported spurious pressure mode like δ^U (others are multiples of this mode). Therefore, locally supported spurious pressure modes are distributed uniformly in this type of mesh. Namely, N_h contains about $O(h^{-2})$ independent spurious pressure modes for either of the two boundary conditions. On the irregular crisscross mesh family, it is known (Douglas and Dupont and Scott and Percell [14]) that the numerical solution for the velocity has an optimal rate of convergence. In the next section, we will show that the recovered pressure also converges optimally.

6.2. Stability and Approximability on Irregular Crisscross Meshes

In this section we will formally discuss the stability and approximation properties of the $\mathcal{P}^3$–$\mathcal{P}^2$ element on irregular crisscross meshes. Again, let $\mathcal{T}_h$ be an irregular crisscross triangulation of a polygonal domain Ω and σ be the number of singular vertices of $\mathcal{T}_h$. For convenience, we let $\mathcal{U}_h$ denote the macroelement partition of $\mathcal{T}_h$ such that each $U \in \mathcal{U}_h$ has a structure like the first graph of Figure 6.4.

Based on the analysis in Section 6.1.2, we have the following lemma.

Lemma 6.2.1. *On an irregular crisscross mesh $\mathcal{T}_h$, if $\boldsymbol{V}_h := \mathring{\boldsymbol{M}}_0^3(\mathcal{T}_h)$ and $P_h := M_{-1}^2(\mathcal{T}_h)$, then*

$$\dim N_h = \sigma + 1,$$

and moreover, all δ^U together with the constant function 1 form a basis for N_h.

Proof. Since the constant function 1 and δ^U are in N_h for all $U \in \mathcal{U}_h$, $\dim N_h \geq \sigma + 1$. In order to prove $\dim N_h \leq \sigma + 1$, we need to show that if there is $p \in N_h$ orthogonal to δ^U for all $U \in \mathcal{U}_h$, then p must be a globally constant.

It is easy to see that such a p must be a piecewise constant function over the macroelement partition $\mathcal{U}_h$ (since χ^U and δ^U form a basis for N_h^U). Since $\boldsymbol{V}_h \times M_{-1}^0(\mathcal{U}_h)$ is a stable mixed finite element, p must be globally constant.

Hence, the constant function 1 and all the δ^U form a basis for N_h. □

The next theorem is about the stability and approximability of the $\mathcal{P}^3$–$\mathcal{P}^2$ element on irregular crisscross meshes. The proof of this theorem is almost identical to the proof of Theorem 4.3.1, and is therefore omitted.

Theorem 6.2.1. *On a regular family of irregular crisscross meshes $\mathcal{T}_h$, we have*

(1) *the reduced inf–sup constant $\bar{\gamma}_h \geq \alpha > 0$, where α is independent of h,*

(2) *if $(\boldsymbol{u}_h, p_h)$ and $(\boldsymbol{u}_h, \bar{p}_h)$ are numerical solutions of (2.4.2) and (2.4.3) from $\boldsymbol{V}_h \times P_h$ and $\boldsymbol{V}_h \times M_h$ respectively, then*

$$\|\boldsymbol{u} - \boldsymbol{u}_h\|_1 + \|p - \bar{p}_h\|_0 \leq Ch^3(\|\boldsymbol{u}\|_4 + \|p\|_3).$$

Here we assume $(\boldsymbol{u}, p) \in \boldsymbol{H}^4(\Omega) \times H^3(\Omega)$ solves (2.1.1). Moreover, $\bar{p}_h$ can be easily recovered from the solution p_h.

The reduced pressure $\bar{p}_h$ can be recovered from p_h just by filtering out the spurious pressure modes by using the process stated in (4.3.1).

The above theorem is also valid for the Stokes equations with traction boundary conditions.

6.3. Stability and Approximability on Mixed meshes

This section is devoted to the $\mathcal{P}^3$–$\mathcal{P}^2$ element on mixed triangulations of diagonal and crisscross structures. The analogous result for the $\mathcal{P}^2$–$\mathcal{P}^1$ element on the mixed mesh family is stated in Section 4.4 of Chapter 4. Again, we only consider the unit square as the domain Ω. Definitions for triangulations $\mathcal{T}_h$, the partition $\mathcal{Q}_h$ of the unit square, crisscross subdivisions, diagonal subdivisions, k–squares, and some related concepts are described in Section 4.4 of Chapter 4.

Theorem 6.3.1. *Suppose that the triangulation $\mathcal{T}_h$ is obtained by triangulating each square in $\mathcal{Q}_h$ with either the diagonal or the crisscross subdivision, and that there is at least one interior singular vertex of $\mathcal{T}_h$. Let σ denote the number of singular vertices of $\mathcal{T}_h$.*

(1) *Then* $\dim N_h = \sigma + 1$. *Moreover, there exists a locally supported spurious pressure mode around each singular vertex of $\mathcal{T}_h$.*

(2) *Consider a family of such triangulations $\mathcal{T}_h$ parametrized by h tending to zero. Suppose that there exists a number k such that every k-square contains at least one 1-square which is crisscross subdivided. Then there exists a positive constant γ depending only on k such that $\bar{\gamma}_h \geq \gamma$.*

Proof. Following the notations in Section 4.4 of Chapter 4, we let $U_1, U_2, \cdots, U_k$ denote all the $K_{i,j}$ such that each of them has an interior singular vertex. For convenience, we denote the spurious pressure mode (shown in Figure 6.4) on U_i by δ^{U_i}, $i = 1, 2, \cdots, k$. Let $\mathcal{T}_h^D$ denote the corresponding diagonal triangulation of the unit square with the same mesh size h. Since $\mathcal{T}_h$ can be viewed as a refinement of $\mathcal{T}_h^D$, $\boldsymbol{V}_h(\mathcal{T}_h^D) \subset \boldsymbol{V}_h(\mathcal{T}_h)$ and $P_h(\mathcal{T}_h^D) \subset P_h(\mathcal{T}_h)$.

If we can show that any $p \in N_h$ is a globally constant provided p is L^2 orthogonal to all δ^{U_i}, then (1) is proved. Suppose $p \in N_h$ is orthogonal to all the δ^{U_i}, then p must be a constant on each U_i. Therefore, $p \in N_h(\mathcal{T}_h^D)$. That is, p is a linear combination of Ψ_i, for $i = 1, 2, 3, 4$. The independence of Ψ_1, Ψ_2, Ψ_3 and Ψ_4 guarantees that p is a globally constant.

The proof of (2) is exactly the same as the proof for the third statement of Theorem 4.4.1. □

Similar to Theorem 4.4.2, we have

Theorem 6.3.2. *Assume $(\boldsymbol{u}, p) \in \boldsymbol{H}^4(\Omega) \times H^3(\Omega)$ solves (2.1.1) and $(\boldsymbol{u}_h, \bar{p}_h) \in \boldsymbol{V}_h \times M_h$ solves (2.4.3). Under the assumptions of Theorem 6.3.1, we have*

$$\|\boldsymbol{u} - \boldsymbol{u}_h\|_{1,\Omega} \leq C \inf_{\boldsymbol{v} \in \boldsymbol{V}_h} \|\boldsymbol{u} - \boldsymbol{v}\|_{1,\Omega} \leq Ch^3 \|\boldsymbol{u}\|_{4,\Omega}, \tag{6.3.1}$$

$$\|p - \bar{p}_h\|_{0,\Omega} \leq Ch^3 \|\boldsymbol{u}\|_{4,\Omega} + C \inf_{q \in M_h} \|p - q\|_{0,\Omega}. \tag{6.3.2}$$

If $K_{1,n}$ and $K_{n,1}$ are crisscross subdivisions, then

$$\|p - \bar{p}_h\|_{0,\Omega} \leq Ch^3 (\|\boldsymbol{u}\|_{4,\Omega} + \|p\|_{3,\Omega}). \tag{6.3.3}$$

If $K_{1,n}$ and $K_{n,1}$ are crisscross subdivisions, then $M_{-1}^2(\mathcal{Q}_h) \subset M_h$. Therefore, (6.3.2) implies (6.3.3). If $\mathcal{T}_h$ has one or two corner singular vertices, then the actual pressure p can be approximated by $\bar{p}_h \in M_h$ with an optimal rate of convergence provided p is orthogonal to the spurious pressure modes associated with the corner singular vertices of $\mathcal{T}_h$.

The pressure is recovered exactly in the way it was for the irregular crisscross meshes.

For the Stokes equations with traction boundary conditions, Theorem 6.3.1 holds and the estimate, under the assumptions of Theorem 6.3.1, is

$$\|\boldsymbol{u} - \boldsymbol{u}_h\|_{1,\Omega} + \|p - \bar{p}_h\|_{0,\Omega} \leq Ch^3 (\|\boldsymbol{u}\|_{4,\Omega} + \|p\|_{3,\Omega}).$$

6.4. Stability and Approximability on Barycentric Trisected Meshes

We shall prove that the $\mathcal{P}^3$–$\mathcal{P}^2$ element is stable on barycentric trisected triangulations in this section. Namely, the space N_h contains only constant functions, and the inf–sup constant γ_h is bounded from below by a positive number independent of h.

Let $\mathcal{S}_h$ be a regular triangulation of a polygonal domain Ω and $\mathcal{T}_h$ be a refinement of $\mathcal{S}_h$ by connecting the three vertices of each triangle in $\mathcal{S}_h$ to its barycenter. We call such a triangulation $\mathcal{T}_h$ a barycentric trisected triangulation. Let $\mathcal{U}_h$ be a macroelement partition of $\mathcal{T}_h$ such that each $U \in \mathcal{U}_h$ is a triangle in $\mathcal{S}_h$.

Let $\hat{U}$ be the triangulation of the reference triangle $\hat{\tau}$ by connecting the three vertices of $\hat{\tau}$ to its barycenter. Clearly, any $U \in \mathcal{U}_h$ is a image of $\hat{U}$ under a linear mapping. Some algebraic computation shows that $N_h^{\hat{U}}$ contains only constant functions. Therefore, by Lemma 3.5.1, N_h^U contains only constant functions for any $U \in \mathcal{U}_h$. Applying the macroelement partition theorem (Theorem 3.2.1), we have the following theorem.

Theorem 6.4.1. *Consider a family of regular barycentric trisected triangulations $\mathcal{T}_h$ parametrized by h tending to zero. Then*

(1) *The $\mathcal{P}^3$–$\mathcal{P}^2$ element is stable on this mesh family.*
(2) *Assume $(\boldsymbol{u}, p) \in \boldsymbol{H}^4(\Omega) \times H^3(\Omega)$ solves (2.1.1) and $(\boldsymbol{u}_h, p_h) \in \boldsymbol{V}_h \times P_h$ solves (2.4.2). Then*

$$\|\boldsymbol{u} - \boldsymbol{u}_h\|_{1,\Omega} \leq C \inf_{\boldsymbol{v} \in \boldsymbol{V}_h} \|\boldsymbol{u} - \boldsymbol{v}\|_{1,\Omega} \leq Ch^3 \|\boldsymbol{u}\|_{4,\Omega},$$
$$\|p - p_h\|_{0,\Omega} \leq Ch^3 (\|\boldsymbol{u}\|_{4,\Omega} + \|p\|_{3,\Omega}).$$

Combining Theorem 4.6.1, Theorem 6.4.1, and the result by Scott and Vogelius [21], we can conclude that $\mathcal{P}^n$–$\mathcal{P}^{n-1}$ element is stable on barycentric trisected triangulations for $n \geq 2$ for the Stokes equations with either the Dirichlet or the traction boundary conditions.

Remark 6.4.1. *The $\mathcal{P}^3$–$\mathcal{P}^2$ element works fine on mixed meshes of diagonal subdivisions and barycentric trisected subdivisions (see Remark 4.6.2) of the unit square. The only spurious pressure modes are from the corner verices on these meshes. We can prove similar results as stated in Theorem 6.3.1 and Theorem 6.3.2 for this type of meshes.*

Chapter 7

STABILITY AND APPROXIMATION PROPERTIES OF THE $\mathcal{P}^1$–$\mathcal{P}^0$ ELEMENT

In this chapter, we will present some theoretical results on the $\mathcal{P}^1$–$\mathcal{P}^0$ element for the Stokes equations. The $\mathcal{P}^1$–$\mathcal{P}^0$ element is defined by

$$\boldsymbol{V}_h = \mathring{\boldsymbol{M}}_0^1(\mathcal{T}_h) \text{ and } P_h = M_{-1}^0(\mathcal{T}_h),$$

on any triangulation $\mathcal{T}_h$. In other words, the velocity space of this element consists of continuous piecewise linear polynomials and the pressure space consists of discontinuous piecewise constants.

This element is probably the simplest finite element for the Stokes equations that preserves the incompressibility condition. Unfortunately, the pressure space P_h is too large on many meshes so that the numerical solution for the velocity is always zero, for example, on the diagonal mesh of the unit square. However, for some meshes this element does have optimal rate of convergence for the velocity, and moreover the pressure can be recovered.

This chapter is organized as follows. First, we introduce Powell's result on the approximation property of C^1 quadratic polynomials over crisscross meshes. Secondly, on the crisscross mesh family of the unit square, we show that the reduced inf–sup constant is Ch. Namely, the element is not reduced stable. However, we can prove that the finite element solution for the velocity converges optimally, and that the solution for the pressure can be recovered. Next, we present some similar approximation results for a general mesh family of a polygonal domain. Furthermore, we display a basis for the space $\boldsymbol{Z}_h$ of all the divergence-free functions in $\boldsymbol{V}_h$ over the crisscross mesh of the unit square, and show that $\boldsymbol{Z}_h$ has optimal approximation properties for any divergence-free functions in $\mathring{\boldsymbol{H}}^1$. Finally, we exhibit a relation between the stabilities of the $\mathcal{P}^1$–$\mathcal{P}^0$ element and the $\mathcal{Q}^1$–$\mathcal{P}^0$ quadrilateral element.

7.1. Known Results

A known result on the $\mathcal{P}^1$–$\mathcal{P}^0$ element is by Powell [20] who considers approximation properties of C^1 quadratic polynomials on the crisscross mesh family. However, Powell's result can be adapted for the $\mathcal{P}^1$–$\mathcal{P}^0$ element on the crisscross mesh of the unit square. That is, the $\mathcal{P}^1$–$\mathcal{P}^0$ element provides a numerical solution for the velocity with an optimal rate of convergence for the Stokes equations with traction boundary conditions. We show also that the $\mathcal{P}^1$–$\mathcal{P}^0$ element works for the Stokes equations with Dirichlet boundary conditions.

7.2. Spurious Modes around a Singular Vertex

For the $\mathcal{P}^1$–$\mathcal{P}^0$ element, there exist spurious pressure modes around each singular vertex of a triangulation $\mathcal{T}_h$. In this section, we explicitly display these modes associated with a singular vertex. The way to determine a spurious pressure mode is similar to that used for the $\mathcal{P}^2$–$\mathcal{P}^1$ element.

We consider spurious pressure modes on a macroelement U which is a quadrilateral divided by its two diagonals (see the first figure of Figure 7.1). Letters a, b, c, and d denote the lengths of the four interior edges of $\mathcal{T}_h^U$. Let the nodal basis functions corresponding to vertices 1, 2, 3, 4, and 5 be denoted by ϕ_1, ϕ_2, ϕ_3, ϕ_4, and ϕ_5 respectively. Since rotations and translations do not change the inf–sup constant, we assume that one diagonal of U lies on the x-axis. For convenience, we denote the directions of the two diagonals of U by $(1,0)$ and (n_1,n_2). The coordinates of the five vertices of $\mathcal{T}_h^U$ are

$$(a,0), \quad (bn_1,bn_2), \quad (-c,0), \quad (-dn_1,-dn_2), \quad \text{and} \quad (0,0).$$

Any arbitrary $\boldsymbol{u} \in \boldsymbol{V}_h^U$ can be written as

$$\boldsymbol{u} = \sum_{i=1}^{5} (u_i, v_i)\phi_i.$$

For any $p \in P_h^U$, its values in the four triangles of $\mathcal{T}_h^U$ are denoted by p_1^U, p_2^U, p_3^U, and p_4^U, starting from the triangle with vertices 1, 2, and 5, and moving in a counterclockwise direction.

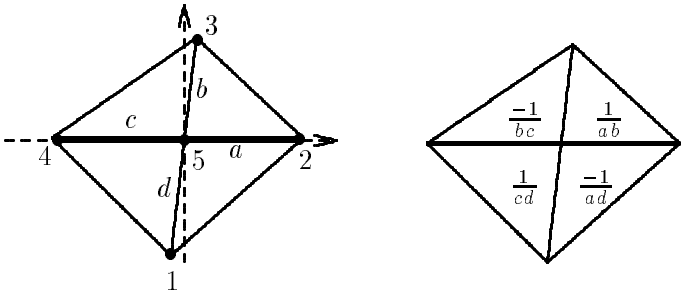

Figure 7.1. Macroelement U and spurious pressure mode.

Set

$$\begin{aligned} 2\int_U p \operatorname{div} \boldsymbol{u} = {} & n_2(dp_1^U + bn_2p_2^U)u_2 + n_2(-bp_3^U - dp_4^U)u_4 + \\ & n_2(-dp_1^U - bp_2^U + bp_3^U + dp_4^U)u_5 + (-ap_1^U - cp_4^U)v_1 + \\ & n_1(-dp_1^U - bp_2^U)v_2 + (ap_2^U + cp_3^U)v_3 + n_1(bp_3^U + dp_4^U)v_4 + \\ & (ap_1^U + dn_1p_1^U - ap_2^U + bn_1p_2^U - cp_3^U - bn_1p_3^U + cp_4^U - dn_1p_4^U)v_5 = 0, \end{aligned}$$

for any $\boldsymbol{u} \in \boldsymbol{V}_h^U$. Solving the system obtained from the above equation, we have

$$p_1^U = -\frac{1}{ad}, \quad p_2^U = \frac{1}{ab}, \quad p_3^U = -\frac{1}{bc}, \quad p_4^U = \frac{1}{cd}, \tag{7.2.1}$$

as a representative of all the spurious pressure modes around the singular vertex of $\mathcal{T}_h^U$ (see the second figure in Figure 6.1). If we solve the linear system corresponding to u_5 and v_5, then the solution space is spanned by χ^U and the one shown in (7.2.1)—this fact is frequently used in latter sections.

If the macroelement U is a square or a parallelogram, then

$$p_1^U = -1, \quad p_2^U = 1, \quad p_3^U = -1, \quad p_4^U = 1,$$

is a basis function of all the spurious pressure modes associated with the singular vertex of $\mathcal{T}_h^U$.

7.3. Stability and Approximability on Crisscross Meshes

In this section, we show that on the crisscross mesh the $\mathcal{P}^1$–$\mathcal{P}^0$ element is unstable even after all spurious pressure modes are removed from the pressure space P_h. That is, $\boldsymbol{V}_h \times M_h$ is unstable. Specifically, we will show that the reduced inf–sup constant $\bar{\gamma}_h$ is Ch. Therefore, we do not expect to get any meaningful estimates for the numerical solution if the standard analysis is directly applied to $\boldsymbol{V}_h \times M_h$. However, with a deeper consideration we show that the numerical solution for the velocity converges optimally and that the pressure can be recovered as well.

For convenience, we consider the unit square $\Omega = [0,1] \times [0,1]$ as the domain in this section. Let $\mathcal{Q}_h$ denote a partition of Ω which has $n \times n$ equal small squares with $h = 1/n$ and n a positive integer. The crisscross triangulation $\mathcal{T}_h$ of Ω is obtained by dividing each small square of $\mathcal{Q}_h$ by its two diagonals. A vertex in $\mathcal{T}_h$ is denoted by (α, β) if the vertex has coordinates $(\alpha h, \beta h)$.

7.3.1. Space of Spurious Pressure Modes

In order to analyze the $\mathcal{P}^1$–$\mathcal{P}^0$ element on the crisscross mesh family on the unit square, we first need to determine the structure of the space N_h on this family. As we have seen in Section 2, for each singular vertex $(i+1/2, j+1/2)$ of the triangulation $\mathcal{T}_h$, there is a spurious pressure mode denoted by $\delta_{i+1/2,j+1/2}$, with four triangles as its support (see the second figure of Figure 7.1). Therefore, all $\delta_{i+1/2,j+1/2}$ are in N_h. We will show that in addition to the $\delta_{i+1/2,j+1/2}$'s there is also a globally supported spurious pressure mode in N_h. Surprisingly, locally and globally supported spurious pressure modes occur simultaneously for the crisscross mesh family.

If $p \in N_h$ is orthogonal to all $\delta_{i+1/2,j+1/2}$, then p must be a constant in each small square in $\mathcal{Q}_h$. For convenience, we denote the value of p by $p_{i+1/2,j+1/2}$ in a small square with $(i+1/2, j+1/2)$ as its center vertex.

Let $\boldsymbol{u} \in \boldsymbol{V}_h$ be arbitrary. We have

$$\boldsymbol{u} = \sum_{1 \le i,j \le n-1} (u_{i,j}, v_{i,j}) \phi_{i,j} + \sum_{0 \le i,j \le n-1} (u_{i+\frac{1}{2},j+\frac{1}{2}}, v_{i+\frac{1}{2},j+\frac{1}{2}}) \phi_{i+\frac{1}{2},j+\frac{1}{2}},$$

where $\phi_{i,j}$ and $\phi_{i+1/2,j+1/2}$ are all the nodal basis functions in $\boldsymbol{V}_h$. Hence,

$$\begin{aligned} \frac{2}{h} \int_\Omega p \operatorname{div} \boldsymbol{u} = \sum_{1 \le i,j \le n-1} \big[& (-p_{i+\frac{1}{2},j+\frac{1}{2}} + p_{i-\frac{1}{2},j+\frac{1}{2}} + p_{i-\frac{1}{2},j-\frac{1}{2}} - p_{i+\frac{1}{2},j-\frac{1}{2}}) u_{i,j} + \\ & (-p_{i+\frac{1}{2},j+\frac{1}{2}} - p_{i-\frac{1}{2},j+\frac{1}{2}} + p_{i-\frac{1}{2},j-\frac{1}{2}} + p_{i+\frac{1}{2},j-\frac{1}{2}}) v_{i,j} \big]. \end{aligned} \tag{7.3.1}$$

Since $u_{i,j}$ and $v_{i,j}$ are arbitrary, by setting (7.3.1) to zero we have the following linear system

$$\begin{aligned} -p_{i+\frac{1}{2},j+\frac{1}{2}} + p_{i-\frac{1}{2},j+\frac{1}{2}} + p_{i-\frac{1}{2},j-\frac{1}{2}} - p_{i+\frac{1}{2},j-\frac{1}{2}} &= 0, \\ -p_{i+\frac{1}{2},j+\frac{1}{2}} - p_{i-\frac{1}{2},j+\frac{1}{2}} + p_{i-\frac{1}{2},j-\frac{1}{2}} + p_{i+\frac{1}{2},j-\frac{1}{2}} &= 0, \end{aligned}$$

for $1 \le i, j \le n-1$. Therefore, we have

$$\begin{aligned} p_{i+\frac{1}{2},j+\frac{1}{2}} &= p_{i-\frac{1}{2},j-\frac{1}{2}}, \\ p_{i-\frac{1}{2},j+\frac{1}{2}} &= p_{i+\frac{1}{2},j-\frac{1}{2}} \end{aligned}$$

for $1 \le i, j \le n-1$.

If we require $\int_\Omega p = 0$, then $p_{i+1/2,j+1/2} = -p_{i-1/2,j+1/2}$, for $1 \le i \le n-1$ and $0 \le j \le n-1$.

Now we are able to conclude that p is a globally supported checkerboard-like spurious pressure mode (see Figure 7.2) denoted by δ_Ω.

-1	1	-1	1
1	-1	1	-1
-1	1	-1	1
1	-1	1	-1

Figure 7.2 Global checkerboard δ_Ω, $h = 1/4$.

Theorem 7.3.1. *On the crisscross mesh $\mathcal{T}_h$ of the unit square with $h = 1/n$, we have*

$$\dim N_h = n^2 + 2.$$

Moreover, any function in N_h can be written as a linear combination of the global constant function 1, the $\delta_{i+1/2,j+1/2}$'s, and the pressure mode δ_Ω.

The proof of the above theorem is immediate.

On the crisscross mesh, the structure of N_h for the $\mathcal{P}^1$–$\mathcal{P}^0$ element is a little different from the one for the $\mathcal{P}^2$–$\mathcal{P}^1$ element. For the $\mathcal{P}^2$–$\mathcal{P}^1$ element, all spurious pressure modes are locally supported. As we will see later on, the globally supported mode δ_Ω and its localized version which appears in each macroelement are the major sources of trouble for the analysis of the approximability and the stability of the $\mathcal{P}^1$–$\mathcal{P}^0$ element.

7.3.2. Reduced inf–sup Constant

In this section, we will prove that the reduced inf–sup constant $\bar{\gamma}_h$ for the $\mathcal{P}^1$–$\mathcal{P}^0$ element is about Ch on the crisscross mesh family of the unit square. First we prove that the reduced inf–sup constant $\bar{\gamma}_h$ is at least Ch, and then we show that $\bar{\gamma}_h$ is at most Ch by an example.

Lemma 7.3.1. *Let $\mathcal{T}_h$ be the crisscross mesh. Then $\boldsymbol{V}_h \times M_h$ is unstable, and moreover, the reduced inf–sup constant*

$$\bar{\gamma}_h \ge Ch,$$

where constant C is independent of h.

Proof. Let $\mathcal{Q}_h$ be a macroelement partition of $\mathcal{T}_h$. Obviously, each macroelement in $\mathcal{Q}_h$ is a translation of any other macroelement in $\mathcal{Q}_h$. Therefore, the local inf–sup constant of $\boldsymbol{V}_h^U \times M_h^U$ is $O(1)$ for any macroelement $U \in \mathcal{Q}_h$. Since M_h^U contains only constants for any macroelement $U \in \mathcal{Q}_h$, the reduced inf–sup constant is at least h if we can prove that $\boldsymbol{V}_h \times Q_h$ ($Q_h := M_{-1}^0(\mathcal{Q}_h) \cap M_h$) has a inf–sup constant greater than Ch.

For any $p \in Q_h$ and $\boldsymbol{u} \in \boldsymbol{V}_h$, we have

$$\begin{aligned}\int_\Omega p \operatorname{div} \boldsymbol{u} = \frac{h}{2} \sum_{1 \le i,j \le n-1} \Big[&(-p_{i+\frac{1}{2},j+\frac{1}{2}} + p_{i-\frac{1}{2},j+\frac{1}{2}} + p_{i-\frac{1}{2},j-\frac{1}{2}} - p_{i+\frac{1}{2},j-\frac{1}{2}})u_{i,j} + \\ &(-p_{i+\frac{1}{2},j+\frac{1}{2}} - p_{i-\frac{1}{2},j+\frac{1}{2}} + p_{i-\frac{1}{2},j-\frac{1}{2}} + p_{i+\frac{1}{2},j-\frac{1}{2}})v_{i,j}\Big].\end{aligned} \tag{7.3.2}$$

In particular, pick $\boldsymbol{u} \in \boldsymbol{V}_h$ such that

$$\begin{aligned} u_{i,j} =& h(-p_{i+\frac{1}{2},j+\frac{1}{2}} + p_{i-\frac{1}{2},j+\frac{1}{2}} + p_{i-\frac{1}{2},j-\frac{1}{2}} - p_{i+\frac{1}{2},j-\frac{1}{2}}), \\ v_{i,j} =& h(-p_{i+\frac{1}{2},j+\frac{1}{2}} - p_{i-\frac{1}{2},j+\frac{1}{2}} + p_{i-\frac{1}{2},j-\frac{1}{2}} + p_{i+\frac{1}{2},j-\frac{1}{2}}), \end{aligned}$$

and

$$\begin{aligned} u_{i+\frac{1}{2},j+\frac{1}{2}} &= 0, \\ v_{i+\frac{1}{2},j+\frac{1}{2}} &= 0. \end{aligned}$$

Then, we have

$$\begin{aligned} \int_\Omega p \operatorname{div} \boldsymbol{u} =& \frac{h^2}{2} \sum_{1 \le i,j \le n-1} \big[(-p_{i+\frac{1}{2},j+\frac{1}{2}} + p_{i-\frac{1}{2},j+\frac{1}{2}} + p_{i-\frac{1}{2},j-\frac{1}{2}} - p_{i+\frac{1}{2},j-\frac{1}{2}})^2 + \\ & (-p_{i+\frac{1}{2},j+\frac{1}{2}} - p_{i-\frac{1}{2},j+\frac{1}{2}} + p_{i-\frac{1}{2},j-\frac{1}{2}} + p_{i+\frac{1}{2},j-\frac{1}{2}})^2\big) \\ =& h^2 \sum_{1 \le i,j \le n-1} \big((p_{i+\frac{1}{2},j+\frac{1}{2}} - p_{i-\frac{1}{2},j-\frac{1}{2}})^2 + (p_{i-\frac{1}{2},j+\frac{1}{2}} + p_{i+\frac{1}{2},j-\frac{1}{2}})^2\big]. \end{aligned} \tag{7.3.3}$$

Define the right hand side of (7.3.3) to be the square of a seminorm of p, denoted by $|p|_h$. It is easy to show that

$$\|\boldsymbol{u}\|_{1,\Omega} \le Ch^{-1}\|\boldsymbol{u}\|_{0,\Omega} \le C|p|_h.$$

Hence, the last inequality together with (7.3.3) implies

$$\frac{b(\boldsymbol{u},p)}{\|\boldsymbol{u}\|_{1,\Omega}} \ge C|p|_h.$$

If we can show that

$$h\|p\|_{0,\Omega} \le C|p|_h, \tag{7.3.4}$$

for any $p \in Q_h$, then we are done.

In order to prove (7.3.4), we need to show

$$\begin{aligned} \sum_{1 \le i,j \le n-1} & \big[(p_{i+\frac{1}{2},j+\frac{1}{2}} - p_{i-\frac{1}{2},j-\frac{1}{2}})^2 + (p_{i-\frac{1}{2},j+\frac{1}{2}} + p_{i+\frac{1}{2},j-\frac{1}{2}})^2\big] \\ & \ge Ch^2 \sum_{0 \le i,j \le n-1} p^2_{i+\frac{1}{2},j+\frac{1}{2}}. \end{aligned} \tag{7.3.5}$$

The left hand side of (7.3.5) can be split into two parts: a part containing all the terms with $i+j$ even and another with all the terms with $i+j$ odd. Each $p_{i+1/2,j+1/2}$ appears in either one of the two parts at most 4 times, and each part has $O(h^{-2})$ terms. If $p_{i+1/2,j+1/2}$ is zero for at least two vertices $(i+1/2, j+1/2)$ one with $i+j$ even and another witj $i+j$ odd, then (7.3.5) holds. Since $|1|_h = 0$ and $|\delta_\Omega|_h = 0$, we can add a function q which is a linear combination of the constant function 1 and δ_Ω to p such that $p+q$ vanishes at two pairs of $(i+1/2, j+1/2)$ with $i+j$ is even and odd each. Hence,

$$\|p\|^2_{0,\Omega} = \|p+q\|^2_{0,\Omega} - \|q\|^2_{0,\Omega} \le \|p+q\|^2_{0,\Omega} \le Ch^{-2}|p+q|^2_h = Ch^{-2}|p|^2_h.$$

(The proof of (7.3.5) can be found in the book by Girault and Raviart [11, § II.3.3] and the paper by Johnson and Pitkäranta [13].) This proves the lemma. □

Lemma 7.3.2. *On the crisscross mesh, there is $q \in M_h$ such that the reduced inf–sup constant $\bar{\gamma}_h$ of $\boldsymbol{V}_h \times P_h$ satisfies*

$$\bar{\gamma}_h \leq Ch,$$

where constant C is independent of h.

Proof. We will find a specific $q \in M_h$ such that

$$\sup_{\boldsymbol{v} \in \boldsymbol{V}_h} \frac{b(\boldsymbol{v}, q)}{\|\boldsymbol{v}\|_{1,\Omega} \|q\|_{0,\Omega}} \leq Ch.$$

The example is exactly the same as the one in Girault and Raviart [11,§ II.3.3] for the $\mathcal{Q}^1$–$\mathcal{P}^0$ element.

Without loss of generality, we consider $\Omega = [-1, 1] \times [-1, 1]$. Let $\mathcal{T}_h$ denote the crisscross triangulation with $h = 1/(2n)$, and let $\mathcal{Q}_{2h}$ denote the macroelement partition of $\mathcal{T}_h$ such that every macroelement has size $2h \times 2h$ and is made up of 16 triangles. A macroelement in $\mathcal{Q}_{2h}$ is denoted by $U_{i,j}$ if (ih, jh) are the coordinates of the center vertex of the macroelement. Let $\delta_{U_{i,j}}$ denote a pressure function which is zero outside of $U_{i,j}$ and has values on $U_{i,j}$ as shown in Figure 7.3.

-1	1
1	-1

Figure 7.3. $\delta_{U_{i,j}}$.

Define

$$q = \sum_{U_{i,j} \in \mathcal{Q}_{2h}} i \delta_{U_{i,j}}.$$

One can easily verify that q is in M_h since q is orthogonal to N_h. After some calculations, we have

$$\sup_{\boldsymbol{v} \in \boldsymbol{V}_h} \frac{b(\boldsymbol{v}, q)}{\|\boldsymbol{v}\|_{1,\Omega} \|q\|_{0,\Omega}} \leq \sqrt{6}h. \quad \square$$

Combining Lemmas 7.3.1 and 7.3.2 we have the following theorem.

Theorem 7.3.2. *On the crisscross mesh, the space $\boldsymbol{V}_h \times M_h$ is unstable and the reduced inf–sup constant $\bar{\gamma}_h$ of $\boldsymbol{V}_h \times P_h$ satisfies*

$$\bar{\gamma}_h = Ch,$$

where constant C is independent of h.

The above theorem implies that we can not directly apply the standard techniques of error analysis to $\boldsymbol{V}_h \times M_h$ since $\bar{\gamma}_h = O(h)$ makes error estimates meaningless. At this point, we don't know whether the numerical solution fails to converge or our analysis is not sharp enough to unveil the real property of the numerical solution. We will give a positive answer to this question in the next section.

7.3.3. Approximation Properties

In this section, we show that the numerical solution approaches the actual solution at a rate of h in the $\boldsymbol{H}^1$ norm. Moreover, we will display a way to recover the numerical solution for the pressure. Since $\boldsymbol{V}_h \times M_h$ is unstable, this means that M_h is still too large. Therefore, we need to remove more modes from M_h and still try to preserve the good approximation properties for the remaining pressure space. It is then necessary to define a new velocity space $\boldsymbol{W}_h \subset \boldsymbol{V}_h$ such that not only is $\boldsymbol{W}_h \times S_h$ stable but also the velocity from $\boldsymbol{W}_h \times S_h$ is exactly the same as the $\boldsymbol{u}_h$ from $\boldsymbol{V}_h \times M_h$. Of course, the space $\boldsymbol{W}_h$ should possess good approximation properties.

The crucial matter here is to determine the bad modes in M_h. Let $h = 1/n$ and $n = 4k$ for some positive integer k, and let $\mathcal{T}_h$ be the crisscross mesh of the unit square. Let $\mathcal{Q}_{4h}$ be a macroelement partition of $\mathcal{T}_h$ such that every $U \in \mathcal{Q}_{4h}$ has 16 $h \times h$ squares. Therefore, $\mathcal{T}_h^U$ consists of 64 triangles. From the analysis of Section 7.3.1, we know that N_h^U is the space spanned by the functions χ^U, δ_U, and $\delta_{i+1/2,j+1/2}$, where $(i+1/2, j+1/2)$ is a singular vertex in $\mathcal{T}_h^U$ (see Figure 7.4 for $\mathcal{T}_h^U$ and δ_U). Obviously, $\delta_{i+1/2,j+1/2}$'s are not in M_h. Since $\delta_\Omega \in \operatorname{span}\{\delta_U, \forall U \in \mathcal{Q}_{4h}\}$, we need to remove $\operatorname{span}\{\delta_U, \forall U \in \mathcal{Q}_{4h}\}$ from M_h.

Define

$$
\begin{aligned}
\bar{N}_h &= \operatorname{span}\{1, \delta_{i+\frac{1}{2},j+\frac{1}{2}}, \delta_U, 1 \le i, j \le n-1, \forall U \in \mathcal{Q}_{4h}\},\\
S_h &= L^2 \text{ orthogonal complement of } \bar{N}_h \text{ in } P_h,\\
\boldsymbol{W}_h &= \{\boldsymbol{v} \in \boldsymbol{V}_h \mid b(\boldsymbol{v}, q) = 0, \forall q \in \bar{N}_h\},\\
S_h^U &= \chi^U S_h,\\
\boldsymbol{W}_h^U &= \{\boldsymbol{v} \in \boldsymbol{W}_h \mid \operatorname{spt} \boldsymbol{v} \subset U\}.
\end{aligned}
$$

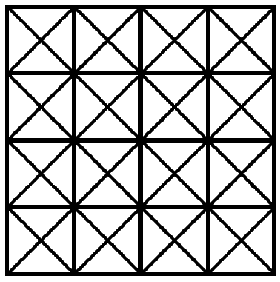

-1	1	-1	1
1	-1	1	-1
-1	1	-1	1
1	-1	1	-1

Figure 7.4. Macroelement U and a bad pressure mode over U.

Theorem 7.3.3. *Let $\mathcal{T}_h$ be a crisscross mesh of the unit square. Assume $(\boldsymbol{u}, p) \in \mathring{\boldsymbol{H}}^2(\Omega) \times H^1(\Omega)$ solves* (2.1.1) *and $(\tilde{\boldsymbol{u}}_h, \tilde{p}_h) \in \boldsymbol{W}_h \times S_h$ solves* (2.4.2)*, then*

$$
\begin{aligned}
\|\boldsymbol{u} - \tilde{\boldsymbol{u}}_h\|_{1,\Omega} &\le Ch\|\boldsymbol{u}\|_{2,\Omega},\\
\|p - \tilde{p}_h\|_{0,\Omega} &\le Ch(\|\boldsymbol{u}\|_{2,\Omega} + \|p\|_{1,\Omega}).
\end{aligned}
$$

Proof. It is easy to verify that

$$
N_h \subset \bar{N}_h, \quad \boldsymbol{M}_0^1(\mathcal{T}_{2h}) \subset \boldsymbol{W}_h, \quad \text{and} \quad M_{-1}^0(\mathcal{Q}_{4h}) \subset S_h.
$$

Therefore, $\boldsymbol{W}_h \times S_h$ has good approximation properties. It only remains to prove that $\boldsymbol{W}_h \times S_h$ is stable.

Define

$$\tilde{N}_h^U = \{q \in S_h^U \mid b(\boldsymbol{v}, q) = 0, \forall \boldsymbol{v} \in \boldsymbol{W}_h^U\}.$$

Then the analysis of Section 7.3.1 implies that $\tilde{N}_h^U$ contains only constant functions. Therefore, $\boldsymbol{W}_h \times \left(S_h \cap (\cup_{U \in \mathcal{Q}_{4h}} \tilde{N}_h^U)\right)$ is stable by the fact that $\boldsymbol{M}_0^1(\mathcal{T}_{2h}) \times M_{-1}^0(\mathcal{Q}_{4h})$ is stable. Finally, by using the macroelement partition theorem we have that $\boldsymbol{W}_h \times S_h$ is stable. □

Theorem 7.3.4. *Let $\mathcal{T}_h$ be the crisscross mesh of the unit square with $h = 1/(4k)$ for some positive integer k. If $(\boldsymbol{u}, p) \in \mathring{\boldsymbol{H}}^2(\Omega) \times H^1(\Omega)$ solves (2.1.1), then the solution $(\boldsymbol{u}_h, p_h) \in \boldsymbol{V}_h \times P_h$ of (2.4.2) satisfies*

$$\|\boldsymbol{u} - \boldsymbol{u}_h\|_{1,\Omega} \le Ch\|\boldsymbol{u}\|_{2,\Omega},$$
$$p_h = \tilde{p}_h + \bar{N}_h,$$

and the pressure can be recovered as a postprocess from p_h.

Proof. Clearly, the solution $(\boldsymbol{u}_h, p_h) \in \boldsymbol{V}_h \times P_h$ of

$$a(\boldsymbol{u}_h, \boldsymbol{v}) + b(\boldsymbol{v}, p_h) = (\boldsymbol{f}, \boldsymbol{v}), \quad \forall \boldsymbol{v} \in \boldsymbol{V}_h,$$
$$b(\boldsymbol{u}_h, q) = 0, \quad \forall q \in P_h$$

satisfies

$$\begin{aligned} a(\boldsymbol{u}_h, \boldsymbol{v}) + b(\boldsymbol{v}, p_h) &= (\boldsymbol{f}, \boldsymbol{v}), \quad \forall \boldsymbol{v} \in \boldsymbol{W}_h, \\ b(\boldsymbol{u}_h, q) &= 0, \quad \forall q \in S_h. \end{aligned} \tag{7.3.6}$$

Since $\boldsymbol{u}_h \in \boldsymbol{W}_h$ and $p_h = (p_h/\bar{N}_h) + n_h$ for some $n_h \in \bar{N}_h$, (7.3.6) implies

$$a(\boldsymbol{u}_h, \boldsymbol{v}) + b(\boldsymbol{v}, p_h/\bar{N}_h) = (\boldsymbol{f}, \boldsymbol{v}), \quad \forall \boldsymbol{v} \in \boldsymbol{W}_h,$$
$$b(\boldsymbol{u}_h, q) = 0, \quad \forall q \in S_h.$$

Since the solution of (2.4.2) in $\boldsymbol{W}_h \times S_h$ is unique, we have

$$\boldsymbol{u}_h = \tilde{\boldsymbol{u}}_h \quad \text{and} \quad p_h/\bar{N}_h = \tilde{p}_h.$$

By Theorem 7.3.3, the velocity $\boldsymbol{u}_h$ and recovered pressure $\tilde{p}_h$ have optimal rates of convergence. It is simple to recover $\tilde{p}_h$ from p_h since we know $\bar{N}_h$ explicitly. □

7.4. Stability and Approximability On a General Mesh Family

The $\mathcal{P}^1$–$\mathcal{P}^0$ element is analyzed on a general mesh family in this section. On this general mesh family, it is shown that the finite element solution for the velocity converges at a order h and the pressure can be recovered by a simple postprocess.

The triangulation $\mathcal{T}_h$ is formed in the following way. First, we partition the polygonal domain Ω into quadrilaterals. This quadrilateral partition is denoted by $\mathcal{Q}_{4h}$. Secondly, each quadrilateral in $\mathcal{Q}_{4h}$ is divided into four subquadrilaterals by linking the intersection of its two diagonals to the middle point of each edge, so $\mathcal{Q}_{2h}$ is formed. Repeating the above process to all quadrilaterals in $\mathcal{Q}_{2h}$, we have $\mathcal{Q}_h$. Finally, partitioning each quadrilateral in $\mathcal{Q}_h$ into 4 triangles by its two diagonals, we obtain the triangulation $\mathcal{T}_h$. The first figure in Figure 7.5 shows how to partition a quadrilateral

in $\mathcal{Q}_{4h}$ into 4 quadrilaterals in $\mathcal{Q}_{2h}$, the second figure shows a macroelement in $\mathcal{Q}_{4h}$ with 64 triangles in $\mathcal{T}_h$.

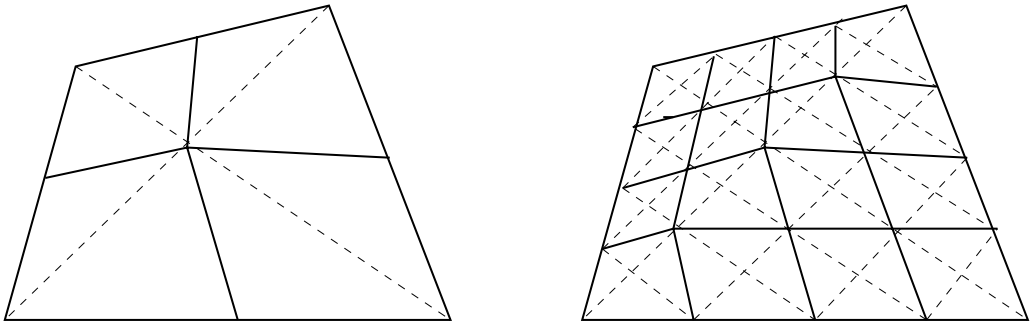

Figure 7.5. Form $\mathcal{Q}_h$ from $\mathcal{Q}_{4h}$.

We will show that on the triangulation $\mathcal{T}_h$, the numerical solution $\boldsymbol{u}_h$ has an optimal rate of convergence and a pressure with an optimal rate of convergence can be recovered from p_h. The measure to achieve this objective is quite similar to what we used for the crisscross mesh. We first remove all possible "bad modes" from P_h, and then consider the pressure in the remaining pressure space. The key issue is to determine bad pressure modes in P_h. We know that spurious pressure modes associated with each singular vertex must be removed from the pressure space P_h. However, this is not enough to guarantee the stability according to our experience with the crisscross mesh. Since the crisscross mesh is a special case of $\mathcal{T}_h$, we definitely need to remove those pressure modes which may degenerate to local spurious modes. Based on this consideration, we will remove all multiples of the mode (shown in Figure 7.6) on each macroelement in $\mathcal{Q}_{2h}$ from the pressure space P_h.

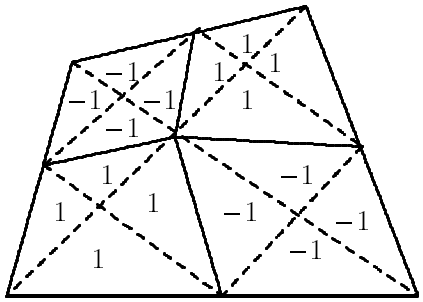

Figure 7.6. "Bad pressure mode" over U_{2h}.

For convenience, we denote a quadrilateral in $\mathcal{Q}_h$ by U_h, a quadrilateral in $\mathcal{Q}_{2h}$ by U_{2h}, one in $\mathcal{Q}_{4h}$ by U_{4h}, and the mode shown in Figure 7.6 by $\delta_{U_{2h}}$. Let δ_{U_h} denote the spurious pressure mode associated with the singular vertex in $U_h \in \mathcal{Q}_h$. We can easily conclude that

$$\int_{\tau} \delta_{U_{2h}} = 0,$$

for any $\tau \in \mathcal{T}_{2h}$, any $U_{2h} \in \mathcal{Q}_{2h}$.

Define

$$\begin{aligned}
\bar{N}_h &= \text{span}\{1, \delta_{U_h}, \delta_{U_{2h}}, \forall U_h \in \mathcal{Q}_h, \forall U_{2\,h} \in \mathcal{Q}_{2\,h}\},\\
S_h &= L^2 \text{ orthogonal complement of } \bar{N}_h \text{ in } P_h,\\
\boldsymbol{W}_h &= \{\boldsymbol{v} \in \boldsymbol{V}_h \mid b(\boldsymbol{v}, q) = 0, \forall q \in \bar{N}_h\},\\
S_h^{U_{4h}} &= \chi^{U_{4h}} S_h,\\
\boldsymbol{W}_h^{U_{4h}} &= \{\boldsymbol{v} \in \boldsymbol{W}_h \mid \text{ spt } \boldsymbol{v} \subset U_{4\,h}\}.
\end{aligned}$$

Theorem 7.4.1. *Let $\mathcal{T}_h$ be a regular triangulation defined at the beginning of this section. If $(\boldsymbol{u}, p) \in \mathring{\boldsymbol{H}}^2(\Omega) \times H^1(\Omega)$ solves (2.1.1) and $(\tilde{\boldsymbol{u}}_h, \tilde{p}_h) \in \boldsymbol{W}_h \times S_h$ solves (2.4.2), then*

$$\begin{aligned}
\|\boldsymbol{u} - \tilde{\boldsymbol{u}}_h\|_{1,\Omega} &\le Ch\|\boldsymbol{u}\|_{2,\Omega},\\
\|p - \tilde{p}_h\|_{0,\Omega} &\le Ch(\|\boldsymbol{u}\|_{2,\Omega} + \|p\|_{1,\Omega}).
\end{aligned}$$

Proof. It is expected that $N_h \subset \bar{N}_h$. This is the case if $\mathcal{T}_h$ is a crisscross mesh. Since $\mathcal{T}_h^{U_{4h}}$ has a special structure, we can show that

$$M_{-1}^0(\mathcal{Q}_{4h}) \subset S_h \text{ and } \boldsymbol{M}_0^1(\mathcal{T}_{2h}) \subset \boldsymbol{W}_h.$$

Therefore, $\boldsymbol{W}_h \times S_h$ has good approximation properties. If we can prove that $\boldsymbol{W}_h \times S_h$ is stable, then we will be done.

Define

$$\tilde{N}_h^{U_{4h}} = \{q \in S_h^{U_{4h}} \mid b(\boldsymbol{v}, q) = 0, \forall \boldsymbol{v} \in \boldsymbol{W}_h^{U_{4h}}\}.$$

We need to show that $\tilde{N}_h^{U_{4h}}$ contains only constant functions. If it does for any $U_{4h} \in \mathcal{Q}_{4h}$, then $\boldsymbol{W}_h \times (S_h \cap (\cup_{U_{4h} \in \mathcal{Q}_{4h}} \tilde{N}_h^{U_{4h}}))$ is stable by the fact that $\boldsymbol{M}_0^1(\mathcal{T}_{2h}) \times M_{-1}^0(\mathcal{Q}_{4h})$ is stable. Therefore, by using the macroelement partition theorem we can prove that $\boldsymbol{W}_h \times S_h$ is stable.

We show that $\dim \tilde{N}_h^{U_{4h}} = 1$. Since $\delta_{U_h} \in \bar{N}_h$, if $q \in \tilde{N}_h^{U_{4h}}$, then q is a constant on each U_h in U_{4h}. Hence, q must be a constant on each $U_{2\,h}$ in U_{4h} since we already removed $\delta_{U_{2h}}$ from the pressure space. Therefore, q must be a constant on each of the four $U_{2\,h}$ in U_{4h}. A simple computation shows that q must a constant on U_{4h}. □

Theorem 7.4.2. *Let $\mathcal{T}_h$ be the triangulation defined at the beginning of this section, then the numerical solution $(\boldsymbol{u}_h, p_h) \in \boldsymbol{V}_h \times P_h$ satisfies*

$$\|\boldsymbol{u} - \boldsymbol{u}_h\|_{1,\Omega} \le Ch\|\boldsymbol{u}\|_{2,\Omega},$$

and $p_h/\bar{N}_h = \tilde{p}_h$. Here we assume $(\boldsymbol{u}, p) \in \mathring{\boldsymbol{H}}^2(\Omega) \times H^1(\Omega)$ solves (2.1.1).

Proof. Use similar arguments in the proof of Theorem 7.3.4. □

7.5. A Space of Divergence-Free Functions on the Crisscross Mesh

In this section, we display a basis for the space $\boldsymbol{Z}_h$ of all divergence-free functions of continuous piecewise linear polynomials on the crisscross mesh $\mathcal{T}_h$. All the basis functions have a very small local support and the space $\boldsymbol{Z}_h$ has optimal approximation properties.

Let the domain Ω be the unit square and $\mathcal{Q}_h$, $h = 1/n$ and n is a positive integer, be a partition of Ω which contains $n \times n$ equal small squares. The triangulation $\mathcal{T}_h$ is obtained from $\mathcal{Q}_h$ by dividing each small square in $\mathcal{Q}_h$ by its two diagonals.

Define

$$\begin{aligned}\boldsymbol{V}_h =& \mathring{\boldsymbol{M}}_0^1(\mathcal{T}_h),\\ \boldsymbol{Z}_h =& \{\boldsymbol{v} \in \boldsymbol{V}_h \mid \operatorname{div} \boldsymbol{v} = 0\}.\end{aligned}$$

A simple calculation shows that

$$\dim \boldsymbol{V}_h = 4n^2 - 4n + 2.$$

In order to study $\boldsymbol{Z}_h$, we define a "pressure" space P_h as

$$P_h = M_{-1}^0(\mathcal{T}_h).$$

Therefore, the analysis of the properties of $\boldsymbol{Z}_h$ can be carried out using the frame work of the analysis of the $\mathcal{P}^1$–$\mathcal{P}^0$ finite element for the Stokes equations with Dirichlet boundary conditions. Since $\operatorname{div} \boldsymbol{V}_h \subset P_h$, we have

$$\boldsymbol{Z}_h = \{\boldsymbol{v} \in \boldsymbol{V}_h \mid \operatorname{div} \boldsymbol{v} = 0\} = \{\boldsymbol{v} \in \boldsymbol{V}_h \mid b(\boldsymbol{v}, q) = 0, \forall q \in P_h\}.$$

Lemma 7.5.1. *On the crisscross triangulation $\mathcal{T}_h$ with $h = 1/n$,*

$$\dim \boldsymbol{Z}_h = (n-2)^2.$$

Proof. Since $\dim P_h = 4n^2$ and $\dim N_h = n^2 + 2$ (see Theorem 7.3.1), the lemma follows. □

In order to find a basis for $\boldsymbol{Z}_h$, we first consider a small macroelement U with size $3h \times 3h$ (see Figure 7.7).

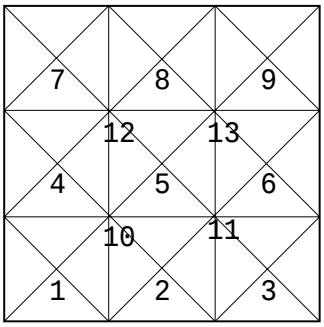

Figure 7.7. Macroelement U.

We denote all the interior vertices of U by $1, 2, \cdots, 13$, as shown in Figure 7.7, and denote the nodal basis functions by $\phi_1, \phi_2, \cdots, \phi_{13}$ accordingly. Let $\boldsymbol{V}_h^U$ denote the subspace of $\boldsymbol{V}_h$ such that all the functions in $\boldsymbol{V}_h^U$ have supports contained in U. We look for functions $\boldsymbol{v} = \Sigma_{i=1}^{13}(u_i, v_i)\phi_i \in \boldsymbol{V}_h^U$ such that $\operatorname{div} \boldsymbol{v} = 0$ in U. Namely, we need to solve a system of 36 linear equations in 26 unknowns. Since $\dim \boldsymbol{Z}_h^U = 1$, we know that this system has one-dimensional solution space. After some algebraic computations, we find that the solution space is

$$\boldsymbol{Z}_h^U = \operatorname{span}\{\boldsymbol{z}^U\},$$

where $\boldsymbol{z}^U = (\xi, \eta)$ and

$$\begin{aligned}\xi =& \phi_2 - \phi_8 + \phi_{10} + \phi_{11} - \phi_{12} - \phi_{13},\\ \eta =& -\phi_4 + \phi_6 - \phi_{10} + \phi_{11} - \phi_{12} + \phi_{13}.\end{aligned}$$

See Figure 7.8 for graphs of ξ and η.

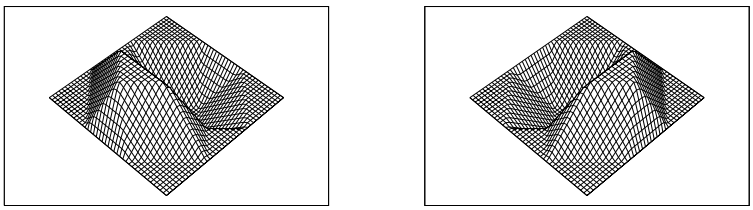

Figure 7.8. The shape of the two components of $\boldsymbol{z}^U$.

Since there are exactly $(n-2)^2$ different macroelement with size $3h \times 3h$ in $\mathcal{T}_h$—the set of all these macroelements is named by $\mathcal{U}_h$—we find a basis for $\boldsymbol{Z}_h$. By the results of Section 7.3, we have

Theorem 7.5.1. *Let $\mathcal{T}_h$ be the crisscross mesh of the unit square with $h = 1/n$. Then*

$$\{\boldsymbol{z}^U \mid \forall U \in \mathcal{U}_h\},$$

form a basis of $\boldsymbol{Z}_h$. Furthermore, if $\boldsymbol{u} \in \mathring{\boldsymbol{H}}^2(\Omega)$ and $\operatorname{div} \boldsymbol{u} = 0$, *then*

$$\inf_{\boldsymbol{v} \in \boldsymbol{Z}_h} \|\boldsymbol{u} - \boldsymbol{v}\|_{1,\Omega} \leq Ch\|\boldsymbol{u}\|_{2,\Omega}.$$

7.6. A Relation between the $\mathcal{P}^1$–$\mathcal{P}^0$ and $\mathcal{Q}^1$–$\mathcal{P}^0$ Elements

In this section, we shall study the relationship between the $\mathcal{P}^1$–$\mathcal{P}^0$ and $\mathcal{Q}^1$–$\mathcal{P}^0$ finite elements. The domain Ω under consideration could be any polygonal domain. We denote a quadrilateral partition of Ω by $\mathcal{Q}_h$ and its corresponding irregular crisscross triangulation by $\mathcal{T}_h$ which is obtained by dividing each quadrilateral in $\mathcal{Q}_h$ by its two diagonals. We assume $\mathcal{T}_h$ is a regular triangulation.

The finite element $\mathcal{Q}^1$–$\mathcal{P}^0$ is defined as

$$\begin{aligned}
\tilde{\boldsymbol{V}}_h &= \{\boldsymbol{v} \in \boldsymbol{C}^0(\Omega) \mid \boldsymbol{v}|_\tau \in Q_\tau^2, \tau \in \mathcal{Q}_h, \boldsymbol{v}|_{\partial\Omega} = 0\},\\
\tilde{P}_h &= \{q \in L^2(\Omega) \mid q|_\tau \in \mathbb{R}\},\\
\tilde{N}_h &= \{q \in \tilde{P}_h \mid b(\boldsymbol{v}, q) = 0, \forall \boldsymbol{v} \in \tilde{\boldsymbol{V}}_h\},\\
\tilde{M}_h &= L^2 \text{ orthogonal complement of } \tilde{N}_h \text{ in } \tilde{P}_h.
\end{aligned}$$

Here

$$Q_\tau = \{w \circ F_\tau^{-1} \mid w \in Q_1(\hat{\tau})\},$$

$\hat{\tau}$ is the reference square, F_τ is the bilinear mapping from $\hat{\tau}$ to τ, and $Q_1(\hat{\tau})$ is the space of all bilinear functions on the reference square $\hat{\tau}$.

For the $\mathcal{P}^1$–$\mathcal{P}^0$ element we use the notations $\boldsymbol{V}_h$, P_h, N_h, M_h, and etc.

It is obvious that

$$\tilde{P}_h \subset P_h.$$

Lemma 7.6.1. *For a polygonal domain Ω, let $\mathcal{Q}_h$ be a quadrilateral partition of Ω. If $\mathcal{T}_h$ is the corresponding irregular crisscross mesh for $\mathcal{Q}_h$, then*

$$\tilde{N}_h \subset N_h.$$

Proof. We state a very simple but important fact first. For any $\boldsymbol{v} \in \boldsymbol{V}_h$, there exists a $\boldsymbol{w} \in \tilde{\boldsymbol{V}}_h$ such that

$$b(\boldsymbol{v}, q) = b(\boldsymbol{w}, q), \forall q \in \tilde{P}_h. \tag{7.6.1}$$

Similarly, for any $\boldsymbol{w} \in \tilde{\boldsymbol{V}}_h$, there is $\boldsymbol{v} \in \boldsymbol{V}_h$ such that (7.6.1) holds.

Since any function $\boldsymbol{w} \in \tilde{\boldsymbol{V}}_h$ is linear on all the edges of $\mathcal{Q}_h$, there exists a function $\boldsymbol{v} \in \boldsymbol{V}_h$ such that $\boldsymbol{v} - \boldsymbol{w}$ vanishes on all the edges of $\mathcal{Q}_h$. Therefore, (7.6.1) follows by using the Green's formula.

From (7.6.1), the lemma follows. □

In order to study the structure of N_h, we consider $\mathcal{Q}_h$ as a macroelement partition of $\mathcal{T}_h$. For any quadrilateral $U \in \mathcal{Q}_h$, there is a spurious pressure mode in P_h associated with the singular vertex of $\mathcal{T}_h^U$ (see Figure 7.1). For convenience, the spurious pressure mode is denoted by δ_U.

Lemma 7.6.2.

$$N_h = \tilde{N}_h + \text{span}\{\delta_U \mid \textit{ for all quadrilaterals } U \in \mathcal{Q}_h \}$$

Proof. Clearly, $\delta_U \in N_h$ for any $U \in \mathcal{Q}_h$. Since N_h^U contains only linear combinations of χ^U and δ_U for each $U \in \mathcal{Q}_h$, any function $q \in N_h$ must be in $\tilde{P}_h$ provided q is orthogonal to all δ_U's. By (7.6.1), $q \in \tilde{N}_h$. Hence, the lemma follows. □

Corollary 7.6.1.

$$M_h \cap \tilde{P}_h = \tilde{M}_h.$$

Theorem 7.6.1. *For a polygonal domain Ω, let $\mathcal{Q}_h$ be a quadrilateral partition of Ω and $\mathcal{T}_h$ the corresponding irregular crisscross mesh for $\mathcal{Q}_h$. Assume $\mathcal{T}_h$ is regular. If $\tilde{\gamma}_h$ and $\bar{\gamma}_h$ denote the reduced inf–sup constants of $\tilde{\boldsymbol{V}}_h \times \tilde{P}_h$ and $\boldsymbol{V}_h \times P_h$ respectively, then*

$$C\tilde{\gamma}_h \le \bar{\gamma}_h \le C^{-1}\tilde{\gamma}_h,$$

where C is a constant independent of h.

Proof. Let $\mathcal{Q}_h$ be a macroelement partition of $\mathcal{T}_h$. On each macroelement $U \in \mathcal{Q}_h$, we have

$$\dim \boldsymbol{V}_h^U = 2, \quad \dim P_h^U = 4,$$
$$\dim M_h^U = 2, \quad \dim N_h^U = 2.$$

Following the arguments of Theorem 4.3.1, we can bound the local inf–sup constants on all macroelements in $\mathcal{Q}_h$ by a positive number which is independent of h. Applying the macroelement partition theorem, we know that the reduced inf–sup constant $\bar{\gamma}_h$ is determined by the stability of $\boldsymbol{V}_h \times (M_h \cap \sum_{U \in \mathcal{Q}_h} N_h^U) = \boldsymbol{V}_h \times \tilde{M}_h$ (by the corollary). This implies that $\boldsymbol{V}_h \times M_h$ has exactly the same stability as $\boldsymbol{V}_h \times \tilde{M}_h$. If we can prove that $\boldsymbol{V}_h \times \tilde{M}_h$ and $\tilde{\boldsymbol{V}}_h \times \tilde{M}_h$ have the same stability, then we are done.

We first show that

$$\bar{\gamma}_h \ge C\tilde{\gamma}_h. \tag{7.6.2}$$

For any $q \in \tilde{M}_h$, by Theorem 2.2.3, there exists a function $\boldsymbol{w} \in \tilde{\boldsymbol{V}}_h$ such that

$$\begin{aligned} b(\boldsymbol{w}, q) &= \|q\|_{0,\Omega}^2, \\ \|\boldsymbol{w}\|_{1,\Omega} &\leq \frac{C}{\tilde{\gamma}_h}\|q\|_{0,\Omega}. \end{aligned} \tag{7.6.3}$$

If we can construct a function $\boldsymbol{v} \in \boldsymbol{V}_h$ such that

$$\begin{aligned} b(\boldsymbol{v}, q) &= \|q\|_{0,\Omega}^2, \\ \|\boldsymbol{v}\|_{1,\Omega} &\leq \frac{C}{\tilde{\gamma}_h}\|q\|_{0,\Omega}, \end{aligned}$$

then (7.6.2) is proved.

Let $\boldsymbol{I}_h := (I_h, I_h) : \tilde{\boldsymbol{V}}_h \to \boldsymbol{V}_h$ be the interpolation operator such that $\boldsymbol{I}_h\boldsymbol{g}$ and $\boldsymbol{g}$ agree at every vertex in $\mathcal{T}_h$ for any $\boldsymbol{g} \in \tilde{\boldsymbol{V}}_h$. Therefore, for any function $\boldsymbol{g} \in \tilde{\boldsymbol{V}}_h$, the interpolation error $\boldsymbol{g} - \boldsymbol{I}_h\boldsymbol{g}$ vanishes at all the edges of the quadrilateral partition $\mathcal{Q}_h$. We will show that there is a constant C independent of h such that

$$\|\boldsymbol{g} - \boldsymbol{I}_h\boldsymbol{g}\|_{1,\Omega} \leq C\|\boldsymbol{g}\|_{1,\Omega}, \tag{7.6.4}$$

for any $\boldsymbol{g} \in \tilde{\boldsymbol{V}}_h$. If this is the case, by taking $\boldsymbol{v} = \boldsymbol{I}_h\boldsymbol{w}$, then

$$\|\boldsymbol{v}\|_{1,\Omega} \leq \|\boldsymbol{w} - \boldsymbol{v}\|_{1,\Omega} + \|\boldsymbol{w}\|_{1,\Omega} \leq C\|\boldsymbol{w}\|_{1,\Omega}.$$

According to the arguments in the proof of Lemma 7.6.1 and (7.6.3), we have

$$\begin{aligned} b(\boldsymbol{v}, q) &= b(\boldsymbol{w}, q) = \|q\|_{0,\Omega}^2. \\ \|\boldsymbol{v}\|_{1,\Omega} &\leq \frac{C}{\tilde{\gamma}_h}\|q\|_{0,\Omega}. \end{aligned}$$

This proves (7.6.2) with the assumption (7.6.4).

Let $U \in \mathcal{Q}_h$ be a macroelement. If we can show that

$$\|g - I_h g\|_{0,U} \leq C\|g\|_{0,U}, \tag{7.6.5}$$

$$|g - I_h g|_{1,U} \leq C|g|_{1,U}, \tag{7.6.6}$$

for any $g \in Q_U$, any $U \in \mathcal{Q}_h$, and any $h > 0$ with constant C independent of h, then we are done. Let $E_\theta(\hat{U})$ denote the set of all the equivalence macroelements of the unit square $\hat{U}$ satisfying the shape constraint (2.3.2). Obviously, translations and dilations of U do not affect (7.6.5) and (7.6.6). Therefore, for simplicity, we assume that the length of the longest diagonals of each macroelement in $E_\theta(\hat{U})$ is one unit, and that the intersection of the two diagonals of any macroelement in $E_\theta(\hat{U})$ has coordinates $(0,0)$. For any macroelement U in $E_\theta(\hat{U})$, we name the intersection of its two diagonals by v_5 and the rest four vertices by v_1, v_2, v_3, and v_4 clockwise. Hence, $S = \{(v_1, v_2, v_3, v_4, v_5) \mid U \in E_\theta(\hat{U})\}$ is a closed set in $\mathbb{R}^{10}$. Let $g \in Q_U$ be arbitrary and it values at v_i be g_i for $i = 1, 2, 3, 4$. For convenience, we denote $(g_1, g_2, g_3, g_4)^t$ by $\bar{g}$. Since $(I_h g)(v_i) = g_i$ for $i = 1, 2, 3, 4$ and $(I_h g)(v_5)$ is determined by g_1, g_2, g_3, and g_4, we have

$$\begin{aligned} \|g - I_h g\|_{0,U}^2 &= \bar{g}^t A_U \bar{g}, \\ \|g\|_{0,U}^2 &= \bar{g}^t B_U \bar{g}. \\ |g - I_h g|_{1,U}^2 &= \bar{g}^t C_U \bar{g}, \\ |g|_{1,U}^2 &= \bar{g}^t D_U \bar{g}. \end{aligned}$$

Here B_U is a symmetric positive definite and A_U, C_U, and D_U, are symmetric positive semi-definite. Clearly, the entries of A_U, B_U, C_U, and D_U are continuous functions of $(v_1, v_2, v_3, v_4, v_5)$.

Since S is a bounded closed set in $\mathbb{R}^{10}$, there exists a constant C_1 independent of h such that

$$\|g - I_h g\|_{0,U} \leq C_1 \|g\|_{0,U}, \tag{7.6.7}$$

for any $U \in E_\theta(\hat{U})$.

It is easy to see that only the constant functions make the both sides of (7.6.6) zeros. Hence, matrix D_U always has exactly three positive eigenvalues which depend on $(v_1, v_2, v_3, v_4, v_5)$ continuously. Since S is a bounded closed set in $\mathbb{R}^{10}$, the smallest nonzero eigenvalue of D_U is bounded away from zero by a positive number independent of h. Due to the same reason, the largest eigenvalue of C_U is bounded above by a constant independent of h. Therefore, there exists a constant C_2 independent of h such that

$$|g - I_h g|_{1,U} \leq C_2 |g|_{1,U}, \tag{7.6.8}$$

for any $U \in E_\theta(\hat{U})$.

Combining (7.6.7) and (7.6.8), we obtain (7.6.5) and (7.6.6). Therefore, we have proved (7.6.2).

Using similar arguments, we can show that $\tilde{\gamma}_h \geq C\bar{\gamma}_h$. $\square$

Theorem 7.6.2. *Let $\mathcal{Q}_h$ be a quadrilateral partition of a polygonal domain Ω and $\mathcal{T}_h$ be the corresponding irregular crisscross mesh for $\mathcal{Q}_h$. If $\tilde{\boldsymbol{V}}_h \times \tilde{P}_h$ is stable, then $\boldsymbol{V}_h \times M_h$ is stable. Moreover, if $(\boldsymbol{u}_h, \bar{p}_h) \in \boldsymbol{V}_h \times M_h$ and $(\boldsymbol{u}_h, p_h) \in \boldsymbol{V}_h \times P_h$ solve (2.4.2), then*

$$\begin{aligned} \|\boldsymbol{u} - \boldsymbol{u}_h\|_{1,\Omega} &\leq Ch\|\boldsymbol{u}\|_{2,\Omega}, \\ \|p - \bar{p}_h\|_{0,\Omega} &\leq Ch(\|\boldsymbol{u}\|_{2,\Omega} + \|p\|_{1,\Omega}). \end{aligned} \tag{7.6.9}$$

Here the constant C is independent of h, $\bar{p}_h = p_h/N_h$, and we assume that $(\boldsymbol{u}, p) \in \mathring{\boldsymbol{H}}^2(\Omega) \times H^1(\Omega)$ solves (2.1.1).

Proof. Stability of $\boldsymbol{V}_h \times M_h$ is a direct consequence of Theorem 7.6.1. It is known that $M^0_{-1}(\mathcal{Q}_h) \subset M_h$, this implies that the approximation properties of M_h are as good as those of P_h. Therefore, (7.6.9) follows. $\square$

References

[1] I. Babuška and M. Suri, *Locking effects in the finite element approximation of elasticity problems*, 1990, Tech. Note BN-1119, Inst. Phys. Sci. Tech., Univ. of Maryland.

[2] J. M. Boland and R. A. Nicolaides, *Stability of finite elements under divergence constraints*, SIAM J. Numer. Anal., 20 (1983), pp. 722–731.

[3] ———, *Stable and semistable low order finite elements for viscous flows*, SIAM J. Numer. Anal., 22 (1985), pp. 474–492.

[4] C. de Boor and R. Devore, *Approximation by smooth multivariate splines*, Trans. Amer. Math. Soc., 276 (1983), pp. 775–788.

[5] C. de Boor and K. Hollig, *Approximation order from bivariate C^1-cubics: a counterexample*, Proc. Amer. Math. Soc., 87 (1983), pp. 649–655.

[6] F. Brezzi, *On the existence, uniqueness, and approximation of saddle point problems arising from Lagrangian multipliers*, RAIRO Anal. Numér., 8 (1974), pp. 129–151.

[7] F. Brezzi and M. Fortin, *Mixed and hybrid finite element methods*, Springer-Verlag, New York–Heidelberg–Berlin, 1991.

[8] C. K. Chui, L. L. Schumaker, R. H. Wang, *On spaces of piecewise polynomials with boundary conditions, II. Type-1 triangulations*, in Second Edmonton Conference on Approximation Theory, Z. Ditzian, A. Meir, and S. Riemenschneider, and A. Sharma, eds., American Mathematical Society, Providence, 1983, pp. 51–66.

[9] P. G. Ciarlet, *The Finite Element Method for Elliptic Equations*, North-Holland, Amsterdam, 1978.

[10] J. F. Ciavaldini and J. C. Nedelec, *Sur l'élément de Fraeijs de Veubeke et Sander*, RAIRO Anal. Numér., 1974.

[11] V. Girault and P. A. Raviart, *Finite element methods for Navier-Stokes equations*, Springer-Verlag, New York–Heidelberg–Berlin, 1986.

[12] C. Johnson, *Numerical solution of partional differential equations by the finite element method*, Cambridge University Press, 1987.

[13] C. Johnson and J. Pitkäranta, *Analysis of some mixed finite element methods related to reduced integration*, Math. of Comp., 158 (1982), pp. 375–400.

[14] J. D. Jr., T. Dupont, P. Percell, and R. Scott, *A family of C^1 finite elements with optimal approximation properties for various Galerkin methods for 2nd and 4th order problems*, RAIRO, 13 (1979), pp. 227–255.

[15] M. Kitahama and P. R. Dawson, *A practical formulation for Lagrangian viscoplastic analyses with adaptive remeshing*, Preprint, Sibley School of Mechanical and Aerospace Engineering, Cornell University, August 1990.

[16] Y-S. Lee and P. R. Dawson, *Obtaining residual stresses in metal forming after neglecting elasticity on loading*, J. of Applied Mechanics, 56 (June 1989), pp. 318–327.

[17] B. Mercier, *A conforming finite element method for two-dimensional incompressible elasticity*, Internat. J. Numer. Methods Engrg., 14 (1979), pp. 942–945.

[18] S. G. Mikhlin, *The spectrum of a family of operators in the theory of elasticity*, Russian Math. Surveys, 28 (1973), pp. 45–88.

[19] J. Morgan and L. R. Scott, *The dimention of the space of C^1 piecewise polynomials* , Preprint, August, 1990.

[20] M. J. D. Powell, *Piecewise quadratic surface fitting for contour ploting*, in Software for Numerical Mathematics, D. J. Evans, ed., Academic Press, New York, 1976, pp. 253–2271.

[21] L. R. Scott and M. Vogelius, *Norm estimates for a maximal right inverse of the divergence operator in spaces of piecewise polynomials* , Math. Modelling Numer. Anal., 9 (1985), pp. 11–43.

[22] ———, *Conforming finite element methods for incompressible and nearly incompressible continua* , Lectures in Applied Mathematics, 22 (1985), pp. 221–244.

[23] L. R. Scott and S. Zhang, *Finite element interpolation of nonsmooth functions satisfying boundary conditions* , Math. Comp., 54 (1990), pp. 483–493.

[24] R. Stenberg, *Analysis of mixed finite element methods for the Stokes problem: a unified approach*, Math. Comp., 42 (1984), pp. 9–23.

[25] ———, *Error analysis of some finite element methods for the Stokes problem*, Math. Comp., 54 (1990), pp. 495–508.